



NTNU – Trondheim
Norwegian University of
Science and Technology

Verifying and Validation of a Manoeuvring Model for NTNU's Research Vessel R/V Gunnerus

Sissel Tjøswold

Marine Technology
Submission date: June 2012
Supervisor: Tor Einar Berg, IMT

Norwegian University of Science and Technology
Department of Marine Technology

MSc. thesis, spring 2012

by

Sissel Tjøswold

Verifying and validation of a manoeuvring model for NTNU's research vessel MV "Gunnerus"

Work description

NTNU's research vessel "Gunnerus" is used as a base for a number of scientific operations. For planning of specific operations it is of interest to have a validated ship motion simulation model for the vessel. This is presently not developed and it has been decided that work should be initiated to build, verify and validate a ship motion simulation model for the vessel.

It is presently under consideration to retrofit a new power and propulsion system to the vessel. In this context it is of interest to compare speed and manoeuvring performance for the vessel with the old and the new propulsion system. Performance information should thus be collected from the present version of the vessel. This master thesis will investigate the manoeuvring performance of the vessel in calm and deep water through field tests in Trondheimsfjorden. In addition to standard IMO manoeuvring tests the student shall discuss other and more operational tests with the navigators on the research vessel.

The master thesis has its origin in the project thesis written fall 2011, where initial simulation studies were performed using MARINTEK's ship motion simulation tools ShipX and VeSim.

Scope of work

1. Review and discuss the basic model formulation used in MARINTEK's ship motion simulation programs SIMAN (ShipX manoeuvring module) og VeSim.
2. Investigate if the basic model formulation is sufficient and valid for the research vessel "Gunnerus".
3. Take part in planning and execution of manoeuvring tests with the vessel.
4. Analyse field test data and discuss measurement accuracy
5. Discuss how the field test results can be used to improve the numerical simulation tools used by MARINTEK
6. Compare test results with simulator results and discuss possible error sources in the field measurements and the numerical simulation models
7. Discuss if the NTNU research vessel "Gunnerus" could be used as a case vessel for an international study to investigate validity of numerical simulation models for different ship types and sizes.

The report shall be written in English and include description of theory, analysis of the results, discussion and a conclusion including a proposal for further work. Source code should be provided on a CD with code listing enclosed in appendix. It is supposed that Department of Marine Technology, NTNU, can use the results freely in its research work, unless otherwise agreed upon, by referring to the student's work.

The report should be well organized and give a clear presentation of the work and all conclusions. It is important that the text is well written and that tables and figures are used to support the verbal presentation. The report should be complete, but still as short as possible.

The thesis should be submitted within 10th of June 2012.

Supervisor: Tor Einar Berg

Trondheim 30 May 2012


Tor Einar Berg

Abstract

MARINTEK's ship motion simulation program SIMAN (ShipX manoeuvring module) is used to develop a ship motion model for NTNU's research vessel R/V Gunnerus. SIMAN uses a 3-DOF linear mathematical model to describe the vessel's motions. In order to verify the SIMAN model of R/V Gunnerus, full-scale trials of R/V Gunnerus were performed in deep water in Trondheimsfjorden. Turning circles, zig-zag- and stopping tests were carried out and analysed. Data was recorded using Seapath and the DP-system installed on R/V Gunnerus. Seapath registered data at 200 Hz, while the DP-system registered data at 1 Hz. Data registration at 1 Hz turned out to be too seldom, especially for the zig-zag manoeuvres.

Full-scale trials are simulated in SIMAN. Measured full-scale results are compared with simulated results, and differences between measured and simulated results are identified. It was expected that differences would occur as SIMAN is developed for conventional vessels and offshore vessels, while R/V Gunnerus is an unconventional vessel ($L = 28.9\text{ m}$, $B = 9.6\text{ m}$). The deviations may be due to inaccurate field test results or errors in the modelling in SIMAN. SIMAN underestimated tactical diameter, transfer and advance in the turning circle manoeuvres. The difference increased with increasing rudder angle (and consequently drift angle), which may indicate errors in modelling of the non-linear damping forces. The damping forces are then modified using Oltmann's polynomial for the cross-flow drag coefficient for a tanker. This improved the results, all with the exception of transfer and advance at rudder angles of 20° . It is also shown that the results are sensitive to rudder angle, so incorrect full-scale measurement will affect the results. The difference between measured and simulated zig-zag trials are significant. However, only a few seconds or degrees difference between the simulated and the measured zig-zag results cause a large percentage difference. Possible reasons for the differences are inadequate data registration of the full-scale trials, or errors in modelling in SIMAN. Overestimated results in SIMAN may indicate an unstable model.

Increasing the models stability index by reducing N_v had a negligible effect on the simulated results. Decreasing rudder angle in the simulations improved the results. Track reach in the stopping manoeuvres are overestimated by SIMAN. This may be due to modelling issues as R/V Gunnerus is much smaller and responds faster than the vessels that SIMAN is developed for.

In the literature there exists several empirical methods to calculate the hydrodynamic coefficients used in manoeuvring equations. The hydrodynamic coefficients of R/V Gunnerus were calculated using approaches given by Wagner Smitt, Norrbin, Inoue, Clarke, Lee and Kijima, as well as using strip theory for a flat plate. Using these coefficients did not improve the simulated results.

In order to create a complete motion model for R/V Gunnerus further investigation is necessary. It is recommended that PMM tests are performed to determine the hydrodynamic coefficients. It can also be useful to investigate the non-linear damping forces. In addition, new full-scale zig-zag tests should be performed in a way that 10/10 and 20/20 tests are obtained. Performing several reruns could be used to determine the precision errors of the full-scale trials.

In the literature there is a need for vessels to be used for validation of simulation tools. R/V Gunnerus can be used as a case vessel to investigate how the simulation tools predict the manoeuvring performance of an unconventional vessel. The 26th ITTC stated that there is a particular need for mathematical models for low speed manoeuvring, and vessels also used for validation of CFD-methods. R/V Gunnerus can be used as a case vessel for this research. It is then necessary to carry out tests intended for these purposes.

Sammendrag

SIMAN (ShipX manøvermodul) er et program utviklet av MARINTEK for å simulere skips bevegelser. Dette programmet er brukt for å lage en manøvermodell for NTNU sitt forskningsfartøy F/F Gunnerus. For å verifisere modellen i SIMAN er full-skala tester med F/F Gunnerus utført i dypt vann i Trondheimsfjorden. Dreiesirkler, sikk-sakk-tester og stoppetester ble gjennomført og analysert. Data ble registrert ved bruk av Seapath og DP-systemet installert på F/F Gunnerus. Seapath registrerte data ved 200 Hz, mens DP-systemet registrerte data ved 1 Hz. 1 Hz viste seg å være for sjeldent, spesielt for sikk-sakk-testene.

Full-skala testene ble deretter simulert i SIMAN. Målte full-skala resultater ble sammenlignet med resultater fra simuleringene, og forskjeller mellom resultatene ble oppdaget. Det var forventet at det ville bli forskjeller siden SIMAN er utviklet for konvensjonelle skip og offshore-fartøy, mens F/F Gunnerus er et ukonvensjonelt skip ($L = 28.9\text{ m}$, $B = 9.6\text{ m}$). Avviket kan dermed skyldes unøyaktige full-skala resultater eller feil med modelleringen for F/F Gunnerus i SIMAN. SIMAN underestimerte taktisk diameter (tactical diameter), sideforflytning (transfer) og vandring (advance) for dreiesirklene. Forskjellen økte ved økende rorvinkel, noe som kan tyde på feil ved modellering av ulineære dempningskrefter. Dempningskreftene ble modifisert ved å bruke Oltmann's polynom for tverr-strøm motstandskoeffisienten (cross-flow drag coefficient) for et tankskip. Dette forbedret resultatene, med unntak av sideforflytning (transfer) og vandring (advance) for manøvre med 20° rorvinkel. Det blir også vist at resultatene er sensitiv til rorvinkel, slik at ukorrekte måling fra full-skala testene vil påvirke simuleringene. Forskjellen mellom målte og simulerte sikk-sakk tester er betydelig. Det må nevnes at kun et par sekunder eller grader forskjell gir stor prosentvis forskjell. Årsaker for forskjellen kan være utilstrekkelig dataregistering i felttestene eller feil knyttet til modelleringen i SIMAN. Overestimerte resultater i SIMAN kan tyde på at modellen er for ustabil. Det å øke modellens stabilitetsindeks ved å redusere den lineære dempnings koeffisienten N_v hadde imidlertid negliserbar virkning. Å redusere

rorvinkelen i simulaeringene forbedret resultatene. SIMAN overestimerte også stoppelengden (track reach) i stoppetestene. Det kan knyttes til modellering siden F/F Gunnerus er mye mindre og responderer raskere enn skipene som SIMAN er utviklet for.

I litteraturen finnes det flere empiriske metoder for å beregne hydrodynamiske koeffisienter som brukes i manøreringsligningene. F/F Gunnerus sine hydrodynamiske koeffisienter ble beregnet ved å bruke metoder gitt av Wagner Smitt, Norrbin, Inoeue, Clarke, Lee og Kijima samt ved bruk av stripeteori. Bruk av disse koeffisientene forbedret ikke resultatene i simuleringene.

For å lage en komplett manøvermodell for F/F Gunnerus er det nødvendig med flere undersøkelser. Det kan anbefales å gjennomføre PMM tester for å bestemme de hydrodynamiske koeffisientene. Det kan også være nyttig å undersøke ulineæreredempningskrefter. I tillegg bør sikk-sakk-testene gjennomføres på en tilfredsstillende måte. Ved å utføre flere enkelstående full-skala tester kan presisjonsfeilen ved full-skala testene finnes.

I litteraturen er det i dag et behov for skip som kan brukes til validering av simuleringsverktøy. F/F Gunnerus kan brukes som et eksempel-skip for å undersøke hvordan simuleringsverktøy estimerer manøvreringsegenskapene til et ukonvensjonelt fartøy. Det er også et særlig behov for matematiske modeller for lavhastighetsmanøvrering, og skip som kan brukes til validering av CFD-metoder. F/F Gunnerus kan brukes som et eksempel-skip for denne forskningen. Det er da nødvendig å utføre tester for disse formålene.

Acknowledgement

This thesis is submitted as a partial fulfilment for the degree of Master of Science in Marine Technology.

I would like to express my gratitude to my supervisor Tor Einar Berg for guidance during this study. I would like to thank Sverre Steen (NTNU) for guidance regarding full-scale trials with R/V Gunnerus. I would also like to thank Edvard Ringen (MARINTEK) for help with ShipX. A special thanks to my office-mates for a good study environment and the encouragement to write this thesis in LaTex.

**Sissel Tjøswold
Trondheim, June 2012**

Contents

1	Introduction	1
1.1	Ship manoeuvring	2
1.1.1	Manoeuvring characteristics	2
1.1.2	Required manoeuvring tests	3
1.2	Manoeuvring prediction methods	7
1.3	Benchmarking models	8
1.4	Thesis organisation	10
2	Forces on a vessel	12
2.1	Reference frames	12
2.1.1	Earth Centered Inertial	12
2.1.2	Earth Centred Earth Fixed	12
2.1.3	North-East-Down	13
2.1.4	Body-fixed	13
2.1.5	Flow axes	15
2.2	Course-, heading- and drift angle	15
2.3	Forces	16
2.4	Damping forces	18
2.5	Circulatory lift and drag	18
2.5.1	Lift	20
2.5.2	Drag	21
2.5.3	Low-speed drag	23
2.6	Non-linear lift (Cross-flow drag)	24
2.7	Roll model	26
2.7.1	The roll angle's influence on lift and drag	26
2.7.2	Roll damping	27
2.8	Total forces	28
2.8.1	Circulatory lift and drag	28
2.8.2	Cross-flow drag	28

2.8.3	Roll damping	28
3	Mathematical models	29
3.1	Linear 3-DOF model	30
3.1.1	Stability calculations	31
3.2	4-DOF low-frequency model	32
4	Calculation of hydrodynamic coefficients	35
4.1	Strip theory	36
4.1.1	Flat plate	36
4.1.2	Surface ship hull	37
4.2	Empirical methods	39
4.2.1	Wagner Smitt	39
4.2.2	Norrbin	39
4.2.3	Inoue	40
4.2.4	Clarke	40
4.2.5	Lee	41
4.2.6	Kijima	43
4.2.7	ShipX Manoeuvring (SIMAN)	45
4.3	Results and discussion	46
5	Full-scale trials	49
5.1	Instrumentation and data registration	50
5.1.1	Seapath	50
5.1.2	DP-system	51
5.2	Analysis of trials	52
5.2.1	Evaluation of data parameters	52
5.2.2	Turning circles	61
5.2.3	Zig-zag trials	67
5.2.4	Stopping tests	70
6	Simulations in ShipX	73
6.1	Method	74
6.2	Simulation of full-scale trials	76
6.2.1	Ship model	76
6.2.2	Manoeuvres	77
6.2.3	Results and discussion	78
6.2.4	Evaluation of parameters in SIMAN	85
6.3	Simulations using calculated hydrodynamic coefficients	92
6.3.1	Ship model	93
6.3.2	Results and discussion	93

7 R/V Gunnerus as a case vessel in research	97
7.1 Current need for research and development	97
7.2 R/V Gunnerus as a case vessel	98
7.3 Recommended trials	98
7.3.1 Planar Motion Mechanism (PMM) tests	98
7.3.2 Full-scale trials	100
8 Conclusion	101
8.1 Further work	103

Appendix	I
A.1 Specifications R/V Gunnerus	II
A.2 4-DOF equations of motion	V
A.2.1 Kirchhoff's equations of motion	V
A.2.2 Rigid body equation of motion	VI
A.2.3 Equations of motion for ships	VII
A.3 Main characteristics of R/V Gunnerus	IX
A.4 Analysis of full-scale trials	X
A.4.1 Turning circles	X
A.4.2 Zig-zag manoeuvres	XIX
A.4.3 Stopping tests	XXIII
A.5 Simulations in ShipX	XXV
A.5.1 Effect of wake fraction and thrust deduction on turning circle manoeuvre	XXV

List of Figures

1.1	Turning circle test	4
1.2	Zig-zag test	5
1.3	Stopping test	6
1.4	Body plan of the benchmarking models KVLCC1 and KVLCC2	9
2.1	Reference frames	13
2.2	Body-fixed axis system used in manoeuvring problems	14
2.3	Course-, heading- and sideslip angle	16
2.4	2D-foil	19
2.5	Lift and drag forces on a vessel	19
2.6	Non-linear flow underneath hull	24
2.7	Aircraft wing with dihedral angle	26
2.8	Dihedral of hull and roll angle	26
4.1	Axis system used in horizontal plane manoeuvring	36
4.2	Stern hull profile used by Lee in derivation of velocity derivatives	42
4.3	Axis system used by Kijima in manoeuvring	44
4.4	Velocity derivatives calculated for R/V Gunnerus	47
4.5	Acceleration derivatives calculated for R/V Gunnerus	48
5.1	R/V Gunnerus' position given by Seapath and DP-system	54
5.2	Trajectory of a turning circle carried out 01/03/2012	55
5.3	Trajectory of a zig-zag manoeuvre	55
5.4	Trajectory of a turning circle carried out 27/02/2012	55
5.5	Trajectories plotted with a two second delay on the DP-data	56
5.6	Heading and rudder angles versus time for a zig-zag manoeuvre	57
5.7	Heading and rudder angles versus time for a turning circle	57
5.8	Speed versus time	58
5.9	Wind speed during a turning circle	59
5.10	Power consumption during a turning circle	60
5.11	Propeller rpm during a stopping test	60

5.12	Turning circle trajectory before and after rotation of trajectory	62
5.13	Rudder angles during a turning circle	63
5.14	Trajectory of a turning circle with points used to predict local current velocity are marked.	64
5.15	Presentation and explanation of turning circle results	65
5.16	Trajectory of a 10/10 zig-zag manoeuvre	68
5.17	Heading and rudder angles versus time in a zig-zag manoeuvre	68
6.1	Measured versus simulated turning circle results	84
6.2	Rudder angle's impact on turning circles with moderate rudder angles	86
6.3	Rudder angle's impact on turning circles with large rudder angles .	86
6.4	Distribution of $C_{cf}(x)$ given by SIMAN and Oltmann's polynomial	88
6.5	Measured versus simulated (using Oltmann's polynomial for $C_{cf}(x)$)	90
6.6	Trajectory of a zig-zag trial simulated using hydrodynamic coefficients predicted by Lee's method	93
6.7	Illustration of how advance varies depending on method used to calculate hydrodynamic coefficients	94
6.8	Illustration of how transfer varies depending on method used to calculate hydrodynamic coefficients	94
6.9	Illustration of how tactical diameter varies depending on method used to calculate hydrodynamic coefficients	95
7.1	Planar Motion Mechanism (PMM)	99
7.2	MARINTEK's multipurpose carriage	100

List of Tables

1.1	Main particulars of benchmarking models	10
2.1	Notation for forces and motions parameters in manoeuvring problems	14
4.1	Velocity derivatives calculated for R/V Gunnerus	47
4.2	Acceleration derivatives calculated for R/V Gunnerus	47
5.1	Parameters recorded by Seapath	50
5.2	Parameters recorded by the DP-system	52
5.3	Results and trial conditions for turning circles carried out 27/02/2012 with 2×425 kW	66
5.4	Results and trial conditions for turning circles carried out 27/02/2012 with 2×142 kW	66
5.5	Results and trial conditions for turning circles carried out 01/03/2012 with 2×425 kW	66
5.6	Results and trial conditions for turning circles carried out 01/03/2012 with 2×142 kW	67
5.7	Results and trial conditions for zig-zag manoeuvres	70
5.8	Results and trial conditions for stopping tests	72
6.1	Simulated turning circle results presented together with measured full-scale results	79
6.2	Simulated zig-zag results presented together with measured full- scale results	80
6.3	Simulated stopping test results presented together with measured full-scale results	81
6.4	Mean differences (%) between simulations and full-scale tests . . .	82
6.5	Hydrodynamic coefficients of R/V Gunnerus predicted by SIMAN	82
6.6	Rudder angle's impact on a turning circle manoeuvre	87
6.7	Mean difference (%) between measured and simulated results when the cross-flow drag coefficient is predicted by SIMAN and Oltmann	89

6.8	Results from zig-zag simulations with varying N_v	91
6.9	Results from zig-zag simulations with varying heading change and rudder angle	92
6.10	Results of zig-zag manoeuvre simulated hydrodynamic coefficients predicted by various methods	96
8.1	Mean difference (%) between measured and simulated turning circles when the cross-flow drag coefficient is predicted by SIMAN and Oltmann	102
8.2	Mean difference (%) between simulations and full-scale tests	102
A.3	w and t 's influence on turning circles with approach speed at 9.8 kn	XXVI
A.4	w and t 's influence on turning circles with approach speed at 9.8 kn	XXVI

Nomenclature

B	Ship's breadth
C_D	Drag coefficient
D	Drag force component
GM	Metacentric height
K	Roll moment
L	= L_{pp} = Ship's length between perpendiculars
L	Lift force component
M	Pitch moment
N	Yaw moment
N'_r	Coefficient for yaw damping
N'_v	Coefficient for yaw damping due to sway velocity
$N'_{\dot{r}}$	Coefficient for hydrodynamic mass moment of inertia in yaw
$N'_{\ddot{v}}$	Coefficient for hydrodynamic mass moment of inertia in yaw due to sway acceleration
Re	Reynolds number
T	Ship's draught
U	Speed of vessel
$U(x)$	Local speed of vessel = $\sqrt{U^2 + (v + xr)^2}$
X	Longitudinal force component
Y	Lateral force component
Y'_r	Coefficient for sway damping due to yaw velocity
Y'_v	Coefficient for sway damping
$Y'_{\dot{r}}$	Coefficient for hydrodynamic mass in sway due to yaw acceleration
$Y'_{\ddot{v}}$	Coefficient for hydrodynamic mass in sway
Z	Vertical force component

Δ	Vessel's weight displacement
Γ	Dihedral angle
β	Drift angle
δ	Rudder angle
∇	Vessel's volume displacement
ϕ	Roll angle
ψ	Heading angle
ρ	Fluid density
p	Roll rate of turning
q	Pitch rate of turning
r	Yaw rate of turning
u	Longitudinal velocity component
v	Lateral velocity component
w	Vertical velocity component

List of Abbreviations

SB	Starboard
PT	Port
AP	Aft perpendicular
FP	Fore perpendicular
DOF	Degree of freedom
MCR	Manufacturers Continuous Rating
IMO	International Maritime Organization
ITTC	International Towing Tank Conference
DP	Dynamic Positioning
CFD	Computational Fluid Dynamics
RANS	Reynolds-averaged Navier–Stokes

Chapter 1

Introduction

Manoeuvring performance is important for ship handling in confined waters. Adequate manoeuvring capability is important for the marine safety and protection of the marine environment. For these reasons International Maritime Organization (IMO) has approved regulations for manoeuvring performance of ships. IMO is a specialised agency of the United Nations, and its main purposes are related to safety and security of shipping, and prevention of marine pollutions by ships. IMO has defined manoeuvring tests which are used to describe the vessel's manoeuvring performance, and requirements that the vessel must fulfil [1]. All ships larger than 100 m, as well as all chemical tankers and gas carriers must fulfil the criteria defined by IMO.

Full-scale trials must be performed to confirm that the vessel satisfies the manoeuvring requirements. The vessel's main dimensions, hull form, speed and propulsion system affect the manoeuvrability, and are decided in the design stage. It is therefore a need to be able to investigate the vessel's manoeuvring capability at this stage. Today it exists several methods to calculate a vessel's manoeuvring performance. It is important that the methods are verified by physical full-scale experiments. A purpose of this study is therefore to perform field tests with NTNU's research vessel R/V Gunnerus. A ship motion model are created in MARINTEK's ship motion simulation tool SIMAN (ShipX Manoeuvring Plug-In). Results from the field tests are compared with results from simulations. Consequently, field test results can be used to improve the simulation tool. R/V Gunnerus has however a ship length of 28.9 m, and is therefore not required to satisfy the manoeuvring criteria stated by IMO. Nevertheless, it is of interest to identify the vessel's manoeuvring performance, and use the result to investigate how simulation tools predict the manoeuvring

performance of an unconventional vessel.

A lot of work regarding manoeuvring of ships is carried out by the International Towing Tank Conference (ITTC). The ITTC is a worldwide association of organisations dealing with prediction of hydrodynamic performance of ships and marine installations based on the results of physical and numerical modeling [2]. The committee is split into many subgroups dealing with their special subject. The manoeuvring committee updates state-of-the-art predictions of manoeuvring characteristic of vessels, reviews IMO procedures and identifies requirements for benchmarking models.

This master's thesis has its origin in the project thesis [3] written autumn 2011. An introduction to ship manoeuvring, as well as initial manoeuvring simulations using SIMAN and VeSim were presented in the project thesis. Simulations in VeSim have however not been performed in the master's thesis due to technical issues and time constraints, but an initial model was established in the project thesis. It has been focused on analysing full-scale trials well and establishing a good model in SIMAN before simulations in VeSim are performed.

In this chapter follows a summary of the introduction to ship manoeuvring presented in the project thesis. Finally, the thesis organisation is presented.

1.1 Ship manoeuvring

1.1.1 Manoeuvring characteristics

The manoeuvring characteristics given by IMO can describe the performance quality and handling ability of a ship [4].

Inherent dynamic stability/straight line stability: If a ship is exposed to a small disturbance, and it afterwards settles on a new straight course without any corrective rudder, then it is said to be dynamically stable on a straight course. The deviation from the original heading is affected by the degree of inherent stability and the magnitude and duration of the disturbance affect.

Course-keeping ability: The course-keeping ability measures a steered vessel's ability to keep a straight path in a predetermined course without use of corrective

rudder. However, if the ship has a small inherent dynamic instability, reasonable course control is accepted.

Initial turning/course-changing ability: The vessel's change-of-heading response to a moderate helm is its course-changing ability. This may be measured as the heading deviation per unit sailed or the distance sailed before a given heading deviation (for instance time to second execute in a zig-zag manoeuvre).

Yaw checking ability: The vessel's response to counter-rudder applied in a certain state of turning is the ship's yaw checking ability. In a zig-zag manoeuvre this may be the heading overshoot reached before the yawing tendency has been cancelled by the counter-rudder.

Turning ability: Turning ability describes the vessel's ability to turn using hard-over rudder. The results may be given as minimum advance or tactical diameter which are found by performing a turning circle manoeuvre.

Stopping ability: Stopping ability is found by measuring the track reach and time to dead in water in a stopping manoeuvre.

1.1.2 Required manoeuvring tests

IMO has defined three required manoeuvring tests, which are commonly referred to as the Standards [4]. The Standards investigate a vessel's manoeuvring characteristics. A turning circle manoeuvre can be used to identify the vessel's turning ability, while course-keeping ability and initial turning/course-changing ability are investigated in a zig-zag manoeuvre and a vessel's stopping ability can be predicted in a stopping test.

Turning circle manoeuvre

A turning circle is performed by obtaining a steady heading and test speed, and then apply a 35° rudder angle (or the maximum allowable rudder angle). The test is complete when a 360° change of heading is obtained. The essential information

to get from this test is tactical diameter, advance and transfer, see Figure 1.1. Transfer is transfer at 90° change of heading, while tactical diameter is transfer at 180° change of heading. Advance is the distance travelled along original heading until the vessel has turned 90° .

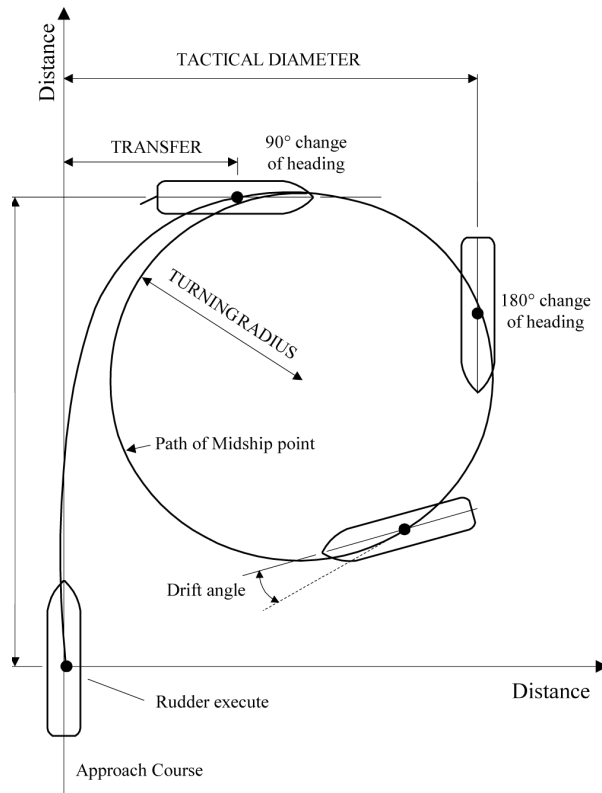


Figure 1.1: Turning circle test [5]

Zig-zag manoeuvre

A zig-zag manoeuvre is performed by obtaining a steady, straight course and then apply a certain rudder angle (first execute). As a given deviation from the vessel's originally course is reached, the rudder angle is shifted (second execute). The vessel will continue yawing in the original direction, but with a decreasing yaw rate. Finally the yaw rate changes sign and the vessel yaws in the same direction as the rudder. The procedure should be repeated until the vessel has

crossed the base course at least two times. The Standards include two zig-zag tests; $10^\circ/10^\circ$ and $20^\circ/20^\circ$. The $10^\circ/10^\circ$ test uses a 10° rudder angle and 10° deviation from the originally heading, while the $20^\circ/20^\circ$ test uses values of 20. The essential information from these manoeuvres is the overshoot angles, time before first counter rudder and time from first (second) counter rudder to first (second) overshoot angle, see Figure 1.2. Overshoot angle is the difference between maximum course change and course change when the rudder is shifted. Time before first counter rudder is the time from first execute to second execute.

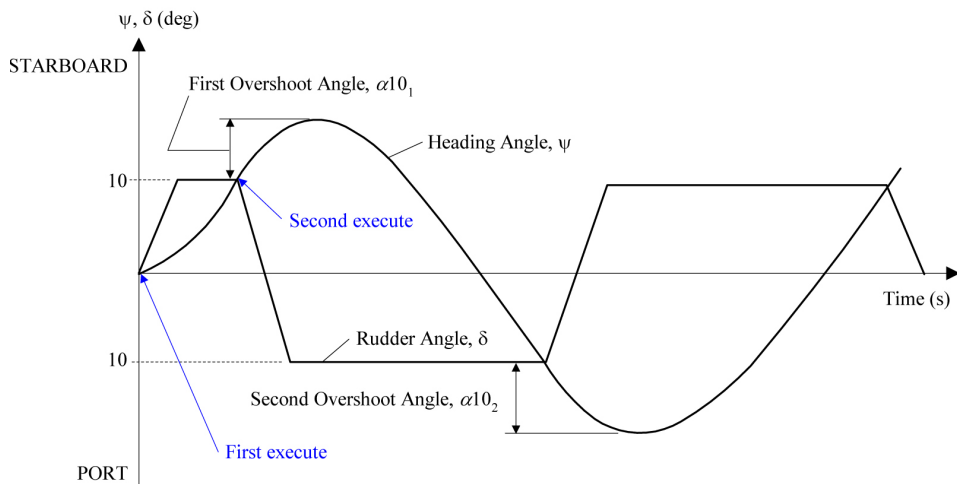


Figure 1.2: 10/10 zig-zag test [5]

Stopping test

A stopping test is performed by obtaining the test speed followed by a full astern stopping order. The rudder should be kept in midship position during the trial. The test is complete when the vessel speed is zero. The essential information from this test is head reach, track reach and lateral deviation, see Figure 1.3. Head reach is the distance travelled in the direction of the vessel's initial course, while lateral deviation is the distance travelled normal to the vessel's initial course. Track reach is the total distance measured along the ship's path.

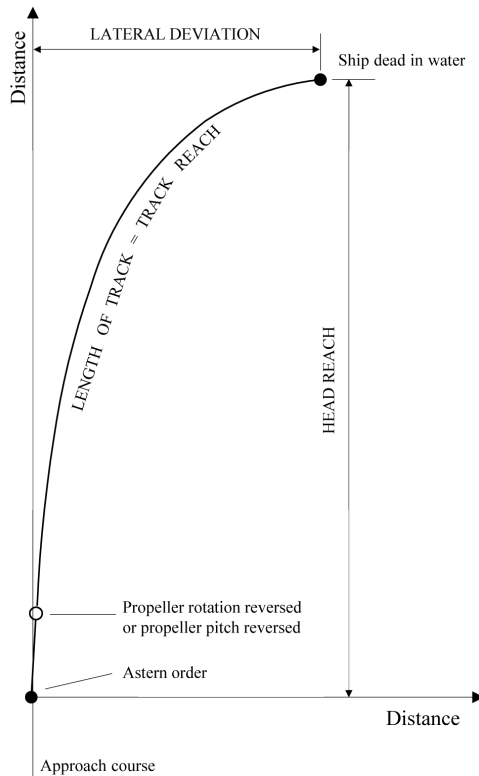


Figure 1.3: Stopping test [5]

Test conditions

The manoeuvring tests should be conducted to both port and starboard under the following conditions [4]:

- deep, unrestricted waters;
- calm environment;
- full load, even keel condition;
- steady approach at the test speed and
- the test speed should be at least 90 % of the vessel's maximum speed.

Comments to the IMO Standards

The Standards are based on experience of conventional vessels with traditional propulsion and steering system, mainly tankers and bulk carriers [6]. As the Standards are based on experience of conventional ship but also used for non-conventional ships, they must be continuously reviewed.

The manoeuvring trials should be performed in a fully-loaded condition. This is however not always practical, especially for dry cargo ships as the change of loading condition affects the manoeuvring performance. Kose stated that for some vessels the directional stability on even keel is worse than in a fully loaded condition [7].

A shortcoming of the Standards expressed by Dand is that the Standards are for deep water and design speed only, which do not consider manoeuvring in ports and other low-speed manoeuvring situations [6].

1.2 Manoeuvring prediction methods

The methods used to predict ship manoeuvring performance can be split into three main categories:

- database methods;
- free model tests and
- numerical simulation of manoeuvring motions.

The database method can be used when manoeuvring parameters are provided from many full-scale trials and free model tests. The manoeuvring performance of the designing vessel can then be predicted based on the database without performing simulations. It is not recommended to use this method unless the designing ship is closely similar to the vessels in the database.

Free model tests can be performed when there is a lack of close similarity between the designing ship and the vessels in the database. These tests give a close reflection of reality, but do not give physical insight in why the vessels manoeuvres the way they do. Free model tests do not give any direct information that can be used for simulations, but they can be used in validations of simulations. When free model tests are performed it is important to consider scale effects.

Numerical simulations of manoeuvring motions is a very useful method to describe a vessel's manoeuvring performance in the design stage. In this case the hydrodynamic forces acting on a vessel must be predicted accurately. The hydrodynamic forces can be obtained by model tests, theoretical calculations (for instance slender body theory or CFD) or empirical methods. CFD (Computational Fluid Dynamics)-methods simulate viscous flow. The most common CFD-method in ship manoeuvring is to use RANS (Reynolds-averaged Navier-Stokes)-calculations. Using CFD gives physical insight in why a ship manoeuvres as it does, and it can also provide information about the flow around the vessel, which would lead to a greater understanding of the manoeuvre. CFD-methods is in development and it is necessary to gain more experience in how the settings in the RANS solvers affect the results. The demand of large computer resources may limit the use of this method. In the design stage it is desired to get a quick prediction of the manoeuvring performance, which can be obtained using empirical methods. The empirical methods use dedicated mathematical models and manoeuvring coefficients. The hydrodynamic coefficients are found using empirical methods or a combination of empiricism and theory. Advantages of using empirical methods are low cost and quick results. In addition depending on mathematical model, they can be used to simulate many manoeuvres. It is underlined that empirical methods are often only applicable for ships similar to the vessels the method is based upon.

1.3 Benchmarking models

Benchmarking models should be used in order to validate manoeuvring prediction methods. However, there is a lack of reliable and well-documented full-scale results of ship manoeuvres that can be used as benchmarking models. Possible reason may be that traditionally manoeuvring performance has had less priority than resistance and propulsion performance. It may also be due to the fact that manoeuvring is a complex process, as the process is unsteady and have parameters (for instance speed and position vectors, propeller rpm and rudder angles) that evolve in time. In addition the vessel is a complex non-linear system. This implies that there has to be strict requirements to the benchmarking test regarding execution and documentation.

A benchmarking model should include:

- full ship documentation, i.e. necessary information regarding lines, engine, propeller, superstructure and

- accurate full-scale trial results.

It is difficult to get access to full ship documentation as such is often classified as confidential information by the ship owner or shipyard. Full-scale trials are conducted outdoor and there are often challenges related to the requirement of calm deep water condition with no current.

In 1979 Crane carefully performed full-scale trials in shallow and deep water with the tanker Esso Osaka ($L_{pp} = 325\text{ m}$, $B = 53\text{ m}$). Esso Osaka has been dominating throughout the years, and much research have used this vessel. Following argument for not using Esso Osaka as a benchmarking model have been expressed:

- Esso Osaka has an old ship design;
- the benchmarking model covers only one ship type and
- there is a lack of propulsion data, which is important for CFD purposes.

For this reasons there has been a request for new benchmarking models with more modern hull form and that cover various ship types. It is however desired to have a limited number of benchmarking models. When the research uses similar benchmark ships it is easier to compare the manoeuvring prediction methods. The Manoeuvring Committee recommends following ship to be used as benchmarking models:

- MOERI KVLCC1 and KVLCC2 Tankers;
- MOERI KCS Container Ship and
- US Navy Combatant TMB 5415.

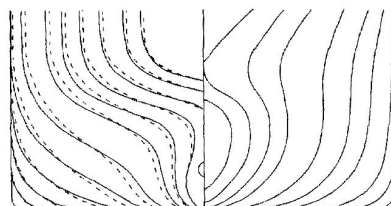


Figure 1.4: Body plan of the benchmarking models KVLCC1 and KVLCC2. Solid line is KVLCC1 and dashed line is KVLCC2 [8].

The MOERI KVLCC Tankers are two tankers with similar main particulars, but

they have different stern shapes, see Figure 1.4. KVLCC1 has a V-shaped stern, while KVLCC2 has a more U-shaped stern. Using these models the manoeuvring performance of two vessels with almost identical main characteristics can be investigated. The full-scale characteristics of the benchmarking models are given in Table 1.1.

Table 1.1: Main particulars of benchmarking models [8]

		KVLCC1	KVLCC2	Container ship	US Navy Combatant
Length	[m]	320	320	320	142
Beam	[m]	58.0	58.0	32.2	19.06
Draught	[m]	20.8	20.8	10.8	6.15
Block coefficient	[‐]	0.8109	0.8098	0.651	0.507

These benchmarking models have modern hull shape. Lines, rudder and propeller documentation as well as results from PMM and free model tests are available. They exist in model scale, but will never be built in full-scale. The Manoeuvring Committee has recommended these vessels as benchmarking models even though full-scale trials never will be conducted.

The development of the new benchmarking models has been in connection with Workshop on Verification and Validation of Ship Manoeuvring Simulation Methods, SIMMAN 2008. The purpose of the workshop was to benchmark the capabilities of various ship manoeuvring simulations using the benchmarking models suggested by the Manoeuvring Committee. A new SIMMAN workshop is planned in 2012.

1.4 Thesis organisation

Chapter 2 starts by defining several reference frames. Further, a description of how hydrodynamic forces in a manoeuvring problem can be modelled using a combination of mathematical and empirical approaches is provided.

Chapter 3 presents two mathematical models that describe calm water manoeuvring. The first model is a linear 3-DOF model derived from Newton's second law, while the other model is a 4-DOF model using an Euler-Lagrangian approach. The relevant motions in calm water manoeuvring are surge, sway, yaw and roll. Roll is neglected in the 3-DOF model, which is acceptable for vessels

with large GM . SIMAN uses a 3-DOF model, while VeSim uses a 6-DOF model. The 4-DOF model describes the principle used in the 6-DOF model used in VeSim.

Chapter 4 contains various approaches to calculate hydrodynamic coefficients. Slender body theory is presented as well as several empirical methods. The approaches are used to calculate hydrodynamic coefficients of R/V Gunnerus.

Chapter 5 deals with full-scale manoeuvring trials of R/V Gunnerus. The trial instrumentation and data registration are evaluated, and turning circles, zig-zag tests and stopping tests are analysed. Some other manoeuvres were also carried out, but these are not analysed in this thesis due to time constraints. Besides, it is assumed that these three manoeuvres provide enough information to evaluate the ship motion model created in SIMaN in this study.

Chapter 6 uses the Ship Manoeuvring-Plug-In in ShipX (SIMAN) to simulate the field manoeuvres of R/V Gunnerus. The results from the simulations did not agree with the full-scale field results, and possible reasons for that are studied. Further, the hydrodynamic coefficients predicted in Chapter 4 are used in manoeuvring simulations. This is done to investigate whether using these coefficient may improve the simulation tool.

Chapter 7 assesses whether R/V Gunnerus can be used as a case vessel to investigate validity of numerical simulation models. The need for a case vessel is discussed and recommended trials are stated.

Chapter 2

Forces on a vessel

2.1 Reference frames

The equations of motion can be derived in several reference frames. However, in certain problems some axis systems are more commonly used than others. In manoeuvring problems a body-fixed frame is a natural choice, but it is also of interest to know how other reference frames are defined. The reference frames used in this study are defined according to notation used by Ross [9] and Fossen [10].

2.1.1 Earth Centered Inertial

The Earth Centred Inertial (ECI) frame, also called $\{i\}$ -frame of reference, has its origin in the centre of the Earth. The frame is fixed in space and given by $\{i\} = \{o_i, \vec{x}_i \, \vec{y}_i \, \vec{z}_i\}$, see Figure 2.1. This frame is used in Newton's laws of motions.

2.1.2 Earth Centred Earth Fixed

The Earth Centred Earth Fixed (ECEF) frame, $\{e\}$ -frame, has its origin in the centre of the Earth. In contrast to the ECI-frame the axes in this frame will rotate. The z-axis rotates with the rotational velocity of the Earth. Consequently is the location time-invariant. The ECEF-frame is defined as $\{e\} = \{o_e, \vec{x}_e, \vec{y}_e, \vec{z}_i\}$, see Figure 2.1.

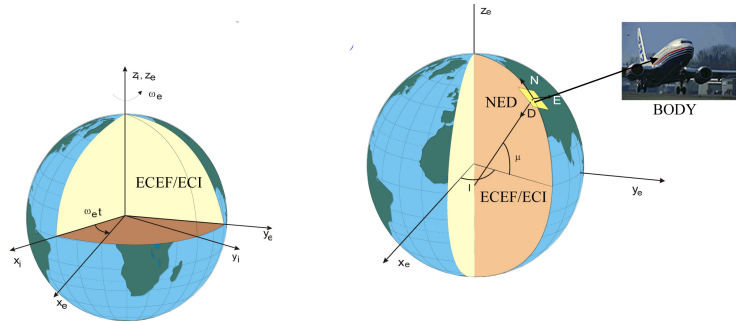


Figure 2.1: Reference frames [11]

2.1.3 North-East-Down

A North-East-Down (NED) frame, $\{n\}$ -frame, is defined relative to the Earth's reference ellipsoid. This is defined according to the World Geodetic System (WGS84), which for instance GPS is based upon. The NED-frame is given by $\{n\} = \{o_n, \vec{x}_n, \vec{y}_n, \vec{z}_n\}$, where \vec{x}_n is the position on the northern axis and \vec{z}_n points downwards against the origin ECEF-frame. In order to comply with the right-hand rule must \vec{y}_n points against east, see Figure 2.1.

2.1.4 Body-fixed

A body-fixed frame, $\{b\}$ -frame, moves with the specified body. In manoeuvring problems the body-fixed axis system has typically its origin where the vessel's mid ship section and the x-y-plane coincide with the calm waterplane. This body-fixed frame is given by $\{b\} = \{o_b, \vec{x}_b, \vec{y}_b, \vec{z}_b\}$, where \vec{x}_b is set positive towards the bow of the vessel, \vec{y}_b towards starboard and \vec{z}_b points downward in order to fulfil the right-hand rule, see Figure 2.2.

The body-fixed frame moves and rotates relative to the NED-frame, which is expressed by:

$$\boldsymbol{\eta} = [n, e, d, \phi, \theta, \psi]^T. \quad (2.1)$$

Further, the $\boldsymbol{\eta}$ -vector can be divided into following translation and rotational components:

$$\begin{aligned} \mathbf{p}^n &= [n, e, d]^T \\ \boldsymbol{\theta} &= [\phi, \theta, \psi]^T, \end{aligned} \quad (2.2)$$

where (n, e, d) are north, east and down position vectors, while (ϕ, θ, ψ) express

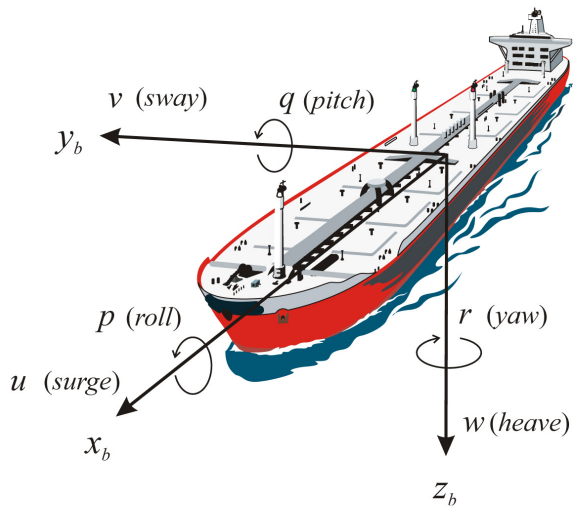


Figure 2.2: Body-fixed axis system used in manoeuvring problems [11]

roll, pitch and yaw angles. The body-fixed velocities are defined as the velocities of the $\{b\}$ -frame relative to the $\{n\}$ -frame and expressed in the $\{b\}$ -frame as:

$$\boldsymbol{\nu} = [u, v, w, p, q, r]^T, \quad (2.3)$$

where u, v, w, p, q, r are the velocities in surge, sway, heave, roll, pitch and yaw respectively.

The nomenclature used in manoeuvring models follows SNAME and ITTC Standards. Forces, moments and motion parameters are defined in Table 2.1 and Figure 2.2.

Table 2.1: Notation for forces and motions parameters in manoeuvring problems

DOF	Motion type		Forces and moments	Linear and angular velocities	Position and Euler angles
1	Linear x-axis	Surge	X	u	x
2	Linear y-axis	Sway	Y	v	y
3	Linear z-axis	Heave	Z	w	z
4	Rotation about x-axis	Roll	K	p	ϕ
5	Rotation about y-axis	Pitch	M	q	θ
6	Rotation about z-axis	Yaw	N	r	ψ

2.1.5 Flow axes

The flow axes, $\{f\}$ -frame, are defined by a body's velocity through a fluid. $\{f\}$ -frame is given by $\{f\} = \{o_f, \vec{x}_f, \vec{y}_f, \vec{z}_f\}$. The flow axes are found by rotating the body-fixed axis system, and it is therefore practical to collocate the origin, o_f , with the body-fixed origin, o_b . \vec{x}_f is defined to point directly into the relative flow, while \vec{z}_f is rotated to be perpendicular to \vec{x}_f . \vec{y}_f must be set to fulfil the right-hand rule.

Flow axes are often used when hydrodynamic forces are calculated as lift is defined perpendicular to the relative flow and drag acts parallel to the flow.

2.2 Course-, heading- and drift angle

Course, heading and drift angles are important parameters used in manoeuvring problems.

Course angle χ : The course angle is defined as the angle from the x_n axis in the NED-frame to the velocity vector U of the vessel, see Figure 2.3. The angle has a positive rotation about z_n according to the right-hand screw rule.

Heading (yaw) angle ψ : The heading angle is defined as the angle from the x_n axis in the NED-frame to the x_b axis in the body-fixed frame, see Figure 2.3. The angle has a positive rotation about z_n according to the right-hand screw rule.

Drift (slideslip) angle β : The drift angle is defined from the x_b axis in the body-fixed frame to the velocity vector U of the vessel, see Figure 2.3. The angle's rotation is set positive about the z_b axis according to the right-hand screw convention.

It is necessary to notice that the drift angle in some cases is defined as::

$$\beta = -\beta. \quad (2.4)$$

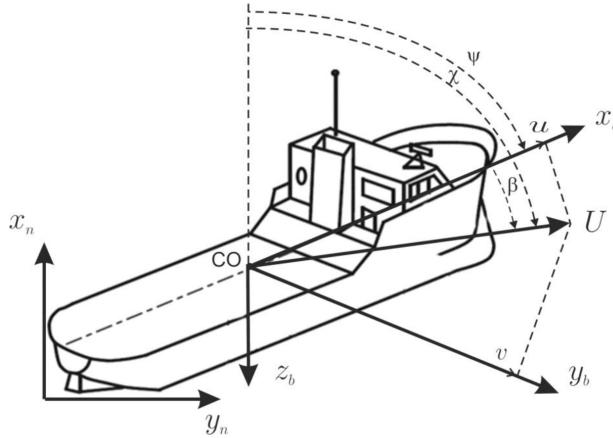


Figure 2.3: Definition of course-, heading- and sideslip angle [10]

2.3 Forces

A vessel's motions during manoeuvring are a result of the balance between the ship's inertia forces and the forces from the water at the hull, control forces and forces from current, wind and waves. The approach used in this chapter to describe the forces on a vessel during manoeuvring is based on "Chapter 4 Forces" in Andrew Ross' Doctoral Theses "Nonlinear Manoeuvring Models for Ships" [9]. Below follows a brief review of forces acting on a vessel during manoeuvring.

Inertial pressure forces: When a vessel is moving the fluid particles close to the hull will be given an accelerated motion that require forces [12]. These forces are typically called added mass and are pressure forces that act in proportion to the acceleration through the fluid.

Potential damping: These are pressure generated damping forces caused by effects from potential flow, i.e. flow in an ideal fluid without friction. When a vessel passes through a fluid, a net force which opposes the motion is created. This is due to a pressure increase in front of the motion and a decrease behind.

Friction: This is a viscous damping force caused by friction between the fluid and the underwater hull as the fluid passes underneath and around the hull.

Vortex shedding: This is also called interference drag and is formed by vortex shedding at sharp edges and consequently creation of vortex sheets.

Lifting forces: Hydrodynamic lift is caused by a pressure difference between upper and lower side of the vessel, and it arises from two physical mechanisms. The first pressure difference causing the lift is related to linear circulation of water around the hull. The other one is cross-flow drag which is a non-linear effect. This drag acts from a momentum transfer from the body to the fluid and it is related to vortex shedding.

Restoring forces: These forces arise from buoyancy, which opposes the vessel's weight and act in the opposite direction as gravity.

Control forces: These forces are created by control surfaces such as rudders or fins, and as propulsive forces from propeller or water jet.

Current forces: A vessel's velocity is normally defined relatively to the seabed. If the sea moves relatively to this fixed point, the difference between them is seen as current forces.

Wind forces: Wind is the flow of air above the Earth's surface, and it creates forces on the superstructure of the vessel.

The hydrodynamic forces on the underwater hull can also be divided in following categories:

- Acceleration dependent forces, i.e. forces related to acceleration of fluid particles.
- Linear dependent forces, i.e. forces that are directly proportional to the velocity of the fluid.
- Non-linear dependent forces, i.e. forces that are proportional to the square or higher order of the velocity of the fluid.

The hydrodynamic forces may be modelled by various methods; for instance using a purely mathematical approach, a purely empirical approach or a purely computational approach. In this chapter the forces are described using a

combination of mathematical and empirical approaches. A description of the hydrodynamic forces, which are related to the first six forces stated above, is provided in this chapter.

2.4 Damping forces

A generic force for a body moving in the free surface of a fluid can generally be written as:

$$F = \frac{1}{2} \rho U^2 S C_F, \quad (2.5)$$

where ρ is fluid density, U is the vessel's speed, S is wetted surface area and C_F is a non-dimensional force coefficient.

Even though the equation is quite simple it is misleading. The wetted surface, S , will not be constant, but vary with the vessel's velocity. This is due to the fact that the wave profile along the ship depends on forward speed, mass distribution and geometry of the vessel. The vessel's speed, U , during manoeuvring varies across the length of the body. It is therefore impractical to use speed only at a single location. The local speed in surge, sway and yaw is given as:

$$U(x) = \sqrt{U^2 + (v + xr)^2}, \quad (2.6)$$

where U is the vessel's speed, v is lateral velocity, r is yaw rate of turning and x is the position along the vessel where the local speed is calculated.

The force coefficient, C_F , is an unknown function which is dependent on other non-dimensional parameters, such as Reynolds number, Froude number or drift angle.

The mentioned points illustrate that it is difficult to model the damping. For this reason the purpose of this chapter is to give a physical description of the forces and derive a structure of the forces, rather than to present specific numbers or formulas. To be able to do so, linear superposition of the damping forces is accepted. Hence, lift, drag, cross-flow drag and other forces can be investigated independently and included in the equations of motion.

2.5 Circulatory lift and drag

A ship can be modelled as a low aspect ratio wing turned on its side. Then the chord is set as ship length and the span is set twice the draught, see Figure 2.4. In

context with manoeuvring, drag and lift refers to forces in the horizontal plane. Lift acts perpendicular to the direction of the motion, while drag acts parallel and opposes the motion, see Figure 2.5. The lift and drag may be expressed respectively as:

$$L = \frac{1}{2} \rho U^2 S C_L(\beta, Re), \quad (2.7)$$

$$D = \frac{1}{2} \rho U^2 S C_D(\beta, Re), \quad (2.8)$$

where S is characteristic area such as Lpp^2 , C_L is non-dimensional lift coefficient, C_D is non-dimensional drag coefficient, β is drift angle and Re is Reynolds number.

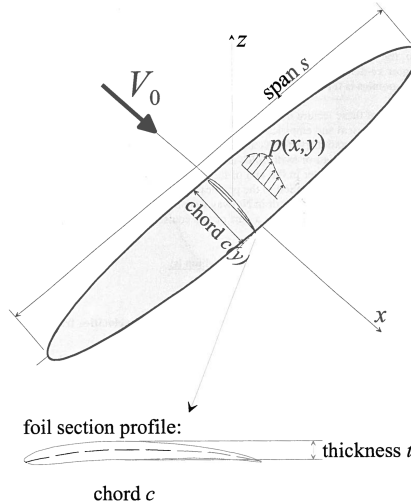


Figure 2.4: Definition of parameters in a 2D-foil [13]

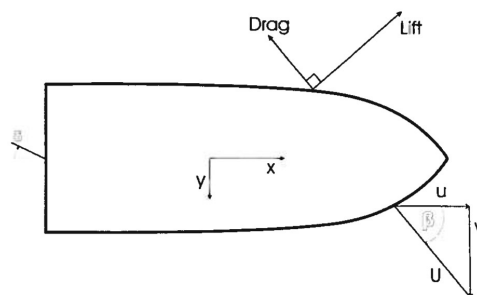


Figure 2.5: Lift and drag forces on a vessel [9]

The lift and drag act in the flow axes and must be converted according to the body fixed axis system using the following transformation matrix:

$$\begin{bmatrix} X_{LD} \\ Y_{LD} \end{bmatrix} = \begin{bmatrix} -\cos(\beta) & \sin(\beta) \\ -\sin(\beta) & -\cos(\beta) \end{bmatrix} \begin{bmatrix} D \\ L \end{bmatrix}. \quad (2.9)$$

Further, the moments are given as:

$$\begin{bmatrix} K_{LD} \\ N_{LD} \end{bmatrix} = \begin{bmatrix} z_{cp} \\ x_{cp} \end{bmatrix} \cdot Y_{LP}, \quad (2.10)$$

where (x_{cp}, z_{cp}) express the location of the vessel's centre of pressure. The drift angle, β , is defined as:

$$\beta = \arctan\left(\frac{v}{u}\right) = \arccos\left(\frac{u}{U}\right) = \arcsin\left(\frac{v}{U}\right). \quad (2.11)$$

The local lift and drag is integrated over the ship length to find the total 3D forces.

2.5.1 Lift

The lift coefficient may be given as:

$$C_L = C_{L\beta} \sin \beta, \quad (2.12)$$

where $C_{L\beta}$ is a constant of proportionality.

The lift includes the drift angle and is therefore a function of longitudinal position and expressed as:

$$\begin{aligned} C_L(x) &= C_{L\beta} \sin \beta(x) \\ &= C_{L\beta} \sin \left(\arcsin \left(\frac{v + xr}{U(x)} \right) \right) \\ &= C_{L\beta} \frac{v + xr}{U(x)}. \end{aligned} \quad (2.13)$$

Equation (2.13) inserted in equation (2.7) gives:

$$\begin{aligned} L(x) &= \frac{1}{2} \rho U(x)^2 S C_L(x) \\ &= \frac{1}{2} \rho U(x) S (v + xr). \end{aligned} \quad (2.14)$$

Using the transformation matrix in equation (2.9), the force may be resolved in the longitudinal direction as:

$$\begin{aligned} X_L(x) &= L(x) \sin(\beta(x)) \\ &= L(x) \frac{v + xr}{U(x)} \\ &= \frac{1}{2} \rho S C_{L\beta} (v + xr)^2. \end{aligned} \quad (2.15)$$

Integrating over the ship length gives the total longitudinal force as:

$$\begin{aligned} X_L &= \int_0^{L_{pp}} X_L(x) dx = \int_0^{L_{pp}} \frac{1}{2} \rho S C_{L\beta} dx \\ &= \frac{1}{2} \rho S C_{L\beta} \frac{1}{3r} (v + L_{pp}r)^3 \\ &= \frac{1}{2} \rho S C_{L\beta} \frac{1}{3r} (3v^2 L_{pp}r + 3v L_{pp}^2 r^2 + L_{pp}^3 r^3) \\ &= \frac{1}{2 \cdot 3} \rho S C_{L\beta} (3v^2 L_{pp} + 3v L_{pp}^2 r + L_{pp}^3 r^2) \\ &= X_{vv} v^2 + X_{rv} rv + X_{rr} r^2, \end{aligned} \quad (2.16)$$

where X_{ij} is a non-linear longitudinal force component, which gives a contribution to the force and is proportional to ij .

The lift is resolved in the transverse direction as:

$$\begin{aligned} Y_L(x) &= -L(x) \cos(\beta(x)) \\ &= -L(x) \frac{u}{U(x)} \\ &= -\frac{1}{2} \rho S C_{L\beta} (uv + uxr). \end{aligned} \quad (2.17)$$

Integrating over the ship length gives the transverse force as:

$$\begin{aligned} Y_L &= \int_0^{L_{pp}} Y_L(x) dx \\ &= -\frac{1}{2} \rho S C_{L\beta} \left(uv L_{pp} + \frac{1}{2} ur L_{pp}^2 \right) \\ &= Y_{uv} uv + Y_{ur} ur. \end{aligned} \quad (2.18)$$

2.5.2 Drag

The drag force acts in opposite direction of the motion, and can be modelled using various techniques. In very slow speed manoeuvring linear modelling is

necessary and sufficient, while higher order terms are necessary for operation in higher speed.

Hoerner and Borst expressed the drag coefficient as:

$$C_D = C_{D0} + C_{D\beta\beta} \sin^2 \beta, \quad (2.19)$$

where C_{D0} is a dimensionless drag coefficient at 0° angle of side slip and $C_{D\beta\beta}$ describes the induced drag proportional to $\sin^2 \beta$.

According to Lewis C_{D0} can in pure surge motion be predicted using the ITTC drag formula:

$$X_{ITTC} = -\frac{1}{2}\rho S(1+k)(c_f + \Delta C_f)|u|u \quad (2.20)$$

$$\Rightarrow C_{D0} = (1+k)(C_f + \Delta C_f), \quad (2.21)$$

where k is a form factor, S is wetted surface area, C_f is flat plate friction from the ITTC-1957 line and ΔC_f is a hull roughness parameter.

In the formula for the drag coefficient as a function of x , a term that acts linearly with the total speed should be included as:

$$\begin{aligned} C_D(x) &= C_{D0} + C_{DU}U(x) + C_{D\beta\beta} \sin^2 \beta(x) \\ &= C_{D0} + C_{DU}U(x) + C_{D\beta\beta} \left(\frac{v + xr}{U(x)} \right)^2. \end{aligned} \quad (2.22)$$

Notice that the drag coefficient C_{DU} has the dimension *time/length* and varies linearly with Reynold's number. Further, the drag force may be expressed as:

$$\begin{aligned} D(x) &= \frac{1}{2}\rho S U(x)^2 C_D(Re, \beta) \\ &= \frac{1}{2}\rho S U(x)^2 \left(C_{D0} + C_{DU}U(x) + C_{D\beta\beta} \left(\frac{v + xr}{U(x)} \right)^2 \right) \\ &= \frac{1}{2}\rho S \left(C_{D0}U(x)^2 + C_{DU}U(x)^3 + C_{D\beta\beta}(v + xr)^2 \right). \end{aligned} \quad (2.23)$$

By combining equation (2.6), (2.9) and (2.23) the drag force in X-direction is

given by:

$$\begin{aligned}
 X_D(x) &= -D(x) \cos \beta(x) = -D(x) \frac{u}{U(x)} \\
 &= -\frac{1}{2} \rho S \left(C_{D0} U(x) u + C_{DU} U(x)^2 u + C_{D\beta\beta} \frac{u}{U(x)} (v + xr)^2 \right) \quad (2.24) \\
 &\cong -\frac{1}{2} \rho S C_{D0} u^2 + C_{DU} u^3 + C_{DU} u v^2 + C_{DU} u x^2 r^2 \\
 &\quad + 2C_{DU} x r u v + C_{D\beta\beta} v^2 + 2v x r + x^2 r^2),
 \end{aligned}$$

Integrating (2.24) over the ship length gives:

$$X_D = X_{uu} u^2 + X_{uuu} u^3 + X_{uvv} u v^2 + X_{urr} u r^2 + X_{urv} u r v + X_{vr} v r + X_{rrr} r^2. \quad (2.25)$$

In sway this drag force is expressed as:

$$\begin{aligned}
 Y_D(x) &= -D(x) \sin \beta(x) \\
 &= -D(x) \frac{v + xr}{U(x)} \\
 &= -\frac{1}{2} \rho S \left(U(x) (v + xr) C_{D0} + U(x)^2 C_{DU} (v + xr) + C_{D\beta\beta} \frac{(v + xr)^3}{U(x)} \right) \\
 &= -\frac{1}{2} \rho S \left((uv + ux r) C_{D0} + U(x)^2 C_{DU} (v + xr) + C_{D\beta\beta} \frac{(v + xr)^3}{U(x)} \right). \quad (2.26)
 \end{aligned}$$

In high speed manoeuvring is usually $U(x) \gg (v + xr)^3$ and the terms with $C_{D\beta\beta}$ may be neglected. This assumption is reasonable for slow speed manoeuvring also, as the side force then is dominated by lower order terms. Hence, the sectional side force is given by:

$$Y_D(x) \cong -\frac{1}{2} \rho S \left(C_{D0} (uv + ux r) + C_{DU} \left(u^2 v + u^2 x r + (v + xr)^3 \right) \right) \quad (2.27)$$

$$\Rightarrow Y_D = Y_{uv} u v + Y_{ur} u r + Y_{uuv} u^2 v + Y_{uur} u^2 r + Y_{rrr} r^3 + Y_{rrv} r^2 v + Y_{rvv} r^2 v + Y_{vvv} v^3. \quad (2.28)$$

2.5.3 Low-speed drag

In low speed manoeuvring, the drag force should be supplemented with a linear component that dominates near $u = 0$ m/s. This linear component will decrease

as u increases, and higher order terms will start to dominate instead. A linear term may be expressed as:

$$D_l = D_U \exp(-aU)U, \quad (2.29)$$

where a is set as $\approx \frac{1}{2}$ to describe the transition between linear and non-linear regimes. The low-speed drag force should be directly implemented in the total drag force as a low-speed drag coefficient will have singularity when $u = 0$.

2.6 Non-linear lift (Cross-flow drag)

In the previous section lift and drag due to circulatory effects were described. Since the ship hull is considered as a low aspect ratio wing, an additional lift component must be considered. This lift component is related to an induced drag term.

Hoerner and Borst stated that in order to have an infinitely long ship there can not be any circulation [9]. For an infinitely long ship there is a lack of leading- and trailing edge. Consequently, there is nothing for the water to circulate about. Nevertheless, a lift caused by deflection of water and momentum transfer to the water is present. According to Hoerner and Borst this is due to the presence of a pair vortex sheets around the lateral edges of a wing. For a vessel this will correspond to a single vortex sheet that curls vertically around the bottom of the hull, see Figure 2.6. It may be natural to assume that these vortices curl horizontally at the bow and stern, but this is not the case for an infinitely long ship. Instead is a cross-flow drag present.

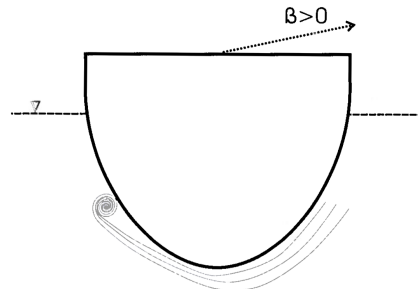


Figure 2.6: Non-linear flow underneath hull [9]

The cross-flow principle can be used to predict the cross-flow coefficients. The

principle assumes that the viscous drag is influenced exclusively by the sway velocity across the hull.

The transverse sectional cross-flow force acting on a vessel may be expressed as:

$$Y_{cf} = \frac{1}{2}\rho \int_0^{Lpp} U(x)^2 C_{cf}(x) T(x) dx, \quad (2.30)$$

where C_{cf} is a cross-flow drag coefficient and $T(x)$ is the local draught.

It is common to express the cross-flow coefficient, C_{cf} , as asymmetric about the sideslip angle β . Two definitions are typically used, either $C_{cf}(x) = C_{cf} \sin \beta(x) |\sin \beta(x)|$ or $C_{cf}(x) = C_{cf} \sin^3 \beta(x)$. Using the first expression give the cross-flow force and moments as:

$$\begin{aligned} Y_{cf} &= \frac{1}{2}\rho \int_0^{Lpp} U(x)^2 C_{cf}(x) \sin \beta(x) |\sin \beta(x)| T(x) dx \\ &= \frac{1}{2}\rho C_{cf} \int_0^{Lpp} (v + xr) |v + xr| T(x) dx, \end{aligned} \quad (2.31)$$

$$K_{cf} = \frac{1}{2}\rho C_{cf} \int_0^{Lpp} z_{cp}(x) (v + xr) |v + xr| T(x) dx \quad (2.32)$$

$$N_{cf} = \frac{1}{2}\rho C_{cf} \int_0^{Lpp} x(x) (v + xr) |v + xr| T(x) dx \quad (2.33)$$

where $z_{cp}(x)$ is the vertical centre of pressure as a function of longitudinal position.

According to Norrbin the cross-flow drag given in (2.31), (2.32) and 2.33) may be approximated using quadratic damping terms in modulus form as [9]:

$$Y_{cf} \cong Y_{|v|v}|v|v + Y_{|r|v}|r|v + Y_{|v|r}|v|r + Y_{|r|r}|r|r \quad (2.34)$$

$$K_{cf} \cong K_{|v|v}|v|v + K_{|r|v}|r|v + K_{|v|r}|v|r + K_{|r|r}|r|r \quad (2.35)$$

$$N_{cf} \cong N_{|v|v}|v|v + N_{|r|v}|r|v + N_{|v|r}|v|r + N_{|r|r}|r|r. \quad (2.36)$$

These approximations give error when v and $x.r$ have different signs.

2.7 Roll model

2.7.1 The roll angle's influence on lift and drag

The lift and drag characteristics of the hull is influenced by the roll angle. This applies particularly for vessel's with low metacentric height. Consequently, an investigation of the roll-sway-yaw interactions are necessary.

The influence of roll angle on the lift and drag may be modelled using an approach related to aerodynamics. An aircraft wing is called dihedral if the wings are turned up at some dihedral angle, Γ , from the horizontal plane, see Figure 2.7. A ship in roll will get the same effect as the aircraft wing. Hence, the roll angle, ϕ , and dihedral angle, Γ , will be conceptually the same, see also Figure 2.8.

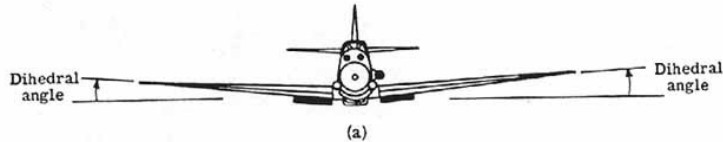


Figure 2.7: Aircraft wing with dihedral angle Γ [14]

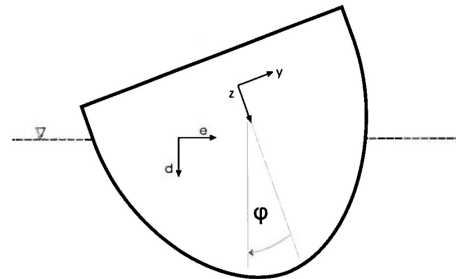


Figure 2.8: Dihedral of hull and roll angle ϕ [9]

The circulatory drag and lift are affected by the roll angle. Hoerner expressed the dihedral angle's effect on the induced drag as:

$$C_{Di} = \frac{C_L^2}{\pi A_R \cos^2 \Gamma}, \quad (2.37)$$

where A_R is the aspect ratio of the wing and Γ is the dihedral angle, i.e. roll angle ϕ . This gives additional contribution to the drag formula given as:

$$\Delta X_D = X_{vv\phi\phi} v^2 \phi^2 + X_{vr\phi\phi} vr \phi^2 + X_{rr\phi\phi} r^2 \phi^2, \quad (2.38)$$

$$\Delta Y_D \cong 0. \quad (2.39)$$

The effect of the dihedral on the lift is expressed by Hoerner and Borst as:

$$\frac{d\alpha}{dC_L} = \frac{1}{2\pi \cos^2 \Gamma} + \frac{1}{\pi A_P \cos^2 \Gamma}, \quad (2.40)$$

where α is the angle of attack.

The additional contribution to the lift formulas caused by roll are given as:

$$\Delta X_L = X_{vv\phi\phi} v^2 \phi^2 + X_{vr\phi\phi} vr \phi^2 + X_{rr\phi\phi} r^2 \phi^2 \quad (2.41)$$

$$\Delta Y_L = Y_{uv\phi\phi} uv \phi^2 + Y_{ur\phi\phi} ur \phi^2. \quad (2.42)$$

2.7.2 Roll damping

Damping is usually related to energy transportation of gravity waves, but in roll it is a more complex process. Roll damping may have following sources:

- wave generation;
- skin friction;
- eddy creation;
- lift generation or
- appendage damping (bilge keels, fins etc.).

Roll damping may be impractical or impossible to model physically. Various empirical formulas are therefore used to predict roll damping. It may be modelled as a linear component plus a quadratic modulus (Ikeda et al.m Lloyd, Himeno) or a linear component plus a quadratic modulus term (Bass, Haddara) Ross [9] uses a cubic model (Perez, Jornee, Massie), which is expressed as:

$$K = K_{pp} + K_{ppp} p^3. \quad (2.43)$$

2.8 Total forces

2.8.1 Circulatory lift and drag

By use of superposition the total surge and sway forces caused by lift and drag can be expressed as:

$$\begin{aligned} X_{LD} &= X_L + X_D + \Delta X_D + \Delta X_L \\ &= X_{uu}u^2 + X_{uuu}u^3 + X_{vv}v^2 + X_{rr}r^2 + X_{vr}vr + X_{uvv}uv^2 \\ &\quad + X_{rvu}rvu + X_{urr}ur^2 + X_{vv\phi\phi}v^2\phi^2 + X_{vr\phi\phi}vr\phi^2 + X_{rr\phi\phi}r^2\phi^2, \end{aligned} \quad (2.44)$$

$$\begin{aligned} Y_{LD} &= Y_L + Y_D\Delta X_D + \Delta X_L \\ &= Y_{uv}uv + Y_{ur}ur + Y_{uur}u^2r + Y_{uuv}u^2v + Y_{vvv}v^3 + Y_{rrr}r^3 \\ &\quad + Y_{rrv}r^2v + Y_{vvr}v^2r + Y_{uv\phi\phi}uv\phi^2 + Y_{ur\phi\phi}ur\phi^2. \end{aligned} \quad (2.45)$$

Roll- and yaw moments are induced by the sway force as:

$$\begin{aligned} K_{LD} &= Y_{LD} \cdot z_{cp} \\ &= K_{uv}uv + K_{ur}ur + K_{uur}u^2r + K_{uuv}u^2v + K_{vvv}v^3 + K_{rrr}r^3 \\ &\quad + K_{rrv}r^2v + K_{vvr}v^2r + K_{uv\phi\phi}uv\phi^2 + K_{ur\phi\phi}ur\phi^2, \end{aligned} \quad (2.46)$$

$$\begin{aligned} N_{LD} &= N_{LD} \cdot z_{cp} \\ &= N_{uv}uv + N_{ur}ur + N_{uur}u^2r + N_{uuv}u^2v + N_{vvv}v^3 + N_{rrr}r^3 \\ &\quad + N_{rrv}r^2v + N_{vvr}v^2r + N_{uv\phi\phi}uv\phi^2 + N_{ur\phi\phi}ur\phi^2. \end{aligned} \quad (2.47)$$

2.8.2 Cross-flow drag

The total forces for cross-flow drag can be modelled as given in the equations (2.34), (2.35) and (2.36).

2.8.3 Roll damping

The roll damping can be modelled as in equation (2.43).

Chapter 3

Mathematical models

Various approaches can be used to derive mathematical models for a body moving through water. The equations of motion can for instance be derived from Newton's second law or the Euler-Lagrange equation. Newton's second law, $\vec{F} = m\vec{a}$, states that the forces acting on a fixed mass are directly proportional to the product of the mass and acceleration. The motions are given relative to a body fixed reference frame. Euler-Lagrange equations are energy based and possess frame-indifference, i.e. the equations can be used for any reference frame.

In this chapter two mathematical models to describe calm water manoeuvring for a port-starboard symmetric vessel are presented. The first model is a linear 3-DOF model derived from Newton's second law, while the other is a 4-DOF model derived using an Euler-Lagrangian approach.

A body can move in six degrees of freedom and the relevant motions in calm water manoeuvring are surge, sway, roll and yaw. Roll is however neglected in the model based upon Newton's second law, which may be acceptable for vessels with large GM . A 4-DOF model is presented using the Euler-Lagrangian approach. The Euler-Lagrangian approach can also be used to model a 6-DOF problem, but this is not done here as only calm water manoeuvring is considered. In addition, the 4-DOF model describes the principle of the 6-DOF model used in Vesim.

3.1 Linear 3-DOF model

The description of the linear 3-DOF model is an abridged version of that given in [3], which is based upon [15] and [7].

The linear 3-DOF model consider motions in the horizontal plan, i.e. surge, sway and yaw. Newtons second law gives the relationship between motion of the vessel and forces from the fluid as:

$$\frac{d}{dt} (M\vec{U}_A) = \vec{F}_1, \quad (3.1)$$

where the force \vec{F}_1 consists of the hydrodynamic forces and control forces from rudders. \vec{U}_A is absolute velocity to the centre of gravity and M is the mass of the body.

The rotational equation of motion can be expressed as:

$$\frac{d}{dt} (I\vec{\omega})_G = \vec{F}_2, \quad (3.2)$$

where the moment \vec{F}_2 includes hydrodynamic moments and control moments from rudders. I is the moment of inertia-matrix and $\vec{\omega}$ is the rotation. The index G indicates that the equation applies to a axis system with origin in the hull's centre of gravity.

This gives rise to equations of motions expressed as:

$$\begin{aligned} X &= M\dot{u} \\ Y &= M(\dot{v} + x_G\dot{r} + ur) \\ N &= I_{zz}\dot{r} + Mx_G(\dot{v} + ur), \end{aligned} \quad (3.3)$$

where x_G is the distance between the vessel's centre of gravity and the origin in the axis system and I_{zz} is the moment of inertia about a vertical axis through the midship point.

Including the hydrodynamic hull forces and control forces from rudder gives following linear equations of motions:

$$\begin{aligned} (X_u - M)\dot{u} &= 0 \\ (Y_v - M)\dot{v} + (Y_r - Mx_G)\dot{r} + Y_v v + (Y_r - Mu)r + Y_\delta \delta &= 0 \\ (N_v - Mx_G)\dot{v} + (N_r \dot{r} - I_{zz})\dot{r} + N_v v + (N_r - Mx_G u)r + N_\delta \delta &= 0. \end{aligned} \quad (3.4)$$

The sway and yaw equations in equation (3.4) can be made dimensionless by dividing the expressions by $\frac{1}{2}\rho L_{pp}^2 U^2$ and $\frac{1}{2}\rho L_{pp}^3 U^2$. The non-dimensional sway and yaw equations are expressed as:

$$\begin{aligned}(Y'_v - M')\dot{v}' + (Y'_r - M'x'_G)\dot{r}' + Y'_V v' + (Y'_r - M')r' + Y'_\delta \delta &= 0 \\ (N'_v - M'x'_G)\dot{v}' + (N'_r \dot{r} - I'_{zz})\dot{r}' + N'_v v' + (N'_r - M'x'_G)r' + N'_\delta \delta &= 0.\end{aligned}\quad (3.5)$$

where ' denotes that the parameter is dimensionless.

3.1.1 Stability calculations

The straight line stability of a vessel can be investigated using following approach. By introducing the differential operator $D = \frac{d}{dt}$, the accelerations can be written as:

$$\begin{aligned}\dot{v}' &= Dv' \\ \dot{r}' &= Dr'.\end{aligned}\quad (3.6)$$

Hence, (3.5) can be rewritten as:

$$\begin{aligned}\left(\left(Y'_v - M'\right)D + Y'_V\right)v' + \left(\left(Y'_r - M'x'_G\right)D + \left(Y'_r - M'\right)\right)r' + Y'_\delta \delta &= 0 \\ \left(\left(N'_v - M'x'_G\right)D + N'_v\right)v' + \left(\left(N'_r - I'_{zz}\right)D + \left(N'_r - M'x'_G\right)\right)r' + N'_\delta \delta &= 0.\end{aligned}\quad (3.7)$$

The sway velocity term may be eliminated by:

- multiplying the sway equation with $\left(\left(N'_v - M'x'_G\right)D + N'_v\right)$;
- multiplying the yaw equation with $\left(\left(Y'_v - M'\right)D + Y'_V\right)$ and
- subtracting the resulting sway equation from the yaw equation.

The result is given by

$$(AD^2 + BD + C)r' = (ED + F)\delta, \quad (3.8)$$

where

$$\begin{aligned}
 A &= (N'_{\dot{r}} - I'_{zz})(Y'_{\dot{v}} - M') - (Y'_{\dot{r}} - M'x'_G)(N'_{\dot{v}} - M'x'_G) \\
 B &= (N'_{\dot{r}} - I'_{zz})Y'_{\dot{v}} + (N'_r - M'x'_G)(Y'_{\dot{v}} - M') - (Y'_{\dot{r}} - M'x'_G)N'_v \\
 &\quad - (Y'_r - M')(N'_{\dot{v}} - M'x'_G) \\
 C &= (N'_r - M'x'_G)Y'_v - (Y'_r - M')N'_v \\
 E &= Y'_\delta(N'_{\dot{v}} - M'_G) - N'_\delta(Y'_{\dot{v}} - M') \\
 F &= Y'_\delta N'_{\dot{v}} - Y'_\delta Y'_{\dot{v}}.
 \end{aligned} \tag{3.9}$$

(3.8) is a first order differential equation, where the yaw speed can be written as:

$$r'(t') = r'_H + r'_p = C_1 \exp(D_1 t') + C_2 \exp(D_2 t') + r'_p, \tag{3.10}$$

where r'_H is the homogeneous solution and r'_p is the particular solution. Setting the rudder angle to zero, the homogeneous solution, r'_H , can be calculated using:

$$\begin{aligned}
 AD^2 + BD + C &= 0, \\
 D_{1,2} &= \frac{-B \pm \sqrt{B - 4AC}}{2A}.
 \end{aligned} \tag{3.11}$$

For a ship with straight line stability the homogeneous solution goes to zero as the time goes to infinity, which is obtained when the exponential coefficients $D_{1,2}$ have real parts. This implies that in order to have straight line stability

$$C > 0. \tag{3.12}$$

This is satisfied if:

$$\frac{N'_r - M'x'_G}{N'_r - M'} > \frac{N'_v}{Y'_v}. \tag{3.13}$$

3.2 4-DOF low-frequency model

A 4-DOF low frequency model is obtained to describe low-frequency operations, i.e. manoeuvring in calm water. In this section the mathematical model is presented, while a more detailed description is given in Appendix A.2. The 4-DOF low-frequency model presented in this study is given by Ross [9] and Fossen [10]. The 4-DOF model can be expressed as:

$$\mathbf{M}\dot{\boldsymbol{\nu}} + \mathbf{C}(\boldsymbol{\nu})\boldsymbol{\nu} + \mathbf{D}(\boldsymbol{\nu}) + \mathbf{g}(\boldsymbol{\eta}) = \boldsymbol{\tau}, \tag{3.14}$$

where

- $\boldsymbol{\nu} = [\boldsymbol{\nu}_1 \ \boldsymbol{\nu}_2] = [u, v, p, r]$ is a generalised velocity vector;
- $\boldsymbol{\eta} = [\boldsymbol{\eta}_1 \ \boldsymbol{\eta}_2] = [x, y, \phi, \psi]$ is a position vector, also called Euler angles;
- $\mathbf{M} = \mathbf{M}_{\text{RB}} + \overline{\mathbf{M}}_{\text{A}}^0$ is the systems inertia matrix including added mass;
- $\mathbf{C}(\boldsymbol{\nu}) = \mathbf{C}_{\text{RB}}(\boldsymbol{\nu}) + \mathbf{C}_{\text{A}}(\boldsymbol{\nu})$ is a Coriolis-centripetal matrix including added mass;
- $\mathbf{D}(\boldsymbol{\nu})$ is a damping matrix;
- $\mathbf{g}(\boldsymbol{\eta})$ is a vector of gravitational/buoyancy forces and moments and
- $\boldsymbol{\tau}$ is a vector of control inputs.

The mass matrices are given as:

$$\mathbf{M}_{\text{RB}} = \begin{bmatrix} m & 0 & 0 & 0 \\ 0 & m & 0 & 0 \\ 0 & 0 & I_x & 0 \\ 0 & 0 & 0 & I_z \end{bmatrix}, \quad (3.15)$$

$$\mathbf{M}_A = - \begin{bmatrix} X_{\dot{u}}^0 & 0 & 0 & 0 \\ 0 & Y_{\dot{v}}^0 & Y_{\dot{p}}^0 & Y_{\dot{r}}^0 \\ 0 & K_{\dot{v}}^0 & K_{\dot{p}}^0 & K_{\dot{r}}^0 \\ 0 & N_{\dot{v}}^0 & N_{\dot{p}}^0 & N_{\dot{r}}^0 \end{bmatrix}, \quad (3.16)$$

$$\overline{\mathbf{M}}_A = \frac{1}{2} (\mathbf{M}_A + (\mathbf{M}_A)^T). \quad (3.17)$$

The Coriolis-centripetal matrices are defined as:

$$\mathbf{C}_{RB}(\boldsymbol{\nu}) = \begin{bmatrix} 0 & 0 & 0 & mv \\ 0 & 0 & mw & -mu \\ 0 & -mw & 0 & I_y q \\ -mv & mu & -I_y q & 0 \end{bmatrix} \quad (3.18)$$

and

$$\mathbf{C}_A(\boldsymbol{\nu}) = \begin{bmatrix} 0 & 0 & Y_{\dot{v}}^0 v + Y_{\dot{r}}^0 r + Y_{\dot{p}}^0 p \\ 0 & 0 & -X_u^0 u \\ 0 & 0 & 0 \\ -Y_{\dot{v}}^0 v - Y_{\dot{r}}^0 r - Y_{\dot{p}}^0 p & X_u^0 u & 0 \end{bmatrix}. \quad (3.19)$$

The damping matrix is modelled as described in Chapter 2. The damping force may be divided into:

- linear lift and drag forces given by the equations (2.44) - (2.47);
- cross-flow drag given by the equations (2.31)-(2.33) and
- roll damping given by equation (2.43).

This gives the damping matrix as:

$$\mathbf{D}(\boldsymbol{\nu}) = \begin{bmatrix} a_{11} & a_{12} & a_{13} & a_{14} \\ a_{21} & a_{22} & a_{23} & a_{24} \\ a_{31} & a_{32} & a_{33} & a_{34} \\ a_{41} & a_{42} & a_{43} & a_{44} \end{bmatrix},$$

where

$$\begin{aligned} a_{11} &= -X_{uu}^L u - X_{uuu}^L u^2 - X_{rvu}^L r v \\ a_{12} &= -X_{vv}^L v - X_{rv}^L r - X_{uvv}^L u v - X_{vv\phi\phi}^L v \phi^2 - X_{vr\phi\phi}^L r \phi^2 \\ a_{13} &= 0 \\ a_{14} &= -X_{rr}^L r - X_{urr}^L u r - X_{rr\phi\phi}^L r \phi \phi \\ a_{21} &= -Y_{uv\phi\phi}^L v \phi^2 - Y_{ur\phi\phi}^L r \phi^2 \\ a_{22} &= -Y_{uv}^L u - Y_{uuc}^L u^2 - Y_{vvv}^L v^2 - Y_{rrv}^L r^2 - Y_{|v|v}^L |v| - Y_{|r|v}^L |r| \\ a_{23} &= 0 \\ a_{24} &= -Y_{ur}^L u - Y_{uur}^L u^2 - X_{rrr}^L r^2 - Y_{vvr}^L v^2 - Y_{|v|r}^L |v| - Y_{|r|r}^L |r| \\ a_{31} &= -K_{uv\phi\phi}^L v \phi \phi - K_{ur\phi\phi}^L r \phi \phi \\ a_{32} &= -K_{uv}^L u v - K_{uuv}^L u^2 - K_{vvv}^L v^2 - K_{rrv}^L r^2 - K_{|v|v}^L |v| - K_{|r|v}^L |r| \\ a_{33} &= -K_p - K_{ppp} p^2 \\ a_{34} &= -K_{ur}^L u r - K_{uur}^L u^2 - K_{rrr}^L r^2 - K_{vvr}^L v^2 - K_{|v|r}^L |v| - K_{|r|r}^L |r| \\ a_{41} &= -N_{uv\phi\phi}^L - N_{ur\phi\phi}^L r \phi^2 \\ a_{42} &= -N_{uv}^L u - N_{uuv}^L u^2 - N_{vvv}^L v^2 - N_{rrv}^L r^2 - N_{|v|v}^L |v| - N_{|r|v}^L |r| \\ a_{43} &= 0 \\ a_{44} &= -N_{ur}^L u r - N_{uur}^L u^2 - N_{rrr}^L r^2 - N_{vvr}^L v^2 - N_{|v|r}^L |v| - N_{|r|r}^L |r|. \end{aligned} \quad (3.20)$$

The restoring matrix can be expressed as:

$$\mathbf{g}(\boldsymbol{\nu}) = \begin{bmatrix} 0 \\ 0 \\ \rho g \nabla G M_T \sin \phi \\ 0 \end{bmatrix}. \quad (3.21)$$

Chapter 4

Calculation of hydrodynamic coefficients

Hydrodynamic coefficients are used to describe a vessel's behaviour in a manoeuvring problem. The coefficients can be found from models test when the lines of the vessel are decided. This a time-consuming and expensive method. It would therefore be practical to calculate the hydrodynamic derivatives based on the vessel's geometry. Then it is not necessary to build the ship model, and small changes on the hull may be easily investigated. Various methods of doing so have been suggested in the literature. However, the accuracy of the methods depend on the particular geometry of the ship.

Several approaches to calculate the hydrodynamic coefficients are presented in this chapter. First two theoretical methods are given, followed by empirical methods. Finally the method used in ShipX (SIMAN) is presented. The coefficients may be used to solve a manoeuvring problem using for instance a 3-DOF linear model presented in Section 3.1. It is important to note that the axis system in Figure 4.1 is used, and the forces and moments are made non-dimensional as:

$$\begin{aligned} Y' &= \frac{Y}{\frac{1}{2}\rho L^2 U^2} \\ N' &= \frac{N}{\frac{1}{2}\rho L^3 U^2}, \end{aligned} \tag{4.1}$$

where ρ is the viscosity of the fluid, L is ship's length between perpendiculars, U is the vessel's velocity and prime denotes that the component is dimensionless.

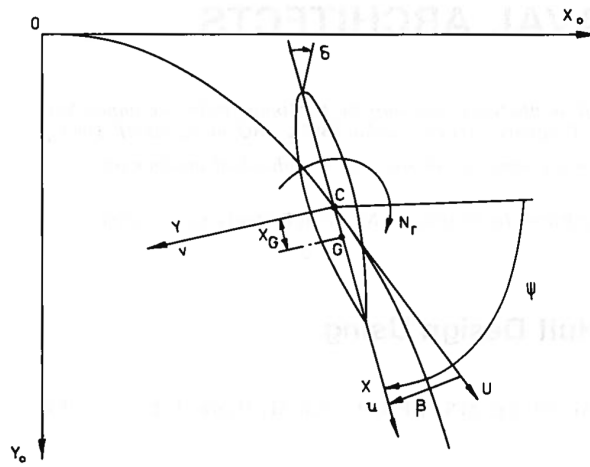


Figure 4.1: Body-fixed axis system used in horizontal plane manoeuvring problems [16]

Furthermore, the methods given in this chapter are used to predict the hydrodynamic coefficients of R/V Gunnerus. In these cases R/V Gunnerus has a loading condition with draught at 2.75 m and no trim. No trim is chosen as the methods do not consider trim effects. Ship characteristics used in the calculations are given in Appendix A.3. Several of the empirical methods are based on older, conventional vessels, while the method used in ShipX (SIMAN) and the method derived by Kijima are based on newer vessels. It is therefore expected that there will be differences in the results.

4.1 Strip theory

4.1.1 Flat plate

Slender body theory and strip methods may be used to estimate the acceleration and velocity derivatives. A rather simplified approach is to consider the ship hull as a low aspect wing turned on its side where the chord is considered as ship length and span is set as twice the draught, see Figure 2.4. The expressions for

this flat plate case are given as [16]

$$\begin{aligned}
 Y'_v &= -\pi \left(\frac{T}{L} \right)^2 \\
 Y'_{\dot{r}} &= 0 \\
 N'_{\dot{v}} &= 0 \\
 N'_{\dot{r}} &= -\pi \left(\frac{T}{L} \right)^2 \cdot \frac{1}{12} \\
 Y'_v &= -\pi \left(\frac{T}{L} \right)^2 \\
 Y'_r &= -\pi \left(\frac{T}{L} \right)^2 \cdot \left(-\frac{1}{2} \right) \\
 N'_v &= -\pi \left(\frac{T}{L} \right)^2 \cdot \frac{1}{2} \\
 N'_r &= -\pi \left(\frac{T}{L} \right)^2 \cdot \frac{1}{4},
 \end{aligned} \tag{4.2}$$

where T and L are the vessel's draught and length.

4.1.2 Surface ship hull

Clarke [17] extended the slender body strip theory for a flat plate using the horizontal added mass coefficients, C_H , for sections along the hull. Consequently the expressions for hydrodynamic coefficients take the effect of hull shape into consideration through the longitudinal added mass distribution. The expressions

for the hydrodynamic derivatives are given as:

$$\begin{aligned}
 Y'_v &= -\pi \left(\frac{T}{L} \right)^2 \int_{X'_B}^{X'_S} C_H dX' \\
 Y'_{\dot{r}} &= -\pi \left(\frac{T}{L} \right)^2 \int_{X'_B}^{X'_S} C_H X' dX' \\
 N'_v &= -\pi \left(\frac{T}{L} \right)^2 \int_{X'_B}^{X'_S} C_H X' dX' \\
 N'_{\dot{r}} &= -\pi \left(\frac{T}{L} \right)^2 \int_{X'_B}^{X'_S} C_H X'^2 dX' \\
 Y'_v &= -\pi \left(\frac{T}{L} \right)^2 (C_H)_{X'} \\
 Y'_{\dot{r}} &= -\pi \left(\frac{T}{L} \right)^2 (C_H)_{X'} \\
 N'_v &= -\pi \left(\frac{T}{L} \right)^2 \left((C_H X')_{X'} + \int_{X'_B}^{X'_S} C_H dX' \right) \\
 N'_{\dot{r}} &= -\pi \left(\frac{T}{L} \right)^2 \left((C_H X'^2)_{X'} + \int_{X'_B}^{X'_S} C_H X' dX' \right),
 \end{aligned} \tag{4.3}$$

where C_H is the zero frequency added mass coefficient at station X' , X' is the non-dimensional distance (X/L) from midships, X'_B is the non-dimensional bow coordinate and X'_S is the non-dimensional stern coordinate. The method of calculating C_H is described by Clarke [17].

It is necessary to consider the effect of viscosity near the stern. This is however challenging as it is not properly understood. Hence, it is difficult to evaluate the expressions for the hydrodynamic coefficients. Schmitz suggested that the integrations should be performed to some point ahead of the stern and further contributions should be neglected. In this manner the hull are effectively truncated. This statement was examined by Clarke and it was found that the point at which truncation should be performed varied for each coefficient [16].

4.2 Empirical methods

4.2.1 Wagner Smitt

Wagner Smitt (1971, 1972) has derived an empirical approach to predict the velocity derivatives. The approach is based on measured values from PMM experiments and the formulas are expressed as [16]:

$$\begin{aligned} Y'_v &= -\pi \left(\frac{T}{L} \right)^2 \cdot 1.59 \\ Y'_r &= -\pi \left(\frac{T}{L} \right)^2 \cdot (-0.32) \\ N'_v &= -\pi \left(\frac{T}{L} \right)^2 \cdot 0.62 \\ N'_r &= -\pi \left(\frac{T}{L} \right)^2 \cdot 0.21, \end{aligned} \tag{4.4}$$

where T and L are the draught and length of the vessel.

4.2.2 Norrbin

An analysis of PMM experiments is also performed by Norrbin in 1971. The expressions for the velocity derivatives are given as [16]:

$$\begin{aligned} Y'_v &= -\pi \left(\frac{T}{L} \right)^2 \cdot \left(1.69 + 0.08 \frac{C_B B}{\pi T} \right) \\ Y'_r &= -\pi \left(\frac{T}{L} \right)^2 \cdot \left(-0.645 + 0.38 \frac{C_B B}{\pi T} \right) \\ N'_v &= -\pi \left(\frac{T}{L} \right)^2 \cdot \left(0.64 - 0.04 \frac{C_B B}{\pi T} \right) \\ N'_r &= -\pi \left(\frac{T}{L} \right)^2 \cdot \left(0.47 - 0.18 \frac{C_B B}{\pi T} \right), \end{aligned} \tag{4.5}$$

where C_B is the vessel's block coefficient and T , L and B are the vessel's draught, length and breadth.

4.2.3 Inoue

In 1981 Inoue [18] investigated manoeuvring performance by studying rotating arm tests and oblique towing tests. Three oil tankers, three dry dock cargo ships, a container ship, a LNG tanker, a RO/RO ship and a carrier were tested. As the manoeuvring performance is strongly dependent of loading condition the vessels were tested in three loading conditions; full, half and ballast condition. The lateral force and yaw moment were then investigated as a function of draught. The velocity derivatives were reformulated to the same form as in previous sections and expressed as [16]:

$$\begin{aligned} Y'_v &= -\pi \left(\frac{T}{L} \right)^2 \cdot \left(1.0 + 1.4 \frac{C_B}{\pi} \frac{B}{T} \right) \\ Y'_r &= -\pi \left(\frac{T}{L} \right)^2 \cdot (-0.5) \\ N'_v &= -\pi \left(\frac{T}{L} \right)^2 \cdot \left(\frac{2.0}{\pi} \right) \\ N'_r &= -\pi \left(\frac{T}{L} \right)^2 \cdot \left(\frac{1.04}{\pi} - \frac{4.0}{\pi} \frac{T}{L} \right), \end{aligned} \quad (4.6)$$

where C_B is the vessel's block coefficient and T , L and B are the vessel's draught, length and breadth respectively.

4.2.4 Clarke

The formulas to predict the velocity derivatives stated in the previous sections differ substantially. Reasons for this may be the use of different data sets, experiment variations or different curve fitting techniques. To get an overview of the various empirical methods Clarke [16] collected acceleration and velocity derivatives that were available in the literature in 1982. Velocity derivatives from 36 rotating arm tests were obtained, as well as velocities and acceleration derivatives from 36 PMM experiments. The normalised coefficients were plotted versus $C_B B/T$ together with lines representing the various methods. A scatter in the results was detected. This may be due to differences in hull form that is not covered in the $C_B B/T$ -parameter or differences in experimental and data reduction techniques. In order to find empirical formulas that could explain the variation of the measured derivatives Clarke used multiple linear regression.

Following regression equation was used:

$$y = b_0 + b_1 x_1 + b_2 x_2 + \dots, \quad (4.7)$$

where y is the dependent variable (i.e. acceleration or velocity derivative), x_1, x_2, \dots are the predictor variables, b_0 is the pre-assigned value of y for the flat plate case and b_1, b_2, \dots are the regression coefficients. Following predictor variables were used:

$$\begin{aligned} & B/T, B/L, T/L, (B/T)^2, (B/L)^2, (T/L)^2, \\ & C_B B/T, C_B B/L, C_B T/L, B^2/TL, BT/L^2. \end{aligned} \quad (4.8)$$

The different terms were investigated statistically and following expression were established:

$$\begin{aligned} Y'_v &= -\pi \left(\frac{T}{L} \right)^2 \cdot \left(1 + 0.16 \frac{C_B B}{T} - 5.1 \left(\frac{B}{L} \right)^2 \right) \\ Y'_r &= -\pi \left(\frac{T}{L} \right)^2 \cdot \left(0.67 \frac{B}{L} - 0.0033 \left(\frac{B}{T} \right)^2 \right) \\ N'_v &= -\pi \left(\frac{T}{L} \right)^2 \cdot \left(1.1 \frac{B}{L} - 0.041 \frac{B}{T} \right) \\ N'_r &= -\pi \left(\frac{T}{L} \right)^2 \cdot \left(\frac{1}{12} + 0.017 \frac{C_B B}{T} - 0.33 \frac{B}{L} \right) \\ Y'_v &= -\pi \left(\frac{T}{L} \right)^2 \cdot \left(1 + 0.40 \frac{C_B B}{T} \right) \\ Y'_r &= -\pi \left(\frac{T}{L} \right)^2 \cdot \left(-\frac{1}{2} + 2.2 \frac{B}{L} - 0.08 \frac{B}{T} \right) \\ N'_v &= -\pi \left(\frac{T}{L} \right)^2 \cdot \left(\frac{1}{2} + 2.4 \frac{T}{L} \right) \\ N'_r &= -\pi \left(\frac{T}{L} \right)^2 \cdot \left(\frac{1}{4} + 0.039 \frac{B}{T} - 0.56 \frac{B}{L} \right). \end{aligned} \quad (4.9)$$

4.2.5 Lee

Stern hull form affects the manoeuvring performance, but this has not been taken into account in the previous methods. Lee [19] investigated PMM tests for modern hull forms, respectively tankers, bulk carries, products carriers, container ships and LNG carriers with stern bulb. An illustration of the stern hull profile is

shown in Figure 4.2. The vessels are tested in full load condition, and some are also tested in ballast condition. Their range of ship particulars are:

$$\begin{aligned} 0.55 &< C_B < 0.87 \\ 0.022 &< \frac{T}{L} < 0.071 \\ 5.0 &< \frac{L}{B} < 8.8 \\ 0.075 &< \frac{C_B B}{L} < 0.166. \end{aligned} \quad (4.10)$$

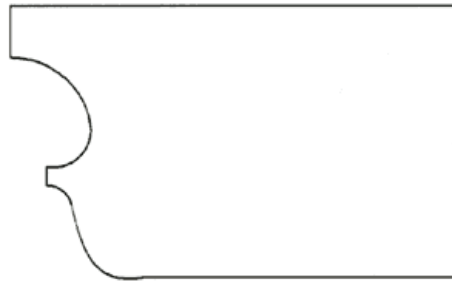


Figure 4.2: Stern hull profile used by Lee in derivation of velocity derivatives [19]

Lee derived an empirical formula where a parameter to represent the stern hull was included. Lee made the forces and moments non-dimensional by dividing the sway and yaw equations with $\frac{1}{2}\rho L T U^2$ and $\frac{1}{2}\rho L^2 T U^2$. In order to make them dimensionless on the same form as the other derivatives in this thesis, Lee's hydrodynamic derivatives are multiplied with $\frac{T}{L}$. Then, the velocity derivatives are expressed as:

$$\begin{aligned} Y'_v &= - \left(0.145 + 2.25 \frac{T}{L} - 0.2 \Delta_{SR} \right) \frac{T}{L} \\ Y'_r &= - (0.282 + 0.1 \Delta_{SR}) \frac{T}{L} + 0.0086 \Delta_{B/L} + 0.004 + m' \frac{T}{L} \\ N'_v &= - (0.222 + 0.1 \Delta_{SR}) \frac{T}{L} + 0.00484 \\ N'_r &= - (0.0424 - 0.03 \Delta_{SR}) \frac{T}{L} - 0.004 \Delta_{C_B} + 0.00027, \end{aligned} \quad (4.11)$$

where

$$\begin{aligned}
 S_R &= \frac{B_{P07}}{B_{PS}} \\
 \nabla' &= \frac{\nabla}{L^2 T} \\
 P_{SR} &= 28.7 \nabla' + 0.54 \\
 \Delta_{SR} &= \frac{P_{SR} - S_R}{P_{SR}} \\
 \Delta_{B/L} &= \frac{0.18 - B/L}{0.18} \\
 P_{C_B} &= 1.12 \frac{T}{L} + 0.735 \\
 \Delta_{C_B} &= \frac{P_{C_B} - C_B}{P_{C_B}} \\
 m' &= \frac{\Delta}{0.5 \rho L^2 T},
 \end{aligned} \tag{4.12}$$

where B_{PS} is half breadth of the vessel at the height of propeller shaft in station 2.0, B_{P07} is half breadth at the height of $0.7R$ (R = propeller radius) in station 2.0, ∇ is the vessel's volume displacement, Δ is its weight displacement and C_B , L , B and T are the ship's block coefficient, length, breadth and draught.

4.2.6 Kijima

In 2003 Kijima and Nakiri [20] published a method for prediction of hydrodynamic coefficients where stern hull shape is taken into consideration. Model test data from 15 ship types and their 48 loading conditions were analysed. Consequently, approximate formulas for the hydrodynamic coefficients were established. Comparison of measured and predicted forces showed close agreement.

The aft hull shape is characterised by e_a , e'_a , σ_a and K . e_a and e'_a describe the fullness of the aft run, σ_a expresses the aft section fullness metric and K is a form

factor. These aft hull parameters are given as:

$$\begin{aligned} e_a &= \frac{L}{B}(1 - C_{pa}) \\ e'_a &= e_a / \sqrt{\frac{1}{4} + \frac{1}{(B/T)^2}} \\ \sigma_a &= \frac{1 - C_{wa}}{1 - C_{pa}} \\ K &= \left(\frac{1}{e'_a} + \frac{1.5}{L/B} - 0.33 \right) (0.95\sigma_a + 0.40), \end{aligned} \quad (4.13)$$

where C_{wa} and C_{pa} are respectively water plane coefficient and prismatic coefficient of aft hull between aft perpendicular and station 5. These coefficients are given as:

$$\begin{aligned} C_{wa} &= \frac{A_{wa}}{L_a B_a} \\ C_{pa} &= \frac{\nabla_a}{A_a L_a}, \end{aligned} \quad (4.14)$$

where A_{wa} is the water plane area of the aft section, A_a is the cross-sectional area equal to the largest underwater section of the aft hull, B_a is the vessel's breadth of the aft hull and L is its length.

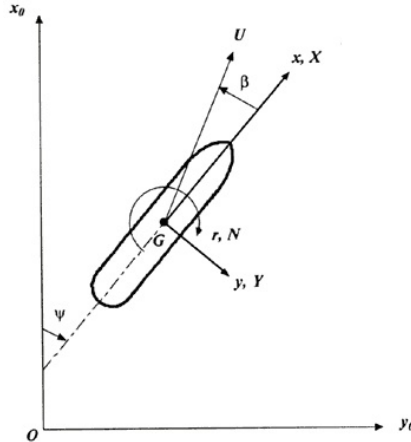


Figure 4.3: Body-fixed axis system used by Kijima [20]

The linear derivatives are originally made non-dimensional by dividing the forces and moments with $\frac{1}{2}\rho LTU^2$ and $\frac{1}{2}\rho L^2TU^2$, like Lee's formulas. Kijima has derived

expressions for Y'_β and N'_β , where β is defined in Figure 4.3 as:

$$\sin \beta = \frac{-v}{U}. \quad (4.15)$$

Y_v and N_v can be expressed by multiplying the expressions for Y'_β and N'_β with (-1) . Consequently are the linear derivatives given as:

$$\begin{aligned} Y'_v &= - \left(\frac{1}{2}\pi K + 1.9257 \frac{C_B B}{L} \sigma_a \right) \cdot \frac{T}{L} \\ Y'_r &= \left(\left(\frac{1}{4}\pi K + 0.052 e'_a - 0.457 \right) + (m' + m'_x) \right) \cdot \frac{T}{L} \\ N'_v &= -K \left(15.0668 \left(T \frac{1 - C_B}{B} e'_a K \right)^2 - 23.819 T \frac{1 - C_B}{B} e'_a K + 1.802 \right) \cdot \frac{T}{L} \\ N'_r &= (-0.54K + K^2 - 0.0477e'_a K + 0.0368) \cdot \frac{T}{L}, \end{aligned} \quad (4.16)$$

where m' and m'_x are the non-dimensional mass and added mass. The mass are made dimensionless by diving it with $1/2\rho L^2 T$. The non-dimensional added mass are predicted as [19]:

$$m'_x = \left(\frac{2.7\rho}{L^2} \right) (C_B L B T)^{5/3}. \quad (4.17)$$

4.2.7 ShipX Manoeuvring (SIMAN)

A model of the vessel, including lines, must be specified in ShipX. Thus, the actual shape of the vessel can be provided. The description given in this section of calculating the hydrodynamic coefficients in ShipX is based on [21].

In ShipX (SIMAN) the hydrodynamic coefficients are calculated based on strip theory as described in Section 4.1.2. The sectional horizontal added mass coefficient, C_H , is integrated from the bow to a certain section in the aftbody. At first the horizontal sectional added mass distribution was calculated as defined in [17]. Comparing this calculated result with results from experiments with segmented models or measurement of pressure distribution indicated a discrepancy between the calculated and the measured results. When the horizontal added mass coefficient was calculated potential flow was assumed, this ignored the viscous effects and a certain discrepancy was expected. This discrepancy was however larger than expected. In order to reduce this discrepancy a correction in the forebody based on waterline angle was applied.

Further, the hull cross sections were increased in size successively from the bow to the stern by increasing the boundary layer thickness using an empirical formulation. The boundary layer correction at the stern is more distinct for full hull forms than for slender hulls. The correction is also larger for model scale Reynolds number than for full-scale Reynolds numbers. Comparing this calculated horizontal sectional added mass distribution with measured C_H for a tanker and a Series 60 hull showed that the corrections improved the sectional added mass distribution. But there was still a discrepancy, especially in the stern, and a straightforward integration of C_H to predict the hydrodynamic coefficients is not recommended. Instead empiricism was introduced. Hydrodynamic coefficients of 25 different ship models were collected, and following procedure to calculate the hydrodynamic coefficients was established:

- Y_v , Y_r , N_v and N_r are set equal to the zero frequency added mass or added moment of inertia calculated in ShipX;
- Y_v is found by applying the maximum value of the C_H -distribution;
- Y_r is found by applying the C_H -value at a section $0.1 \times L_{pp}$ forward of the aft perpendicular and
- N_v and N_r are found by applying the C_H -value at a section $0.1 \times L_{pp}$ forward of the aft perpendicular and carrying out the remaining integration from the forward perpendicular and to this section.

4.3 Results and discussion

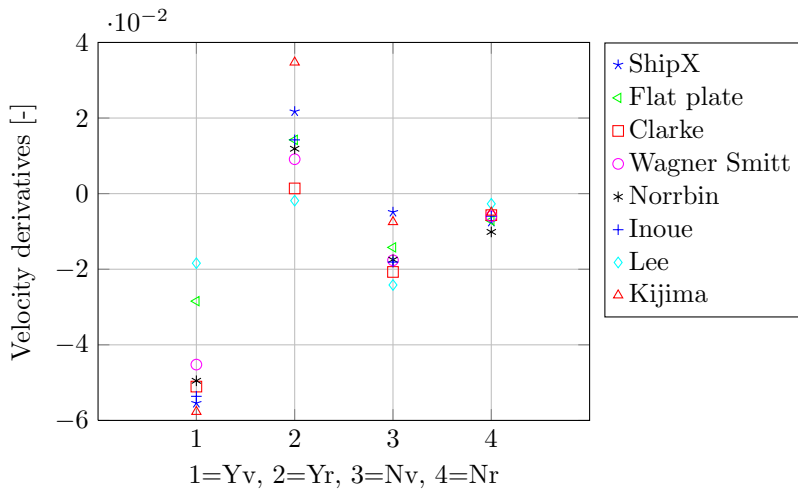
The calculated hydrodynamic coefficients for R/V Gunnerus are presented in the Tables 4.1 and 4.2, and in the Figures 4.4 and 4.5. As expected there are differences between the empirical methods as they are derived from different data sets. The results should be questioned as R/V Gunnerus is an unconventional vessel and differs significantly from the vessel used in the empirical methods. In Section 6.3 these hydrodynamic coefficients will be used in simulations of turning circle and zig-zag manoeuvres.

Table 4.1: Velocity derivatives calculated for R/V Gunnerus

	Y_v	Y_r	N_r	N_v
ShipX	-0.05542	0.02172	-0.00749	-0.00489
Flat plate	-0.028446	0.014223	-0.007111	-0.014223
Wagner Smitt	-0.045229	0.009103	-0.005974	-0.017636
Norrbin	-0.049512	0.011873	-0.010132	-0.017486
Inoue	-0.053625	0.014223	-0.005970	-0.018109
Clarke	-0.051047	0.001379	-0.005693	-0.020719
Lee	-0.018404	-0.0019	-0.002695	-0.024168
Kijima	-0.057696	0.034731	-0.0049843	-0.007492

Table 4.2: Acceleration derivatives calculated for R/V Gunnerus

	\bar{Y}_r	\bar{Y}_v	\bar{N}_r	\bar{N}_v
ShipX	0.00227	-0.02881	-0.00212	0.00227
Flat plate	0	-0.028446	-0.002370	0
Clarke	-0.005187	-0.021478	-0.000213	-0.006323

**Figure 4.4:** Velocity derivatives calculated for R/V Gunnerus.

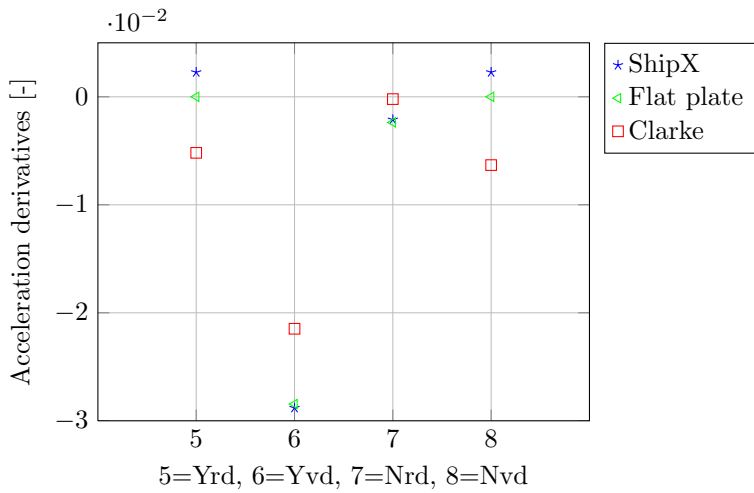


Figure 4.5: Acceleration derivatives calculated for R/V Gunnerus

Chapter 5

Full-scale trials

Field tests with R/V Gunnerus were carried out in deep water in Trondheimsfjorden from Monday 27 February to Thursday 1 March 2012. The trials were a part of NTNU's research cooperation with Rolls-Royce Marine University Technology Centre (UTC) "Performance in a Seaway".

Performing full-scale trials had two main objectives:

1. Investigate speed and manoeuvring performance
2. Obtain well-documented full-scale results of ship manoeuvres.

The first objective is due to installation of a new propulsion system on R/V Gunnerus. As the propulsion system it is going to be replaced by a new system it of great interest to document any changes in speed and manoeuvring performance. The second objective focuses on establishing of a data set that can be used to compare full-scale results with results from manoeuvring simulations and model tests. Prediction of manoeuvring performance and processing of full-scale manoeuvring trials are treated in this study.

During the four days in Trondheimsfjorden, speed trials, zig-zag tests, stopping tests, spiral tests and turning circles followed by pull-out tests were carried out. Turning circles, zig-zag manoeuvres and stopping tests are investigated in this study.

In this chapter a description of the instrumentation and an evaluation of the data parameters used in the analysis are provided. Further, a description of how the manoeuvres are analysed, and the results of the full-scale trials are presented.

Data from the full-scale trials and Matlab-scripts used to analyse the tests, as well as plots from the trials are provided on CD.

5.1 Instrumentation and data registration

R/V Gunnerus is equipped with Kongsberg Seapath 300 and the Dynamic Positioning (DP) system Kongsberg SDP-11/cPos. These systems were used to record necessary data during the trials. As the trials were carried out, the data was used to analyse the manoeuvres in order to obtain full-scale results for R/V Gunnerus.

5.1.1 Seapath

The Seapath 300 product is developed specifically for the hydrographic and other high precision applications where heading, position, roll, pitch, heave and timing are critical measurements. The product combines inertial technology together with GPS satellite signals. [22]

Seapath has two built-in GPS receivers for determination of position and velocity, which makes the system robust against GPS dropouts. If one GPS drops out, the other receiver will provide the vessel's position and heading, while an inertial sensor provides heading from its internal sensors.

Seapath registered data at 200 Hz. Table 5.1 shows parameters of interest obtained by Seapath and which scaling that is used.

Table 5.1: Parameters recorded by Seapath

Parameter	Scaling
Time, seconds	s
Time, fraction of second	0.0001 s
Latitude	$2^{30} = 90^\circ$
Longitude	$2^{30} = 90^\circ$
Heading	$2^{14} = 90^\circ$
North velocity	cm/s
East velocity	cm/s

Seapath register time as Unix time, which is the numbers of seconds after 1 January 1970 GMT time ignoring leap seconds. GMT time is one hour behind

Norwegian standard time. A conversion calculator are used to convert date and time to Unix time and vice versa [23].

5.1.2 DP-system

A vessel is subjected to forces from wind, waves and current. These forces represent the forces that the thrusters in a dynamic positioning (DP)- system must be able to balance in order to control the vessel's motion in the horizontal plane.

R/V Gunnerus is equipped with cPos, a compact DP control system. cPos is intended for smaller vessels and operations. On R/V Gunnerus is the system operation station located at the bridge and it provides control of the vessel using joystick, DP or autopilot. cPos may have following operational modes [24]:

- ***Joystick mode:*** Allows the operator to control the vessel manually using a joystick for position and heading control
- ***Auto Heading mode:*** Automatically maintains the required heading
- ***Auto Position mode:*** Automatically maintains the required position and heading
- ***Autopilot mode:*** Enables the vessel to steer automatically on a predefined course
- ***Track Line mode:*** Makes the vessel follow a specified track line

The DP-system registered many parameters, in Table 5.2 is some parameters of interest outlined. Data from the DP-system was registered at 1 Hz.

Table 5.2: Parameters recorded by the DP-system. PT and SB are used as abbreviations for respectively port and starboard.

Parameter	Description	Scaling
Thr2AziFeedb	Time	yyyy-mm-dd hh.mm.ss
Thr3AziFeedb	PT rudder angle	deg
UTMposMeasN1	SB rudder angle	deg
UTMposMeasE1	Latitude	UTM coordinates
Gyro1	Longitude	UTM coordinates
Gen1Power	Heading	deg
Gen2Power	Power generator 1	kW
Gen3Power	Power generator 2	kW
GPSspeed1	Power generator 3	kW
Thr2RpmFeedb	Speed of vessel	kn
Thr3RpmFeedb	PT propeller rpm	%
WindSpeed	SB propeller rpm	%
	Wind speed	kn

5.2 Analysis of trials

The test data is post-processed in Matlab in order to analyse the manoeuvres.

In this section is an evaluation of some of the parameters recorded by Seapath and the DP-system provided. Further follows a description of how the full-scale manoeuvres are post-processed, and finally the results are outlined.

5.2.1 Evaluation of data parameters

R/V Gunnerus' position, heading and speed are obtained by both Seapath and the DP-system. Three data sets are used to compare data from Seapath and the DP-system.

Data set 1: 1 March 2012 from 07:57:43 to 07:59:43 GMT. This set includes the beginning of the first manoeuvre (turning circle) that was carried out that day.

Data set 2: 27 February 2012 from 15:16:50 to 15:18:20 GMT. This set includes the beginning of a zig-zag manoeuvre.

Data set 3: The third set is from 27 February 2012 from 16:29:17 to 16:30:47 GMT. This set includes the beginning of a turning circle.

Position

The UTM-reference system is a Cartesian coordinate system with meter at its axes, and is used to give locations on the surface of the Earth. The Earth is divided into 60 zones that is used for map projection. Trondheim is located in zone 32V. In order to analyse the trials it is convenient to have R/V Gunnerus' position in UTM (Universal Tranverse Marcator)-coordinates (instead of latitude and longitude as Seapath uses) as it has meter on its axes.

Seapath gives R/V Gunnerus' position using latitude and longitude recorded in a binary format. As the trials were post-processed, the latitude and longitude were converted to degrees by multiplying them with $90/2^{30}$. Further, the latitude and longitude positions were converted into UTM-coordinates using the script deg2utm.m [25]. The DP-system give R/V Gunnerus' position directly in UTM-coordinates.

Ideally should the UTM-coordinates from Seapath and the DP-system be equal. However, this was not the case. An online UTM to latitude and longitude converter [26] was used to obtain the vessel's position, and then the vessel's position could be plotted in a map. Figure 5.1 shows the vessel's position 01/03/2012 at 07:57:43 GMT. Point A is the vessel's position given by Seapath and point B is its position given by the DP-system. The trials were performed in Trondheimsfjorden, and the position given by the DP-system is incorrect.

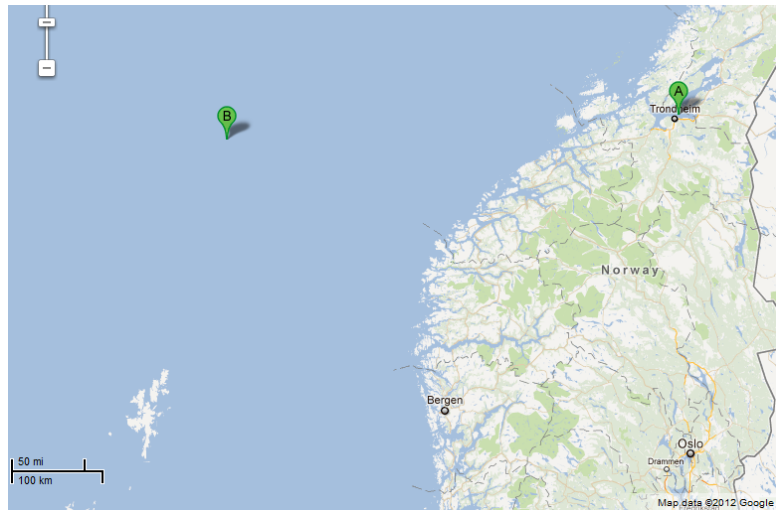


Figure 5.1: R/V Gunnerus' position at 01/03/2012 07:57:43 GMT. A is position (7038778.267843, 572663.804260) given by Seapath while B is the position (7038778.888000, 72662.912390) given by the DP-system.

In the Figures 5.2, 5.3 and 5.4 the first position of the trajectory is set as origin. Consequently it can be seen that Seapath and the DP-system give similar trajectories. As it is the vessel's relative movement that is of interest, it does not affect the results that R/V Gunnerus' position is not registered at the same location. In the mentioned figures the DP-system's data points are plotted. Figure 5.2 illustrates the problem that the DP-system did not update the position every second, and the trajectory is inadequate. This was the case for data from 1 March 2012, and was due to the settings the DP-system was operated with that day. A difference in the trajectories given by Seapath and the DP-system is shown in Figure 5.3 and Figure 5.4. The vessel turns later according to the positions given by the DP-system. In Figure 5.5 the positions from the DP-system are plotted with a delay of two seconds, and hence the trajectories correspond better with each other. It may then look like there is a delay of approximately two seconds in the registration of the position in the DP-system.

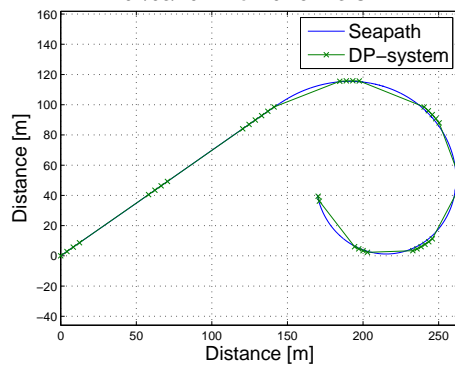


Figure 5.2: Trajectory of data set 1

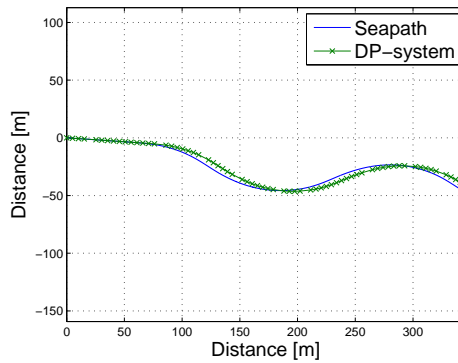


Figure 5.3: Trajectory of data set 2

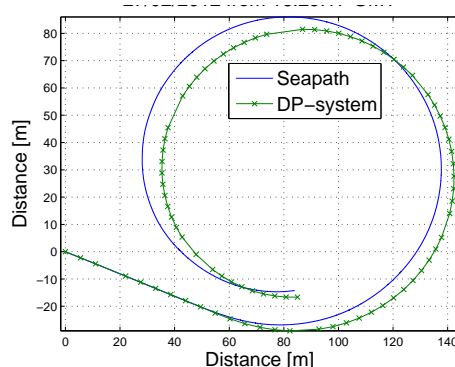


Figure 5.4: Trajectory of data set 3

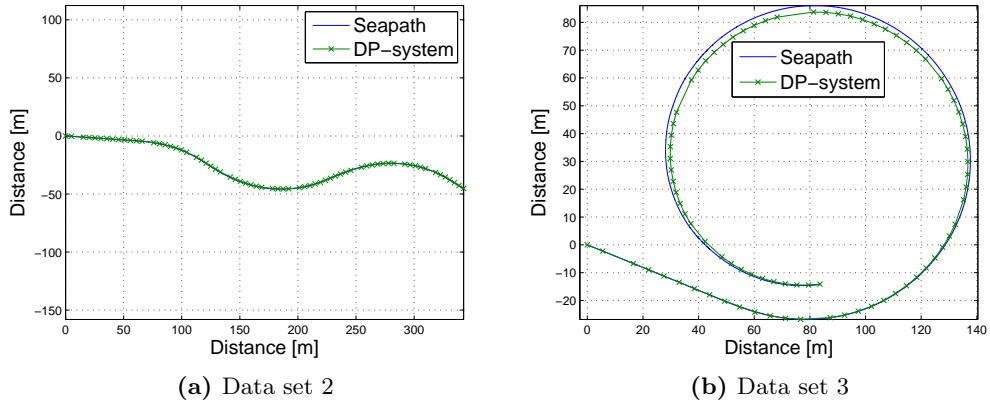


Figure 5.5: The trajectories of data set 2 and 3 are plotted with a two second delay on data from the DP-system

Heading

Seapath predicts R/V Gunnerus' heading using GPS, while the DP-system predicts the heading using gyro.

Heading and rudder angles versus time for data set 2 and data set 3 are plotted in Figure 5.6 and Figure 5.7. The heading at the start of the manoeuvre is set as origin. It can be seen that there is a small difference between the heading measured by Seapath and the DP-system. The heading given by the DP-system is however not always updated as often as it should. For instance, in the zig-zag manoeuvre in data set 2 the heading change is registered as 21.8° after both 28, 29 and 30 seconds, -11.4° after 41 and 42 seconds and -13.9° after 43 and 44 seconds.

It is also of interest to investigate how R/V Gunnerus responds to a change of rudder angles. From Figures 5.6 and 5.7 it may be seen that R/V Gunnerus change heading almost instantaneously as the rudder angles change. A short response time seems reasonable as R/V Gunnerus is a small vessel and she reacts quick according to the crew aboard.

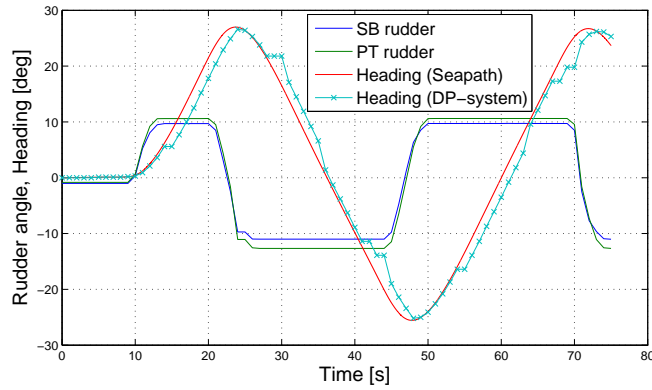


Figure 5.6: Heading and rudder angles versus time for data set 2

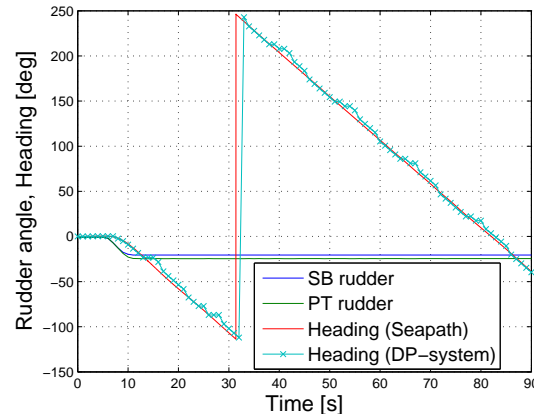


Figure 5.7: Heading and rudder angles versus time for data set 3

Speed

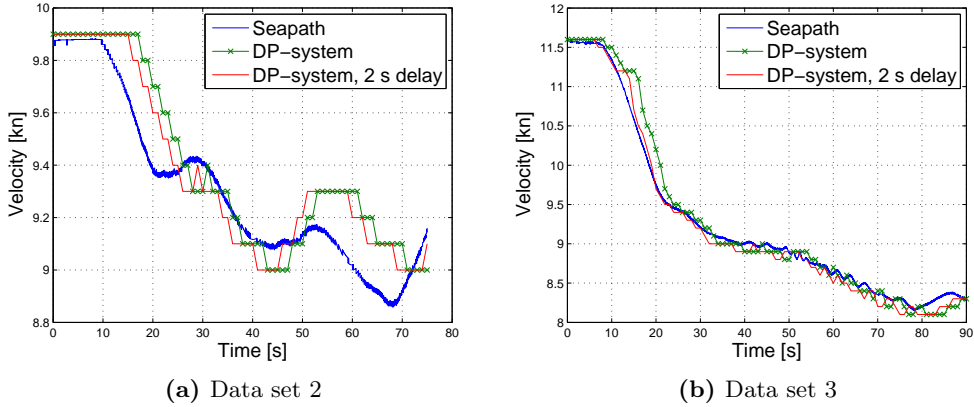


Figure 5.8: Speed versus time for data set 2 and 3

The ship speed for data sets 2 and 3 are plotted in Figure 5.8. Seapath uses GPS to measure R/V Gunnerus' velocity, which is given by north velocity and east velocity. Hence, the vessel's speed can be predicted as:

$$Speed = \sqrt{(NorthVelocity)^2 + (EastVelocity)^2}. \quad (5.1)$$

The DP-system provides R/V Gunnerus' speed directly. The speed is measured by GPS using a VTG telegram. The VTG telegram has usually a resolution of 0.01 kn or 0.01 m/s depending on what the GPS is set up to send [27]. However, in Figure 5.8 it can be seen that the speed is registered with a resolution of 0.1 kn.

Figure 5.8a shows that the speed measured by Seapath and the DP-system differs considerably for data set 2. There is also a varying delay in the registration of the heading. This was a frequent problem for the zig-zag manoeuvres.

The speed of R/V Gunnerus in a turning circle manoeuvre is shown in Figure 5.8b. In this case speed measured by the DP-system corresponds better with speed from Seapath. The speed from the DP-system is also plotted with a delay of two seconds. This may reduce the difference between Seapath and the DP-system, but it is difficult to evaluate.

Rudder angles

R/V Gunnerus is equipped with two rudders, which in this study are referred to as SB (starboard) rudder and PT (port) rudder. The rudder angles are recorded every second using the DP-system. The rudder angles are registered with an offset on approximately 1° to port. The reason for this is not known, but two possible reasons are suggested. The rudders may have this offset, or it may be some errors in the data registration. It can be recommended that the rudders position should be investigated during a dry docking. Furthermore, the offset will not be corrected for in the analysis.

Wind speed

The wind speed is measured by the DP-system using a wind sensor. There is a parameter, `WindSpeed1[kn]` (not used in this thesis), which register the wind speed at the sensor. The parameter `WindSpeed[kn]` gives the DP-model's wind speed, i.e. a filtered value that takes the speed of the vessel into account [27]. The wind speed varies with time as it can be seen in Figure 5.9. Average wind speed is calculated as the mean value of the wind speed in a time interval, typically a manoeuvre.

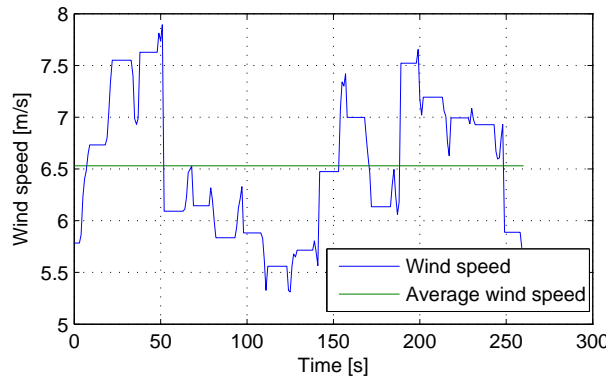


Figure 5.9: Wind speed during a turning circle

Power

R/V Gunnerus' main electric propulsion is at $2 \times 500\text{ kW}$, and its consumption can be controlled from the bridge by the captain. Three generators of 450 kW each provide the vessel with power. The DP-system register the power at each

generator. In Figure 5.10 power consumption is plotted versus time for a 2×142 kW turning circle. The given power is the sum of the power from the three generators, which includes the propulsion power as well as all other power consumption aboard.

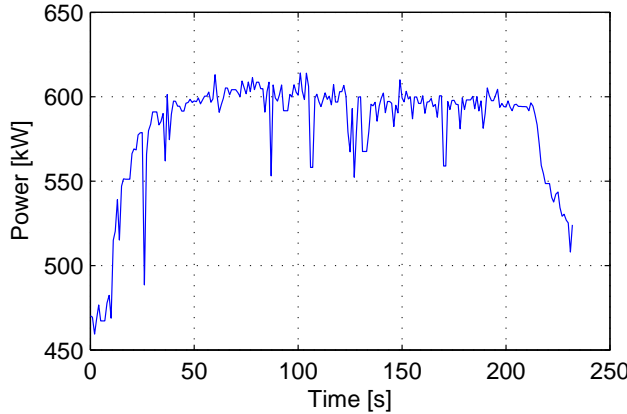


Figure 5.10: Power consumption during a turning circle

Propeller rotation

The propeller's rotation are recorded by the DP-system and are given as a percentage value. After the trials had been conducted it have been tried to find which value that is set as 100 %, but this was not obtained.

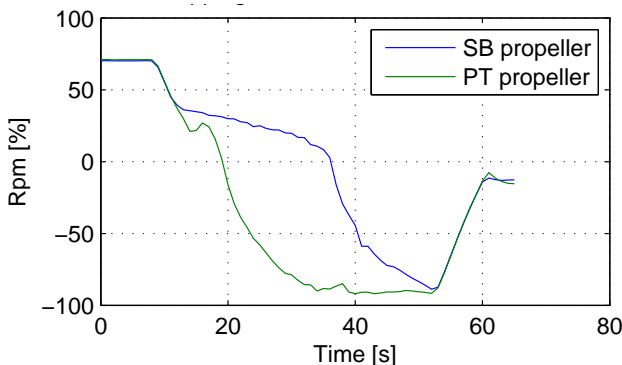


Figure 5.11: Propeller rpm during a stopping test

The propeller's rpm is of interest in a stopping manoeuvre. In Figure 5.11 is

propeller rpm plotted versus time for a stopping test. As it can be seen in Figure 5.11, SB propeller reverses slower than PT propeller. Siemens, which delivered the main electric propulsion, was contacted to find out what was causing this problem. No reasons were detected, except that it is probably due to an error in the propulsion unit.

Data to be used in the analysis

The decision of what data that was going to be used in the analysis of the manoeuvres had to be based upon the observations stated above. It is also necessary to mention that sometimes when the vessel was subjected to large and sudden movements the GPS system used to predict the vessel's position in the DP-system dropped out. The vessel's position and speed given by the DP-system were in these incidents incorrect.

Since the positions and velocity were recorded too seldom by the DP-system 1 March 2012, it was necessary to use the position and velocity data from Seapath. Turning circles were carried out both 27 February and 1 March. The same parameters should be used in order to compare the tests from the various days. Hence, the position and speed from Seapath are used.

Position and velocity data from Seapath are used for the other manoeuvres as well. This is because Seapath is considered more accurate. In addition, the data in the DP-system is recorded once per second, which is too seldom as R/V Gunnerus responds quickly. The other data are obtained by the DP-system, since these parameters only are recorded by the DP-system.

It has been questioned whether there is a delay in the data registration in the DP-system. As this is not certain, it has not been corrected for. It is however necessary to consider it when the results are being evaluated.

5.2.2 Turning circles

Turning circles were performed Monday 27 February and Thursday 1 March 2012. Both days were 720° turning circles with 20° and 35° rudder angles to starboard and port carried out. The trials were executed with an engine power of $2 \times 425\text{ kW}$ and $2 \times 142\text{ kW}$, which correspond to 85% MCR and 28.4% MCR.

The rudder angles and engine power were controlled manually by the captain aboard, but the rudder angles and power could also be given by the DP-system.

Turning circles carried out Monday 27 February 2012 were performed with incorrect rudder angles. For instance, what was supposed to be a 35° turning circle was carried out with SB rudder angle at 42.9° and PT rudder angle at 36.1° . This was caused by incorrect factors in the DP-system and was corrected Tuesday 28 February 2012. It was however necessary to carry out a new set of turning circles with correct rudder angle, which was done 1 March 2012.

Post-processing

In this section follows a description of how the turning circles are post-processed. Flow chart is given i Appendix A.4.1, and Matlab-scripts and additional plots are provided on CD. Parameters from the DP-system that are used are rudder angles, wind speed and generator power. Time, latitude, longitude, heading, east velocity and north velocity are imported from Seapath.

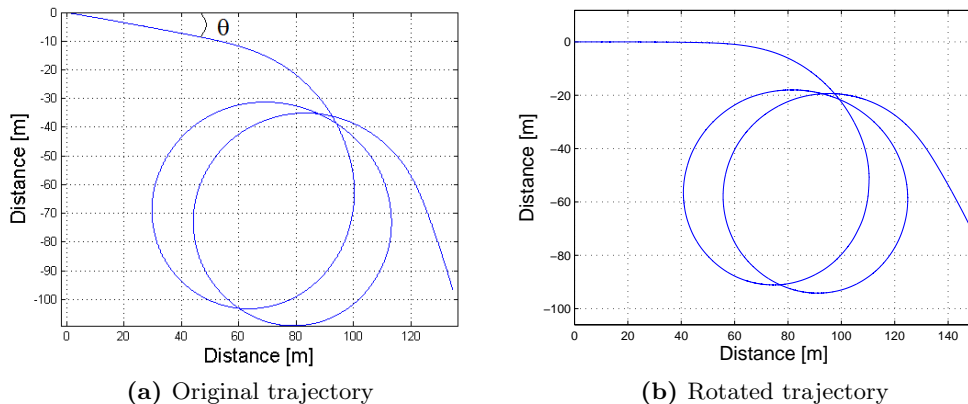


Figure 5.12: Turning circle trajectory before and after rotation of trajectory

One turning circle manoeuvre is investigated at a time by defining its time range. This first position of a test is defined as origin, see Figure 5.12a. In order to get the vessel's start course along the x-axis, the trajectory are rotated using the transformation matrices. A rotated trajectory is presented in Figure 5.12b. For rotation by an angle θ clockwise about the origin is the transformation matrix expressed as:

$$\begin{bmatrix} x' \\ y' \end{bmatrix} = \begin{bmatrix} \cos \theta & \sin \theta \\ -\sin \theta & \cos \theta \end{bmatrix} \begin{bmatrix} x \\ y \end{bmatrix}, \quad (5.2)$$

where x and y are the original position coordinates and x' and y' are the rotated coordinates.

Likewise for a counter clockwise rotation is the transformation matrix given as:

$$\begin{bmatrix} x' \\ y' \end{bmatrix} = \begin{bmatrix} \cos \theta & -\sin \theta \\ \sin \theta & \cos \theta \end{bmatrix} \begin{bmatrix} x \\ y \end{bmatrix}. \quad (5.3)$$

Further, rudder angles versus time are plotted, see Figure 5.13.

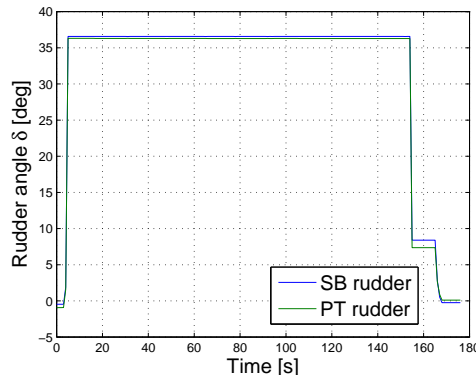


Figure 5.13: Rudder angles during a turning circle

Wind, waves and current affect the vessel's manoeuvrability. These environmental forces can make it difficult for the vessel to maintain its course. Another consequence may be varying resistance to the vessel's forward motion, which will result in varying demand of power to achieve a given speed. For this reasons the manoeuvring trials should be carried out in calm weather conditions. This was not the case for the full-scale trials with R/V Gunnerus, and a correction of the trajectory was required. The corrections are predicted using IMO's Prediction Guidance [4]. The effect of a constant current can be estimated when a turning circle of at least a 720° change of heading has been performed and the vessel's track, heading and elapsed time are recorded. The positions (x_{1i}, y_{1i}, t_{1i}) and (x_{2i}, y_{2i}, t_{2i}) , see Figure 5.14, are used to predict the current velocity. Eight points are chosen manually, such that four local current velocities are predicted. The local current velocity vector, \vec{v}_i for two corresponding positions can be estimated as:

$$\vec{v}_i = \frac{(x_{2i} - x_{1i}, y_{2i} - y_{1i})}{(t_{2i} - t_{1i})}, \quad (5.4)$$

where x and y are positions and t is time. Further, the current velocities in x- and y-direction, v_{cx} and v_{cy} , can be taken as:

$$\vec{v}_c = \begin{bmatrix} v_{cx} \\ v_{cy} \end{bmatrix} = \begin{bmatrix} \frac{1}{n} \sum_{i=1}^n \frac{x_{2i} - x_{1i}}{t_{2i} - t_{1i}} \\ \frac{1}{n} \sum_{i=1}^n \frac{y_{2i} - y_{1i}}{t_{2i} - t_{1i}} \end{bmatrix}. \quad (5.5)$$

When the current velocity, \vec{v}_c , is predicted from a 720° turning test it also includes the effect of wind and waves.

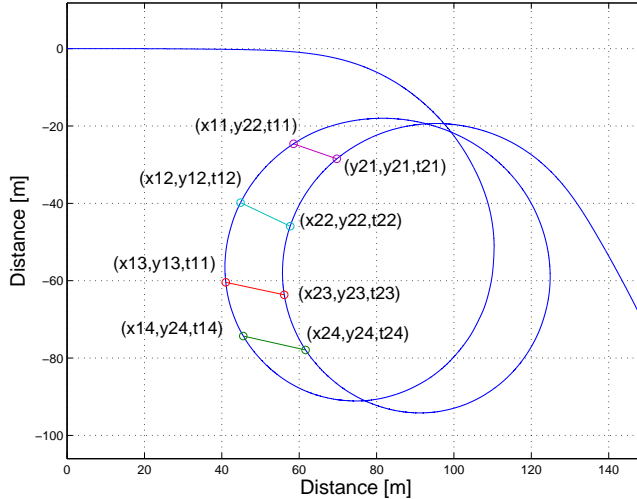


Figure 5.14: Trajectory of a turning circle with points used to predict local current velocity are marked.

Subsequently were all trajectories corrected according to:

$$\begin{aligned} \vec{x}'(t) &= \vec{x}(t) - v_{cx} \vec{t} \\ \vec{y}'(t) &= \vec{y}(t) - v_{cy} \vec{t}, \end{aligned} \quad (5.6)$$

where $\vec{x}(t)$ and $\vec{y}(t)$ are measured x- and y-position vectors, $\vec{x}'(t)$ and $\vec{y}'(t)$ are the corrected position vectors, and t is time. A corrected trajectory is shown in Figure 5.15.

Transfer and advance are measured as the vessel has a 90° change of heading after rudder execute, while tactical diameter are measured at a 180° change of heading. In this study the trials are defined such that rudder execute is three seconds after

start of the trial. Finally a plot of the turning circle trajectory with transfer, advance and tactical diameter marked is presented, see Figure 5.15.

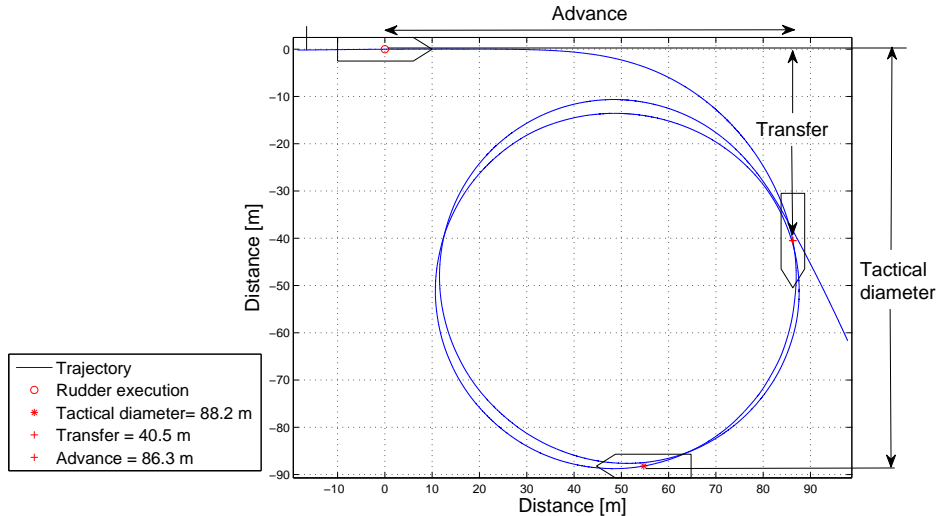


Figure 5.15: Presentation and explanation of turning circle results

Results and discussion

Plots of trajectory with correction point and corrected turning circles with results are provided in Appendix A.4.1. Every trial's tactical diameter, transfer and advance as well as trial conditions are outlined in the Tables 5.3, 5.4, 5.5 and 5.6. The test's approach speed and generator power are recorded at the start of rudder execution, while average wind speed is the mean value of the wind speed during the test. The given power includes engine power as well as all other power consumption aboard.

The turning circles are carried out to both starboard and port. Ideally, under similar conditions turning circles to starboard and port should give similar results. But the full-scale results differ. The turning circle carried out Monday 27/02/2012 show relatively good similarity between starboard and port turn. These tests were carried out with varying rudder angles, and the wind speed was lower than at the trials performed Thursday 01/03/2012. The tests are however corrected for environmental conditions.

More turning circle manoeuvres must be carried out in order to predict the precision error of the full-scale trials.

Table 5.3: Results and trial conditions for turning circles carried out 27/02/2012 with 2×425 kW

		20° SB	20° PT	35° SB	35° PT
Tactical diameter	[m]	110.5	113.2	83.1	80.3
Transfer	[m]	52.4	51.4	37.6	34.3
Advance	[m]	89.2	92.4	77.2	73.7
PT rudder angle	[°]	20.5	20.6	37.0	36.1
SB rudder angle	[°]	22.4	24.5	40.6	42.8
Approach speed	[kn]	11.8	11.6	11.9	11.6
Average wind speed	[m/s]	4.9	4.3	2.7	2.3
Power	[kW]	1119	1113	1126	1119

Table 5.4: Results and trial conditions for turning circles carried out 27/02/2012 with 2×142 kW

		20° SB	20° PT	35° SB	35° PT
Tactical diameter	[m]	110.7	112.6	88.1	88.9
Transfer	[m]	52.6	47.2	40.9	36.9
Advance	[m]	86.6	91.6	77.2	83.9
PT rudder angle	[°]	20.5	20.7	36.9	36.1
SB rudder angle	[°]	22.4	24.5	40.5	42.9
Approach speed	[kn]	9.6	8.9	9.6	9.3
Wind speed	[m/s]	4.8	6.0	4.0	4.4
Power	[kW]	471	477	468	463

Table 5.5: Results and trial conditions for turning circles carried out 01/03/2012 with 2×425 kW

		20° SB	20° PT	35° SB	35° PT
Tactical diameter	[m]	115.9	130.0	88.2	78.9
Transfer	[m]	54.4	56.1	40.5	34.5
Advance	[m]	110.4	98.6	86.3	84.4
PT rudder angle	[°]	20.4	18.5	36.3	33.8
SB rudder angle	[°]	20.2	20.2	36.6	36.4
Approach speed	[kn]	12.3	11.9	12.3	12.0
Wind speed	[m/s]	7.0	6.2	5.9	5.7
Power	[kW]	1109	1127	1119	1120

Table 5.6: Results and trial conditions for turning circles carried out 01/03/2012 with 2×142 kW

		20° SB	20° PT	35° SB	35° PT
Tactical diameter	[m]	121.2	127.2	89.0	86.2
Transfer	[m]	52.7	51.8	34.6	36.9
Advance	[m]	97.8	120.7	89.3	87.1
PT rudder angle	[°]	20.4	18.7	36.3	33.8
SB rudder angle	[°]	20.2	20.3	36.5	36.4
Approach speed	[kn]	9.8	9.7	9.7	9.8
Wind speed	[m/s]	6.5	6.2	6.8	5.8
Power	[kW]	449	457	459	455

5.2.3 Zig-zag trials

Zig-zag trials were carried out Monday 27 February 2012. $10^\circ/10^\circ$ test and $20^\circ/20^\circ$ test at both 2×425 kW and 2×250 kW were performed. The manoeuvres were operated using a predefined program in the DP-system.

In retrospect it has been seen that the solution of operating the zig-zag manoeuvres using the DP-system did not work properly as the rudders shifted too late. In a $10/10$ ($20/20$) manoeuvre, the rudders are ordered to 10° (20°) to starboard/port. When a 10° (20°) change of heading from the base course is obtained, the rudders should be shifted to 10° (20°) to port/starboard, but this did not happen. At what heading the rudders shifted are found using the plot of heading and rudder angles versus time, see Appendix A.4.2. For the $10/10$ zig-zag manoeuvre at 2×425 kW are the first four rudder changes at respectively 29.2° , 26.6° , 26.8° and 24.4° change of heading. The manoeuvre's heading change is then estimated as the average of the four heading changes, which in this case is 27° . Hence, this test is not a $10/10$ manoeuvre, but a $10/27$ manoeuvre.

Post-processing

The zig-zag manoeuvres are post-processed using Matlab. Flow chart is presented in Appendix A.4.2, while Matlab-scripts and additional plots are provided on CD. UTM positions, rudder angles, heading and power are imported from the DP-system, while latitude, longitude, heading, speed north velocity and east velocity are imported from Seapath.

The full-scale zig-zag manoeuvres were carried out such that the ship heading passed the base course more than five times. In the post-processing is the range of a manoeuvre defined such that the ship heading pass the base course at least three times. A test's trajectory is plotted in Figure 5.16. The vessel's heading at first execute are defined as origin. Then the vessel's heading and rudder angles versus time are plotted, see Figure 5.17. Furthermore, the vessel's speed, wind speed and power consumption during the manoeuvre are plotted.

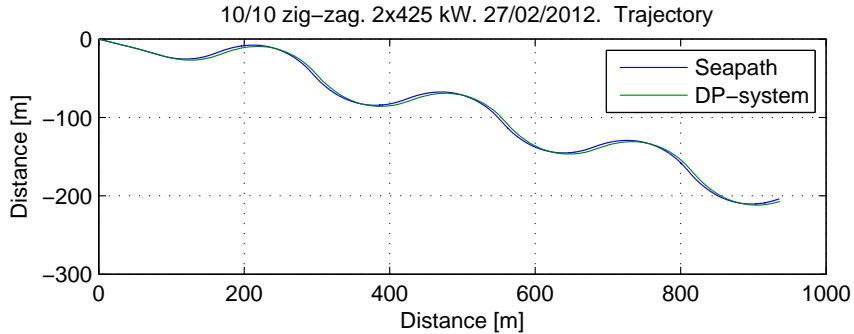


Figure 5.16: Trajectory of a 10/10 zig-zag manoeuvre

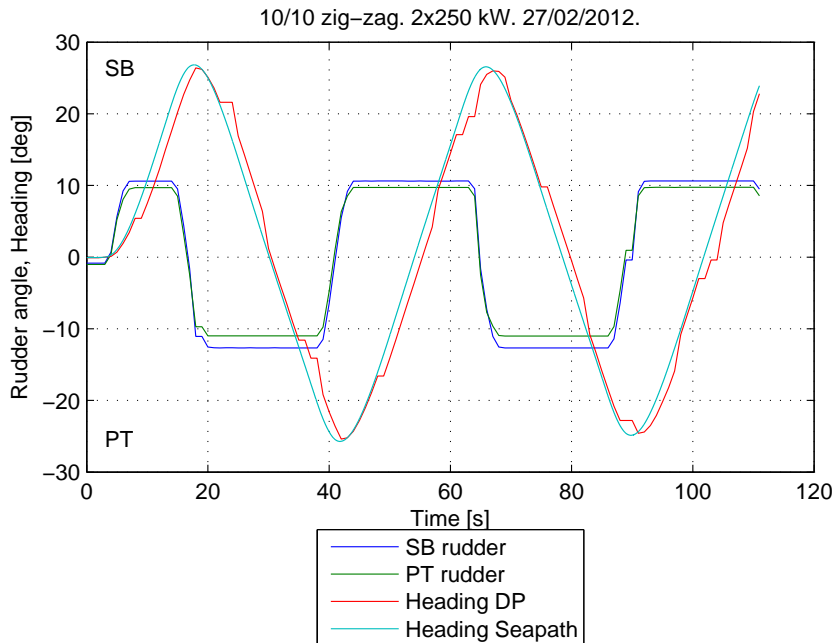


Figure 5.17: Heading and rudder angles versus time in a zig-zag manoeuvre

Results and discussion

The results of the zig-zag manoeuvres are read by the plots of heading and rudder angles versus time, see Appendix A.4.2. It can be questioned how accurate this reading is. In Table 5.7 the essential information from the manoeuvres is provided. The overshoot angles are defined as the difference between maximum heading change and the heading change when the rudders are shifted. In Table 5.7 the overshoot angles are predicted using two definitions. The first definition uses the heading change when the rudders are shifted, while the other (overshoot angle, average) uses the average change of heading. The power indicates the generator power at the start of first rudder execution, and it includes engine power as well as other power consumption aboard.

10/27, 10/21, 20/44 and 20/39 manoeuvres were obtained instead of 10/10 and 20/20 manoeuvres. In these zig-zag manoeuvres it was high speed and large motions. In addition, there is strict requirements to registration of heading change and response to rudder. The DP-system is not intended for operations like this. From the plots of heading and rudder angles versus time it looks like the rudders are shifted approximately 5 s too late. This might be explained by the fact that the frequency of the DP-controller is 1 Hz, i.e. in worst case it may take 2-3 s before the command is given from the DP-system to the rudder. After that, the rudders must be shifted, which also takes time. Hence, a delay of 5 s seems reasonable. It may be concluded that for R/V Gunnerus, a small vessel that responds rapidly, the DP-system is too slow for zig-zag manoeuvres [27].

The full-scale zig-zag manoeuvres can not be compared with 10/10 and 20/20 manoeuvres, but should be compared with 10/27, 10/21, 10/44 and 20/39 tests. However, a solution of how 10/10 and 20/20 test can be obtained should be found.

Table 5.7: Results and trial conditions for zig-zag manoeuvres

		2 × 425 kW 10/10	2 × 250 kW 20/20	2 × 250 kW 10/10	2 × 250 kW 20/20
Approach speed	[kn]	12.0	11.6	9.9	10.8
Heading change, average	[°]	27	44	21	39
Time before 1st counter rudder	[s]	12	12	11	12
Time from 1st counter rudder to 1st overshoot angle	[s]	3.0	4.5	3.8	5.8
Time from 2nd counter rudder to 2nd overshoot angle	[s]	2.8	4.8	3.6	3.7
Time from 3rd counter rudder to 3rd overshoot angle	[s]	3.8	5.9	2.9	6.0
1st overshoot angle	[°]	4.6	12.1	5.4	14.8
2nd overshoot angle	[°]	4.0	13.2	5.4	6.8
3rd overshoot angle	[°]	6.8	17.8	3.4	14.8
4th overshoot angle	[°]	6.4	18.0	5.5	14.4
1st overshoot angle, average	[°]	7.0	15.8	5.4	13.4
2nd overshoot angle, average	[°]	3.9	15.8	5.4	12.2
3rd overshoot angle, average	[°]	6.8	13.5	3.4	13.8
4th overshoot angle, average	[°]	4.0	15.8	5.5	11.6
SB rudder angle to SB	[°]	10.6	22.4	10.6	22.4
SB rudder angle to PT	[°]	12.7	24.6	12.7	24.6
PT rudder angle to SB	[°]	9.8	20.6	9.7	20.5
PT rudder angle to PT	[°]	11.0	20.7	11.0	20.7
Power	[kW]	1108	1117	683	672

5.2.4 Stopping tests

Three stopping were executed Tuesday 28 February 2012:

Stopping test 1: Carried out with an engine power of 2×142 kW. Operated by the captain at R/V Gunnerus.

Stopping test 2: Carried out with an engine power of 2×425 kW. Operated by the captain at R/V Gunnerus.

Stopping test 3: Carried out with an engine power of 2×142 kW. Operated using the DP-system.

Post-processing

The post-processing of the stopping manoeuvres is performed using Matlab. Flow chart is given i Appendix A.4.3, and Matlab-scripts and additional plots are provided on CD. Information about position, rudder angles, propeller rpm, speed, generator power and wind speed are obtained from the DP-system. While latitude, longitude, north velocity and east velocity are given by Seapath.

The test data are first imported to Matlab. Then latitude and longitude are converted to UTM-coordinates. Each stopping test is defined by its time range. The transformation matrices are used to get the test's start course along the axis. The start of a stopping manoeuvre is when the propellers start to reverse, while the manoeuvre is finished when the ship is dead in water. In this case the ship is said to be dead in water when the speed is at its minimum. After this point the speed is negative, but this cannot be seen in the velocity plot as the the speed is predicted as an absolute value. Furthermore, the rotated stopping trajectory is plotted, and lateral deviation, head reach and track reach are predicted. In addition are information regarding ship speed, propeller rpm and generator power at the start of the manoeuvre as well as average wind speed found.

Results and discussion

The trajectory and results of the stopping tests are presented in Appendix A.4.3. In Table 5.8 the results are provided along with trial conditions. Power and maximum revolution are given at the start of propeller reversing. It is not know what rpm that is set as 100 %.

As mentioned in Section 5.2.1, SB propeller reversed slower than PT propeller. A consequence of this is higher time to reverse revs. More tests must be carried out in order to predict the prediction error of the full-scale trials.

Table 5.8: Results and trial conditions for stopping tests

		Stopping test 1	Stopping test 2	Stopping test 3
Lateral deviation	[m]	4.4	11.8	2.9
Head reach	[m]	152.7	186.8	130.9
Track reach	[m]	154.8	189.2	132.4
Approach speed	[kn]	9.6	12.1	9.5
Max revolutions astern	[%]	70.2	98.9	69.8
Power	[kW]	465	1087	469
Average wind speed	[m/s]	8.3	7.3	8.1
Time to Reverse revs	[s]	49	56	46
Average wind speed	[m/s]	8.3	7.3	8.1

Chapter 6

Simulations in ShipX

ShipX Manoeuvering is a plug-in to the hydrodynamic workbench ShipX which is developed at MARINTEK. ShipX can be used to perform several hydrodynamic analysis of a vessel in a design stage. ShipX is originally developed for investigation of conventional cargo ships (bulk carriers, container ship etc.). During the last years it has been improved such as it is valid for more modern vessel's (such as offshore vessels) as well. Simulation of manoeuvring trials can be performed using ShipX Manoeuvring Plug-In. The plug-in consists of two software tools; HullVisc and SIMAN. The manoeuvring trials are performed in SIMAN, while Hull-Visc is a pre-processor to SIMAN and calculates hydrodynamic data of the vessel. The hydrodynamic data is calculated based on the vessel's general arrangement plan and loading condition. While information regarding rudders, propellers and environmental conditions must be provided to SIMAN. ShipX Manoeuvring Plug-In is in this study referred to as ShipX or SIMAN.

In this chapter full-scale manoeuvring trials are simulated in SIMAN. In order to be able to evaluate the results a description of the method used in the simulations is provided. R/V Gunnerus is significantly smaller and has a different hull shape than the vessels that SIMAN is developed for. As R/V Gunnerus is outside SIMAN's application range, it is expected that there will be differences between the measured field results and SIMAN-simulations. Parameters that may influence the full-scale results are investigated.

6.1 Method

The method described in this section is based on [21] and [28]. A 3-DOF model, including surge, sway and yaw, are used to describe the vessel's motions. This 3-DOF model is an modified version of the 3-DOF model presented in Section 3.1. The equations of motion used in SIMAN are expressed as:

$$(M - X_{\dot{u}})\ddot{u} = (M + X_{vr})vr + (Mx_G + X_{rr})r^2 + X_{res} + X_{vv}v^2 + X_{vvvv}v^4 + X_{prp} + X_{rud} + X_{thr} + X_{cu} + X_{wa} + X_{tug} \quad (6.1)$$

$$(M - Y_{\dot{v}})\ddot{v} + (Mx_G - Y_{\dot{r}})\dot{r} = -Mur + Y_vv + Y_{Uv}Uv + Y_r r + Y_{Ur}Ur - X_{\dot{u}}ur + Y_{cf} + Y_{prp} + Y_{rud} + Y_{thr} + Y_{wi} + Y_{cu} + Y_{wa} + Y_{tug} \quad (6.2)$$

$$(I_{zz} - N_{\dot{r}})\dot{r} + (Mx_G - N_{\dot{v}})\dot{v} = -Mx_{Gur} + N_r r + N_{Ur}Ur + N_v v + N_{Uv}Uv + N_{cf} + N_{prp} + N_{rud} + N_{thr} + N_{wi} + N_{cu} + N_{wa} + N_{tug}, \quad (6.3)$$

where:

- m and I_{zz} are ship mass and mass moment of inertia;
- Y_v , N_r , Y_r and N_v are velocity coefficients for linear damping;
- $X_{\dot{u}}$, $Y_{\dot{v}}$, $N_{\dot{r}}$, $Y_{\dot{r}}$ and $N_{\dot{v}}$ are acceleration coefficients for linear damping;
- Y_{Uv} , Y_{Ur} , N_{Uv} and N_{Ur} are the Froude number influence;
- X_{res} is ship resistance;
- X_{vr} and X_{rr} are coefficients for ideal fluid force contribution;
- X_{vv} and X_{vvvv} are coefficients for force contribution at drift angle;
- \dot{u} and u are surge acceleration and velocity;
- U is total ship speed;
- \dot{v} and v are sway acceleration and velocity;
- \dot{r} and r are yaw acceleration and velocity;
- x_g is distance of centre of gravity from midship;

and the subscripts indicates:

- cf is cross-flow non-linear damping;
- prp , rud and thr are contribution from propeller, rudder and tunnel thruster and

wi, *cu*, *wa* and *tug* are external contributions from wind, current, waves and tugs.

A description of how the velocity and acceleration coefficients for linear damping are predicted is given in Section 4.2.7.

The non-linear damping is calculated according to the cross-flow principle. The linear sway and yaw derivatives are predicted using potential flow calculations, which lead to a lack of transverse forces in the aft body. Consequently, a cross section in the aft where it is assumed that flow separation occurs is introduced. At small drift angles the section in the aft ship with most curvature is defined as the separation section. In front of the separation section it is assumed that there is no non-linear transverse force, while aft of it cross-flow drag is present. This non-linear damping is calculated as a transverse cross-flow force, where the sectional cross-flow force acting on a vessel may be calculated as described in Section 2.6 as:

$$Y_{cf} = \frac{1}{2}\rho \int U(x)^2 C_{cf}(x) T(x) dx, \quad (6.4)$$

where $C_{cf}(x)$ is a sectional cross-flow drag coefficient. The sectional cross-flow drag coefficient is of quadratic form. The cross-flow drag coefficient is estimated based on data available in the literature. The coefficient is given for forebody hull-sections, midbody sections and aftbody sections as a function of B/T . The flow condition at large drift angles, β , is taken into account by assuming that the section for flow separation moves forward with increasing drift angle. It is then assumed that the complete hull is subjected to cross-flow force and moment at $\beta = 90^\circ$. Similar, it is assumed that when the yaw velocity angle, γ , equals 90° the complete hull is subjected to cross-flow force and moment.

The longitudinal ship resistance can be calculated using either Holtrop's empirical method, an automatic polynomial method or a manual method. Using the automatic polynomial method, HullVisc will generate polynomial coefficients for the resistance based on Holtrop's method, but they are modified based on MARINTEK's resistance database. Using the manual polynomial database enables the user to specify the resistance curve for the ship or a similar ship.

The coefficients Y_{Uv} , Y_{Ur} , N_{Uv} and N_{Ur} should take the effect of Froude number on linear damping into account. At the moment they are however set as zero as they are difficult to calculate.

The effect of drift angle is taken into account by the coefficients X_{vv} and X_{vvvv} , which improve the calculation with regard to speed loss.

A description of how the propeller and rudder forces are predicted is given in [21]

and [28].

6.2 Simulation of full-scale trials

6.2.1 Ship model

A ShipX model of R/V Gunnerus was established for MARINTEK during the vessel's design stage. The vessel's lines and principle characteristics are defined in this ship model. Loading conditions for design waterline ($T = 2.9$ m) and normal operative ($T = 2.6$ m) were established. In order to use the ShipX Manoeuvring Plug-in, the ship model had to be further developed. As a part of the project thesis [3] a loading condition with draught at 2.6 m and service speed at 9.4 kn was established. This condition was investigated in resistance tests in model-scale [29].

Tuesday 28 February 2012 R/V Gunnerus was measured with $T_m = 2.75$ m, $T_{FP} = 2.23$ m and $T_{AP} = 3.33$ m. The draughts were measured manually by the crew aboard to the best of theirs ability. The manoeuvring trials should be simulated in conditions as similar to the full-scale conditions as possible. For that reason a new loading conditions with $T = 2.75$ m and trim was created. The ShipX vessel is provided on CD.

ShipX Manoeuvring Plug-In consists of HullVisc and SIMAN. HullVisc calculates the hydrodynamic data. In HullVisc it is specified that the vessel is a conventional merchant vessel. Some hull and thruster data as well as service speed must be provided here. It is also specified that the resistance should be calculated using Holtrop's empirical method. The resistance prediction methods' impact on the manoeuvring were investigated in the project thesis [3]. The resistance was then calculated using polynomials obtained from model test. This showed that at a loading condition with $T = 2.6$ m, the resistance method had a negligible impact on the manoeuvring characteristics. Hence, it is expected that Holtrop's method is suitable for the full-scale loading condition as well.

SIMAN requires information regarding hull, propulsion, rudder and environment. The necessary input data was obtained from specifications in Appendix A.1, model test [29], general arrangement drawings and information from the crew aboard R/V Gunnerus. The information from the general arrangement drawings are predicted using the software program DraftSight. No information regarding the bow thruster is specified as this thruster will not be in use during the simulated manoeuvring tests. No environmental effects are

selected.

Wake fraction and thrust deduction must be specified in ShipX Manoeuvring Plugin. w and t are predicted for R/V Gunnerus in the model tests. The model tests were performed with $T = 2.6$ m and velocities from 8.0 kn to 14.0 kn. As this is the only available information, a sensitivity analysis of how wake and thrust deduction influence the results of a turning circle manoeuvre is carried out, see Appendix A.5.1. Based on the sensitivity analysis it was chosen to run the simulations with $w = 0.260$ and $t = 0.280$, as it was done in the initial simulation in the project thesis [3].

6.2.2 Manoeuvres

Turning circles, zig-zag manoeuvres and stopping tests are simulated in SIMAN. As far as it is possible, the manoeuvres should be simulated with similar conditions as the full-scale trials. Every manoeuvre is simulated at the loading condition with $T_m = 2.75$ m and trim where $T_{AP} = 3.33$ m.

Simulations of R/V Gunnerus in ShipX have shown that the vessel is symmetric as she obtains similar results for simulations to both starboard and port [3]. Hence, whether a manoeuvre is performed to either starboard or port should not have any influence on the results.

Turning circle

In order to simulate a turning circle manoeuvre rudder angle, maximum heading, service speed (also referred to as approach speed) and direction of turn must be specified. The rudder angle and maximum heading can be given with a precision of 1.0° , which is poorer than the data from the field tests. R/V Gunnerus is equipped with two rudders, but the rudder angles in the simulations can not be specified individually. The rudder angles used in the simulations are therefore set as the average of the two rudder angles from the full-scale trials. The approach speed can be given with a precision of 0.1 kn, which is as good as a steady speed was measured.

The turning circles are simulated with a maximum heading of 360° , i.e. a 360° turning circle.

Zig-zag manoeuvre

In a zig-zag manoeuvre rudder change, heading change and service speed (approach speed) must be specified. The direction of first turn and number of overshoot angles to be calculated (from one to four) must also be decided. Rudder change and heading change can be specified with a precision of 1.0° , while service speed has a precision of 0.1 kn.

Stopping test (Full astern stopping)

The stopping manoeuvre in SIMAN is called Full astern stopping. In this manoeuvre rudder angle and service speed (approach speed) must be specified. Rudder angle and approach speed can be given with a precision of 1.0° and 0.1 kn.

The manoeuvre can be simulated by either controlling propeller revolutions or controlling propeller pitch. As R/V Gunnerus has fixed pitch propellers, the stopping tests were carried out by controlling propeller revolutions. Necessary input data to this simulation is time to reverse revolutions and max revolutions astern. Time to reverse revolutions is the time it takes to go from the propeller revolutions at service speed to maximum revolutions astern, which is found from the full-scale trials. Max revolutions astern is the desired maximum propeller revolutions astern and it is predicted by SIMAN.

The stopping test are simulated with 0° rudder angle as this was done in the full-scale trials.

6.2.3 Results and discussion

The results of the simulations are presented in the Tables 6.1, 6.2 and 6.3. Together with the results are rudder angles and approach speed from both simulations and field tests given. The results from the simulations are compared with full-scale results. *Dif* states how many percent larger SIMAN results are compared to measured full-scale results. Mean differences between measured and simulated results are presented in Table 6.4. In addition, the hydrodynamic coefficients predicted by SIMAN for the field test condition is presented in Table 6.5.

Table 6.1: Simulated turning circle results presented together with measured full-scale results. FS indicates full-scale results, while Diff indicates how many percent larger SIMAN results are compared to the full-scale result.

		$20^\circ SB$		$20^\circ PT$		$35^\circ SB$		$35^\circ PT$		
		FS	SIMAN	Dif	FS	SIMAN	Dif	FS	SIMAN	Dif
<i>27/02/12 - 2 × 425kW:</i>										
Rudder angle [°]	22.4/ 20.5	22	24.5/ 20.6	22	40.6/ 37.0	39	42.6/ 36.1	39	36.1	11.6
Approach speed [kn]	11.8	11.8	11.6	11.6	11.9	11.9	11.6	11.6	11.6	11.6
Tactical diameter [m]	110.5	99	-10.4	113.2	99	-12.5	83.1	56	-32.6	80.3
Transfer [m]	52.4	49	-6.5	51.4	49	-4.7	37.6	31	-17.6	34.3
Advance [m]	89.2	95	6.5	92.4	95	2.8	77.2	77	-0.3	73.8
<i>27/02/12 - 2 × 142kW:</i>										
Rudder angle [°]	22.4/ 20.5	21	24.5/ 20.7	22	40.5/ 36.9	39	42.9/ 36.1	39	36.1	9.3
Approach speed [kn]	9.6	9.6	8.9	8.9	9.6	9.6	9.6	9.3	9.3	9.3
Tactical diameter [m]	110.7	111	0.3	112.6	106	-5.9	88.1	58	-34.2	88.9
Transfer [m]	52.6	55	4.6	47.2	53	12.3	40.9	32	-21.8	36.9
Advance [m]	86.6	98	13.2	91.6	96	4.8	77.2	76	-1.6	83.9
<i>01/03/12 - 2 × 425kW:</i>										
Rudder angle [°]	20.2/ 20.4	20	20.2/ 18.5	19	36.6/ 36.3	39	36.4/ 33.8	35	33.8	11.9
Approach speed [kn]	12.3	12.3	11.9	11.9	12.3	12.3	12.3	11.9	11.9	11.9
Tactical diameter [m]	115.9	108	-6.8	130	117	-10.0	88.2	59	-33.1	78.9
Transfer [m]	54.4	53	-2.6	56.1	57	1.6	40.5	32	-21.0	34.5
Advance [m]	110.4	99	-10.3	98.6	103	4.5	86.3	79	-8.5	84.4
<i>01/03/12 - 2 × 142kW:</i>										
Rudder angle [°]	20.2/ 20.4	20	20.3/ 18.7	20	36.5/ 36.3	39	36.4/ 33.8	35	33.8	9.8
Approach speed [kn]	9.8	9.8	9.7	9.7	9.7	9.7	9.7	9.8	9.8	9.8
Tactical diameter [m]	121.2	117	-3.5	127.2	117	-8.0	89	62	-30.3	86.1
Transfer [m]	52.7	57	8.2	51.8	58	12.0	34.6	33	-4.6	36.9
Advance [m]	97.8	101	3.3	120.7	101	-16.3	89.3	78	-12.7	87.2

Table 6.2: Simulated zig-zag results presented together with measured full-scale results. FS indicates full-scale results, while Dif indicates how many percent larger SIMAN results are compared to the full-scale result.

	10/10 - 2 × 425 kW			20/20 - 2 × 425 kW			10/10 - 2 × 142 kW			20/20 - 2 × 142 kW		
	FS	SIMAN	Dif									
Rudder angle [°]	10	27		20	44		10	21		20	39	
Heading [kn]	12	12		11.6	11.6		9.9	9.9		10.8	10.8	
Approach speed [s]	12	14	16.7	12	14	16.7	11	15	36.4	12	14	16.7
Time before 1st counter rudder [s]	3	5	66.7	4.5	7	55.6	3.8	6	57.9	5.8	7	20.7
Time from 1st counter rudder to 1st overshoot angle [s]	2.8	5	78.6	4.8	7	45.6	3.6	6	66.7	3.7	7	89.2
Time from 2nd counter rudder to 2nd overshoot angle [s]	4.6	9.1	97.8	12.1	20.8	71.9	5.4	7.7	42.6	14.8	19.7	33.1
1st overshoot angle [°]	4	9.4	135.0	13.2	21.6	63.6	5.4	7.3	35.2	6.8	19.8	191.2
2nd overshoot angle [°]	6.8	9.4	38.2	17.8	21	18.0	3.4	7.2	111.8	14.8	19	28.4
3rd overshoot angle [°]	6.4	9.3	45.3	8	21	162.5	5.5	7.2	30.9	14.4	19.3	34.0
4th overshoot angle [°]	7	30.0	15.8		31.6	5.4			42.6	13.4		47.0
1st overshoot angle, mean [°]	3.9	141.0	15.8		36.7	5.4			35.2	12.2		62.3
2nd overshoot angle, mean [°]	6.8	38.2	13.5		55.6	3.4			111.8	13.8		37.7
3rd overshoot angle, mean [°]	4	132.5	15.8		32.9	5.5			30.9	11.6		66.4

Table 6.3: Simulated stopping test results presented together with measured full-scale results. FS indicates full-scale results, while Dif indicates how many percent larger SIMAN results are compared to the full-scale result.

Table 6.4: Mean differences [%] between simulations and full-scale tests. Positive value indicates that the parameter is overestimated in the simulations.

	Mean difference [%] between simulations and full-scale trials
<i>Turning circle:</i>	
Tactical diameter (20°)	-7.1
Transfer (20°)	3.1
Advance (20°)	1.0
Tactical diameter (35°)	-30.3
Transfer (35°)	-12.5
Advance (35°)	-5.6
<i>Zig-zag test:</i>	
Time before 1st counter rudder	21.6
Time from counter rudder to overshoot angle	60.1
Overshoot angle	71.2
Overshoot angle, mean	51.0
<i>Stopping test:</i>	
Track reach	64.0
Time to stop	95.0

Table 6.5: Hydrodynamic coefficients of R/V Gunnerus predicted by SIMAN at a loading conditions with $T_m = 2.75$ m and trim

Coefficient	Value [-]
Y_v	$-6.79E - 02$
Y_r	$2.63E - 02$
N_v	$-6.27E - 04$
N_r	$-8.06E - 03$
$Y_{\dot{r}}$	$3.96E - 03$
Y_d	$-3.01E - 02$
$N_{\dot{r}}$	$-2.29E - 03$
$Y_{\ddot{r}}$	$3.96E - 03$
X_{rr}	$-3.96E - 03$
$X_{\dot{u}}$	$-4.49E - 03$
X_{vr}	0.0123372
X_{vv}	$6.64E - 03$
X_{vvvv}	0.1244353

As can be seen in the Tables 6.1, 6.2 and 6.3 there are differences between measured full-scale results and results from simulations in SIMAN. This differences may be related to:

- possible errors in the full-scale trials;
- inaccurate simulation conditions and
- modelling issues in SIMAN.

The first two points are also discussed in Chapter 5.

Measured versus simulated transfer, advance and tactical diameter are presented in Figure 6.1. Most of the data is located around the one-the-one line, but especially one group stands out. The group of data that differs most from the one-to-one line is tactical diameter for turning circles with 35° rudder angle. There are also a tendency of underestimating transfer and advance for 35° manoeuvres. This may indicate error with non-linear damping.

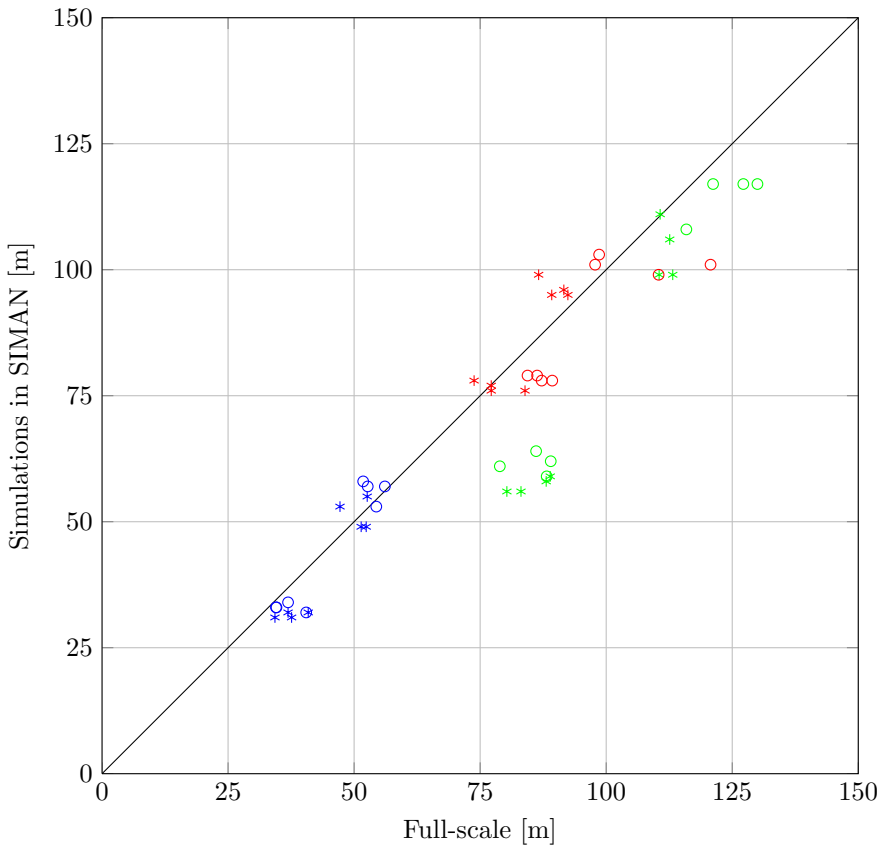


Figure 6.1: Measured versus simulated turning circle results Blue indicates transfer, red indicates advance and green indicates tactical diameter. Results from trials carried out 27 February 2012 are plotted using stars, while results from 1 March 2012 are plotted using circles.

As seen in 6.2, the difference between simulated and measured results of zig-zag manoeuvres and stopping tests is significant. However, only a few seconds or degrees difference between the simulated and the measured zig-zag results may cause a large percentage difference. Challenges regarding execution and reading results from full-scale trials are discussed in Chapter 5. Nevertheless, simulated zig-zag results are larger than full-scale results, which may imply that the SIMAN model is too unstable. The difference in zig-zag and stopping test results may also be due to other modelling issues as R/V Gunnerus is smaller and responds faster than the vessels that SIMAN are developed for.

6.2.4 Evaluation of parameters in SIMAN

As stated in the previous section, the simulated results differs from the measured results. The differences can be related to both field tests and the simulation tool. It is desired to identify what causes the deviations, and thus improve the simulation tool and ship motion model for R/V Gunnerus. Several parameters that may influence the simulated results are evaluated in this section.

Effect of rudder angle on turning circle

R/V Gunnerus is equipped with two rudders. In SIMAN only one rudder angle can be specified for a turning circle manoeuvre. Hence, the manoeuvre must be simulated with equal rudder angle at both rudders. Unfortunately, for some of the full-scale manoeuvres the rudders did not have the same rudder angle, and one value must be chosen for the simulations. Data from full-scale trials give the rudder angles with a precision of approximately 0.1° , but in SIMAN the rudder angle can only be specified with a precision of 1.0° . As mentioned in Section 5.2.1 there is also raised a question of how accurate the rudder data from the full-scale trials is. It is therefore of great interest to perform a sensitivity analysis to investigate how turning circle manoeuvres in SIMAN are influenced by the rudder angle.

The sensitivity analysis investigates how tactical diameter, transfer and advance are affected by rudder angles from 18° to 24° and from 33° to 39° . In the Figures 6.2 and 6.3 are the tactical diameter, transfer and advance plotted for manoeuvres with approach speed at 9.8 kn and 11.9 kn. Advance, transfer and tactical diameter's average difference when the rudder angle is increased by 1.0° are given in Table 6.6.

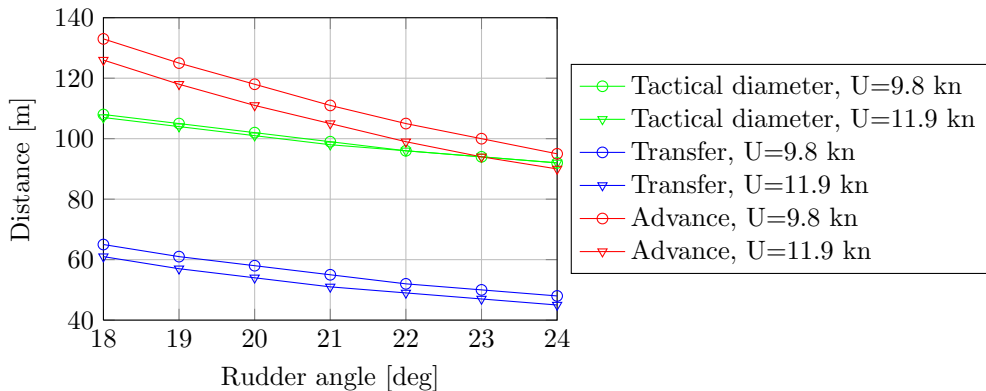


Figure 6.2: Illustration of the rudder angle's impact on a turning circle manoeuvre with approach speed on 9.8 kn and 11.9 kn. Rudder angles from 18° to 24° .

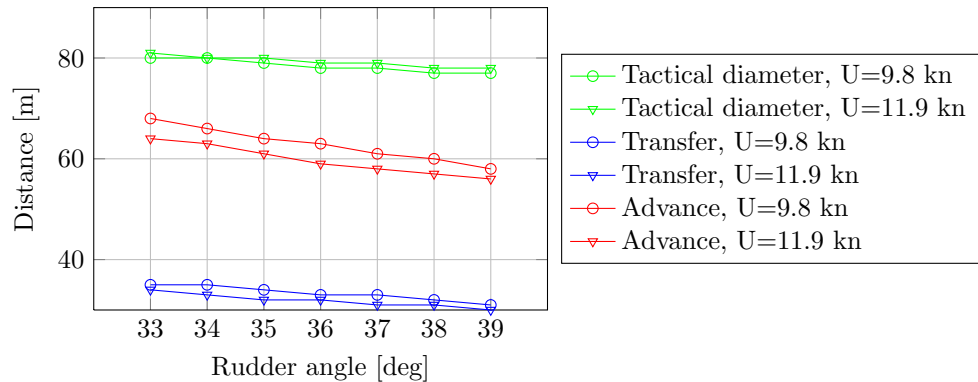


Figure 6.3: Illustration of the rudder angle's impact on a turning circle manoeuvre with approach speed on 9.8 kn and 11.9 kn. Rudder angles from 33° to 39° .

Table 6.6: Rudder angle's impact on a turning circle manoeuvre

	Approach speed [kn]	Average reduction for 1.0° increase of rudder angle [m] [%]	
<i>Advance:</i>			
18-24 degrees	9.8	2.7	2.6
	11.9	2.5	2.5
33-39 degrees	9.8	0.5	0.6
	11.9	0.5	0.6
<i>Transfer:</i>			
18-24 degrees	9.8	2.8	4.9
	11.9	2.7	4.9
33-39 degrees	9.8	0.7	2.0
	11.9	0.7	2.1
<i>Tactical diameter:</i>			
18-24 degrees	9.8	6.3	5.5
	11.9	6.0	5.5
33-39 degrees	9.8	1.7	2.6
	11.9	1.3	2.2

It can be seen that both tactical diameter, transfer and advance decrease as rudder angle increases. The decrease is less for larger rudder angles. The decrease reduces as the speed increases. A 2° rudder angle error in a 20° turning circle manoeuvre, may change the advance, transfer and tactical diameter by 5 m, 5 m and 12 m respectively. The difference between simulations and measured results is however largest at large rudder angles, and the difference between simulated and measured results are largest at large rudder angles.

Effect of non-linear damping on turning circle

Simulated and measured results from turning circles differs. The differences increases with increasing rudder angle (and consequently increasing drift angle). The non-linear damping force is calculated as a transverse cross-flow force. The cross-flow force in response to its transverse motion is relatively large, as the hull has low longitudinal frequency and high transverse frequency [30]. This may indicate that the damping force is inaccurate predicted in SIMAN.

The non-linear damping force is calculated as a transverse cross-flow force. The sectional cross-flow acting on a vessel can be expressed as:

$$Y_{cf} = \frac{1}{2}\rho \int U(x)^2 C_{cf}(x) T(x) dx, \quad (6.5)$$

where $U(x)$ is local transverse velocity, $C_{cf}(x)$ is local cross-flow drag coefficient and $T(x)$ is local draught.

The cross-flow force is integrated from the stern to a section where it is assumed that flow separation is initiated. By changing the location of the separation point, the cross-flow force can be modified. The force can also be modified by modifying the cross-flow drag coefficient.

Cross-flow drag coefficient

In SIMAN, the local cross-flow drag coefficient are estimated using data in the literature. The coefficient are separated into sets fore forebody hull-sections, midbody sections and aftbody section, and given as a function of B/T . The collected data and the trendlines representing the used values are given in [28]. The cross-flow coefficient used in the simulations is presented in Figure 6.4. There is a drop in the $C_{cf}(x)$ -curve at section 11 and 12. Section 11 defines the transition from midbody to forebody, and hence the coefficient are calculated using a new formulation.

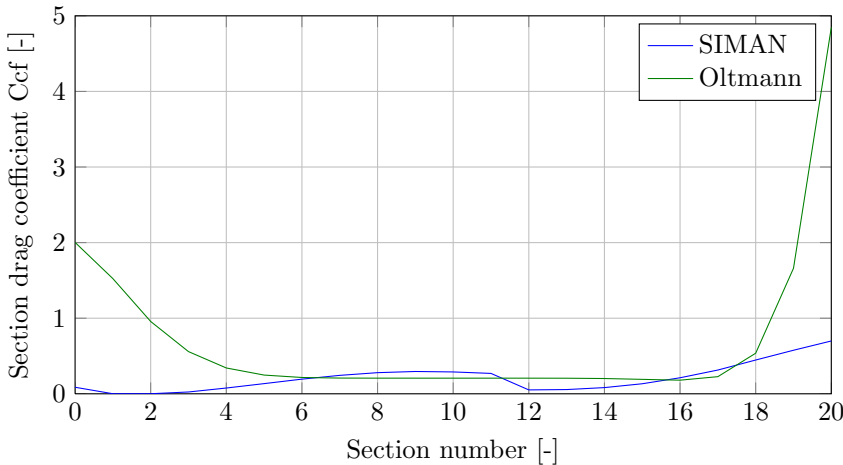


Figure 6.4: Distribution of $C_{cf}(x)$ given by SIMAN and Oltmann's polynomial

In 1984 Oltmann and Sharma [30] presented a high-order four term polynomial to predict the local cross-flow coefficient. It is assumed that the length of the aftbody and forebody are equal and that the draught is constant along the hull. The polynomial is then expressed as:

$$C_{cf}(x) = a_0 + a_7 \left(\frac{x}{l} \right)^7 + a_8 \left(\frac{x}{l} \right)^8 + a_9 \left(\frac{x}{l} \right)^9, \quad (6.6)$$

where x is longitudinal position at the hull, l is half ship length, and a_0, a_7, a_8 and

a_9 are unknown coefficients.

The four unknown coefficients, a_0, a_7, a_8 and a_9 , can be linked to four measured values of side force and yaw moment coefficients at zero forward speed ($\beta = 90^\circ$ and $\gamma = 90^\circ$). In this case the cross-flow effects can be observed without interference from ideal fluid and lifting effects. Oltmann identified the four coefficients for a tanker as:

$$\begin{aligned} a_0 &= 0.207 \\ a_7 &= 5.31 \\ a_8 &= 3.218 \\ a_9 &= -6.732. \end{aligned} \tag{6.7}$$

Oltmann's expression for the cross-flow drag coefficient of a tanker is used as cross-flow drag coefficient in simulations of R/V Gunnerus. R/V Gunnerus' hull is divided into 20 sections. In this case, for simplicity section 0 is located at $x/l = -1$, section 1 at $x/l = -0.9$ section 2 at $x/l = -0.8$ and so on. The distribution of the local cross-flow drag coefficient using Oltmann's polynomial for a tanker is shown in Figure 6.4. The full-scale trials are then simulated using this cross-flow drag coefficient. Mean difference between measured and simulated results when the cross-flow drag coefficient is predicted by SIMAN and Oltmann is presented in Table 6.7. The results are improved for tactical diameter and transfer at 35° rudder angle, but reduced for transfer and advance at 20° rudder angle.

Table 6.7: Mean difference [%] between measured and simulated results when the cross-flow drag coefficient is predicted by SIMAN and Oltmann. Positive value indicates that the parameter is overestimated in the simulations.

	Rudder angle	SIMAN	Oltmann
Tactical diameter	20°	-7.1	-0.6
Transfer	20°	3.1	19.6
Advance	20°	1.0	7.7
Tactical diameter	35°	-30.3	-21.8
Transfer	35°	-12.5	-7.1
Advance	35°	-5.6	-5.9

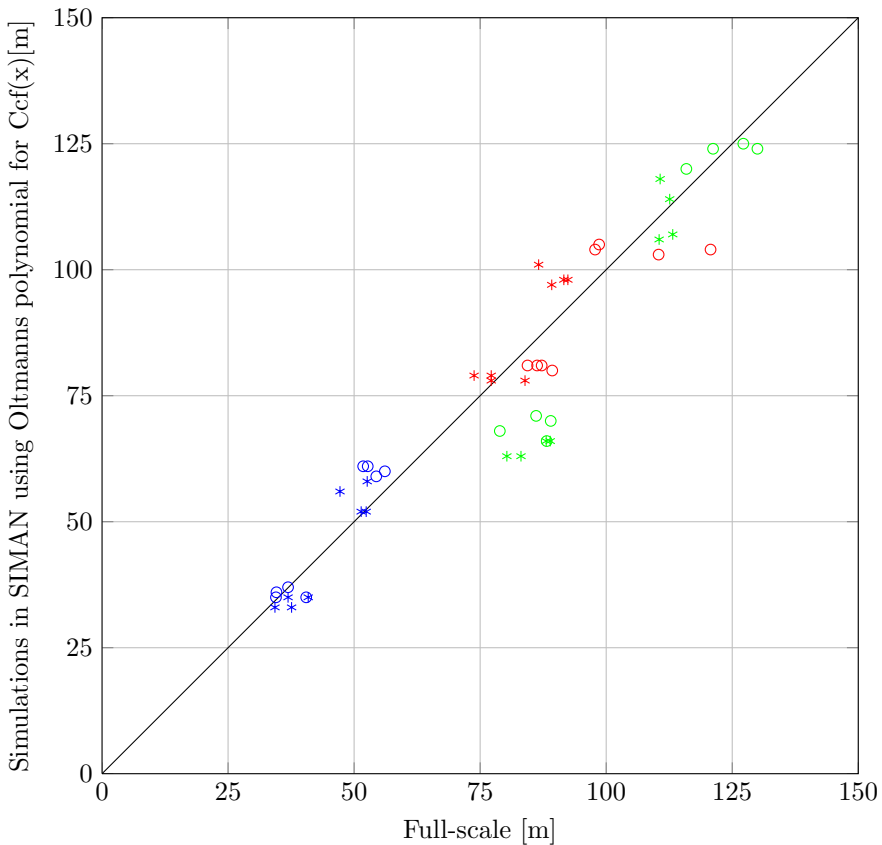


Figure 6.5: Measured versus simulated (using Oltmann's polynomial for $C_{cf}(x)$). Blue indicates transfer, red indicates advance and green indicates tactical diameter. Results from trials carried out 27 February 2012 are plotted using stars, while results from 1 March 2012 are plotted using circles.

Location of separation section

SIMAN locates the separation section at section 1. Since it is desired to reduce the damping forces, it will not have any impact to change the location of the separation point.

Effect of stability index on zig-zag manoeuvre

SIMAN overestimates the results in the simulated zig-zag manoeuvre. This can be an indication of an unstable SIMAN model. By reducing the coupled damping derivative, N_v , the stability index will increase, which implies that the model's

stability increases. N_v is reduced with 20%, 40% and 60%. In addition a situation where the stability index increased by SIMAN to $88.27 \cdot 10^{-5}$ is investigated. Results from simulations of a 10/21-zigzag is presented in Table 6.8. This shows that increasing the stability index by reducing N_v has almost no impact on the zig-zag manoeuvre. Letting SIMAN increase the stability index, gives better results for the overshoot angles, but not for time before 1st counter rudder.

Table 6.8: Results from zig-zag simulations with varying N_v

Stability index	$[10^{-5}]$	Full-scale	N_v	0.8 N_v	0.6 N_v	0.4 N_v	88.27
			30.63	30.79	31.25	31.36	
Rudder angle	[deg]		10	10	10	10	
Heading	[deg]		21	21	21	21	21
Approach speed	[kn]	9.9	9.9	9.9	9.9	9.9	9.9
Time before 1st counter rudder	[s]	11	15	15	15	15	17
Time from 1st counter rudder to 1st overshoot angle	[s]	3.8	6	6	6	6	5
Time from 2nd counter rudder to 2nd overshoot angle	[s]	3.6	6	6	6	6	6
1st overshoot angle	[deg]	5.4	7.7	7.6	7.4	7.4	5.7
2nd overshoot angle	[deg]	5.4	7.3	7.6	7.4	7.4	5.8
3rd overshoot angle	[deg]	3.4	7.3	7.5	7.3	7.3	5.7
4th overshoot angle	[deg]	5.5	7.2	7.5	7.3	7.3	5.7

Effect of heading change and rudder angle on a zig-zag manoeuvre

Heading change and rudder angle are specified in the simulations of zig-zag-maneuvres. The heading change is estimated as an average value of the first four heading changes in the full-scale tests, as described in Section 5.2.3. It has been questioned how accurate the change of heading and rudder angles are measured, and it is therefore of interest to investigate their impact on a zig-zag manoeuvre. This is studied using the 10/21 (10/10) manoeuvre at 2×142 kW, and the results are presented in Table 6.9. The effect of hanging heading change was not significant. The overshoot angles and times from counter rudder to overshoot angle decrease with decreasing rudder angle, which improved the results significantly for the overshoot angles.

Table 6.9: Results from zig-zag simulations with varying heading change and rudder angle

			Full-scale Simulations				
			10	10	8	12	
Rudder angle	[deg]						
Heading	[deg]		21	19	23	21	21
Approach speed	[kn]	9.9	9.9	9.9	9.9	9.9	9.9
Time before 1st counter rudder	[s]	11	15	14	16	17	14
Time from 1st counter rudder to 1st overshoot angle	[s]	3.8	6	6	6	5	6
Time from 2nd counter rudder to 2nd overshoot angle	[s]	3.6	6	6	6	5	6
1st overshoot angle	[deg]	5.4	7.7	7.7	7.7	5.9	9.3
2nd overshoot angle	[deg]	5.4	7.3	7.5	7.5	5.9	9.2
3rd overshoot angle	[deg]	3.4	7.3	7.4	7.5	5.8	9.4
4th overshoot angle	[deg]	5.5	7.2	7.4	7.3	5.8	9.4

6.3 Simulations using calculated hydrodynamic coefficients

Turning circles and zig-zag manoeuvres are simulated using the hydrodynamic coefficients predicted in Chapter 4. This is done in order to evaluate the calculated coefficients and investigate whether using these coefficients will improve the simulated results. Only ShipX (SIMAN), flat plate theory and Clarke have derived expressions for both velocity and acceleration derivatives. For the methods that only predict the velocity derivatives, the acceleration derivatives predicted by SIMAN are used. This is not a correct approach, but is a necessary assumption in this study.

As shown in Section 6.2, SIMAN overestimates the manoeuvring performance in a turning circle, i.e. it is desired to increase simulated advance, transfer and tactical diameter. On the other hand, in the zig-zag manoeuvre it is desired to decrease the simulated results.

6.3.1 Ship model

The simulations is performed with draught at 2.75 m and no trim. Similar ship model as described in Section 6.2.1, but without trim, is used in the simulations. The reason why trim is not included is that the methods used to predict the hydrodynamic coefficients do not consider trim.

6.3.2 Results and discussion

The hydrodynamic coefficients derived by Lee could not be used in the simulations. A stability index at $-90 \cdot 10^{-5}$ gave a significantly unstable vessel. The track of a 10/21 zig-zag manoeuvres are shown in Figure 6.6. Turning circles could not be performed as the vessel lost its speed.

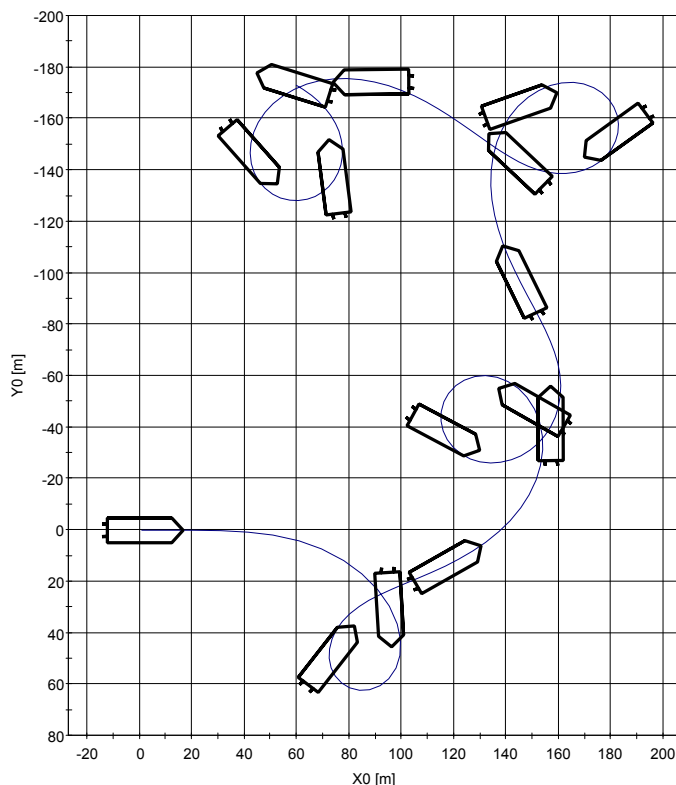


Figure 6.6: Trajectory of a simulated zig-zag manoeuvre using hydrodynamic coefficients predicted by Lee's approach. This track history shows a very unstable model.

Advance, transfer and tactical diameter simulated using the different coefficients are presented in the Figures 6.7, 6.8 and 6.9. As mentioned, comparisons of measured full-scale results and simulated trials showed that SIMAN underestimates advance, transfer and tactical diameter. None of these methods to calculate the hydrodynamic coefficients gave better results than SIMAN.

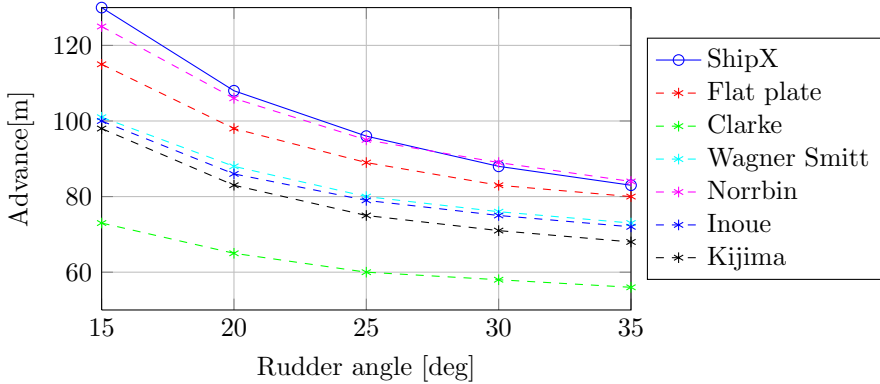


Figure 6.7: Illustration of how advance varies depending on method used to calculate hydrodynamic coefficients

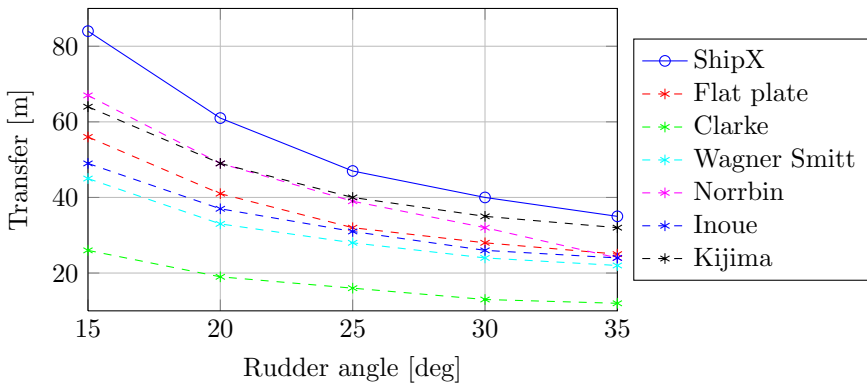


Figure 6.8: Illustration of how transfer varies depending on method used to calculate hydrodynamic coefficients

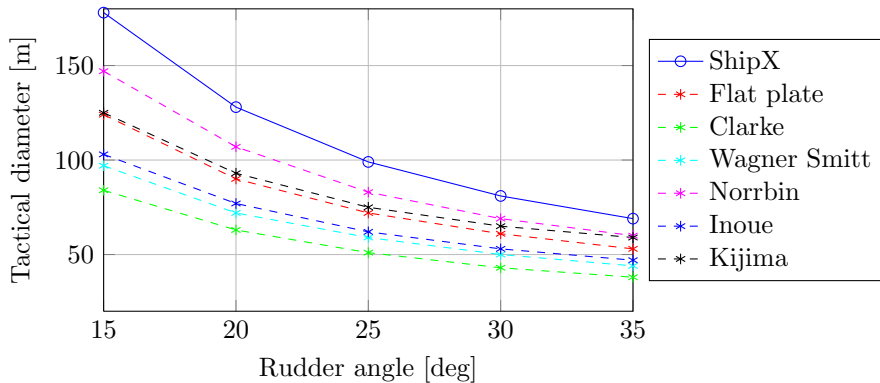


Figure 6.9: Illustration of how tactical diameter varies depending on method used to calculate hydrodynamic coefficients

Results from a 10/21 zigzag manoeuvre are presented in Table 6.10. Based on comparisons of measured and simulated results, it was desired that the new simulations should give smaller results than the simulation using coefficients calculated by SIMAN. This was however not obtained.

It should also be mentioned that only coefficients predicted by SIMAN and Kijima give positive stability index, i.e. the other methods give an unstable vessel. This can also underline that these approaches (Flat, plate, Wagner Smitt, Norrbin, Inoue and Clarke) are not suited for R/V Gunnerus.

Table 6.10: Results of zig-zag manoeuvre simulated hydrodynamic coefficients predicted by various methods

		SIMAN	Flat plate	Clarke	Wagner Smit	Norrbin	Inoue	Kijima
Stability index	[10^{-5}]	25.09	-15.78	-51.65	-28.38	-0.70	-16.78	17.92
Rudder angle	[deg]		10	10	10	10	10	10
Heading	[deg]		21	21	21	21	21	21
Approach speed	[kn]	9.9	9.9	9.9	9.9	9.9	9.9	9.9
Time before 1st counter rudder	[s]	16	14	9	13	15	13	13
Time from 1st counter rudder to 1st overshoot angle	[s]	6	7	6	7	6	7	6
Time from 2nd counter rudder to 2nd overshoot angle	[s]	6	7	6	8	7	7	6
1st overshoot angle	[deg]	6.7	10.5	16.4	14.2	8.7	13.6	11.7
2nd overshoot angle	[deg]	6.7	11.4	16.4	16.2	9.3	14.6	11.9
3rd overshoot angle	[deg]	6.7	11.2	15.1	15.4	9.2	14.5	11.7
4th overshoot angle	[deg]	6.5	11.5	15.0	15.5	9.0	14.6	11.5

Chapter 7

R/V Gunnerus as a case vessel in research

7.1 Current need for research and development

The 26th ITTC [31], held in Rio in 2011, investigated the current need for research and development. Some issues from their work are highlighted in this section.

During the last three years there has been a remarkable development of numerical methods for manoeuvring prediction. Most of the development is regarding CFD (particularly RANS) methods, while the development of new empirical methods has not been significant. Nevertheless, CFD's introduction to the commercial market has been less than expected.

The 26th ITTC stated that there is a particular need for mathematical models for low speed manoeuvring. Manoeuvring in harbours, subsea equipment installation and offloading are examples of low speed manoeuvring operations. Standard manoeuvres have moderate drift angles (typically 30°), and manoeuvring forces can be obtained from conventional manoeuvring model tests. Low speed manoeuvres require large drift angles, and the hydrodynamic forces acting on the hull are different than at traditional manoeuvres. This requires a new mathematical model. Several papers present simulations of manoeuvring at low speed, but they do not specify the manoeuvring models that is used. For that matter it is necessary to standardise mathematical models for low speed and large drift angles. Model test, CFD simulations and some empirical methods can be used to derive mathematical models. For low speed

manoeuvring validation are performed on force level, i.e. forces predicted by a mathematical model are compared to forces measured on a physical model. If the validation should be based on motion level, it is necessary to standardise some typical low speed manoeuvres that can be used for validation.

7.2 R/V Gunnerus as a case vessel

In the literature there is a need for vessels that can be used for validation of mathematical models. It is however not recommended that R/V Gunnerus is used as a benchmarking model for validation of numerical models. The most obvious reason is that the R/V Gunnerus differs significantly from the ships that must satisfy IMO's criteria of manoeuvring capability. Nevertheless, ship design is in constant development, and manoeuvring prediction methods (especially empirical methods) should be revised continuously to be able to describe the vessels well. Using the unconventional vessel R/V Gunnerus, one might increase the methods' field of applicability and thereby stay one step ahead of the development of new ship design. In this study it has been shown that R/V Gunnerus manoeuvring capability can be described using the numerical model in SIMAN, but the model requires modification as R/V Gunnerus is outside its application range.

As mentioned, there is a distinct need for mathematical models for low speed manoeuvring. It is assumed that R/V Gunnerus can be used to participate in the development of low speed manoeuvring models. R/V Gunnerus can also be used for CFD purposes. This is in compliance with the purpose of R/V Gunnerus, namely to be used for research and educational purposes.

7.3 Recommended trials

In this section it is suggested some manoeuvring trials that can be conducted. Which tests that are going to be carried out depends on the purpose of the study.

7.3.1 Planar Motion Mechanism (PMM) tests

PMM-tests should be performed in order to determine the hydrodynamic coefficients used in manoeuvring equations.

PMM tests are regarded as the most reliable and controlled method for

determination of the hull forces as input to the manoeuvring equations. The main draw back with PMM testing is the complexity and cost connected to running these tests. To establish a complete set of hull forces data a large number of test cases are required. [32]

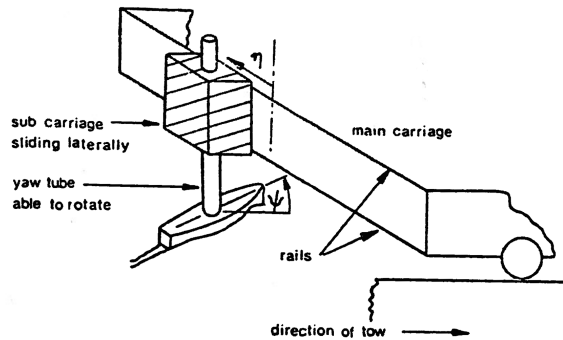


Figure 7.1: Planar Motion Mechanism (PMM) [32]

PMM is mounted to a towing carriage in a towing tank or a seakeeping basin, see Figure 7.1. The model is usually free to heave and pitch, and fixed roll. A PMM test consists of following tests:

- oblique towing tests;
- pure sway tests;
- pure yaw tests and
- yawing with drift.

Hull forces in sway and surge, as well as yaw moment are recorded during the tests. Rudder lift forces should be measured if rudder is applied. Bare hull tests can be used for CFD purposes. The PMM tests should be carried out with drift angles that represent both conventional manoeuvring and low speed manoeuvring.

At MARINTEK PMM tests are executed using a multipurpose carriage with 6 DOF hexapod motion platform in the towing tank, see Figure 7.2. The hexapod is free to move in all DOF, maximum carriage speed is 5 m/s and maximum transverse carriage speed is 2 m/s.

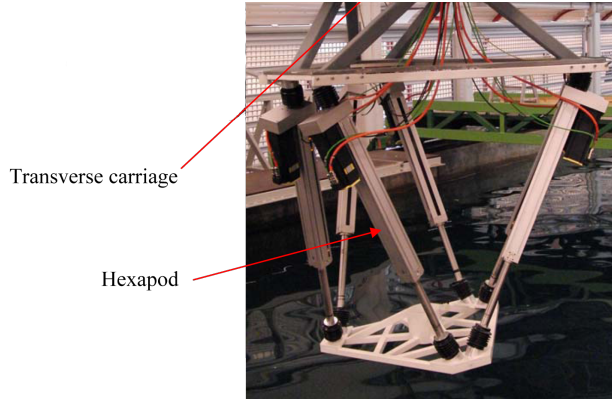


Figure 7.2: MARINTEK's multipurpose carriage with 6 DOF hexapod motion platform used for PMM tests [33]

7.3.2 Full-scale trials

It is recommended that more full-scale trials should be conducted. By running several repetitions the uncertainty of the precision errors, i.e. the scatter in the trials, can be predicted. Before new field tests are carried out the offset in rudder recording should be investigated, this is also mentioned in Section 5.2.1. In addition, a better solution of conducting the zig-zag tests must be suggested.

Turning circles, zig-zag manoeuvres and stopping tests should be performed, as well as low speed trials.

Chapter 8

Conclusion

Full-scale trials of R/V Gunnerus have been conducted in deep water in Trondheimsfjorden. Turning circles, zig-zag manoeuvres and stopping tests have been analysed to predict the vessel's manoeuvring performance. Data during full-scale trials was registered by Seapath at 200 Hz and by DP-system at 1 Hz.

A ship motion model of R/V Gunnerus has been created in SIMAN, and simulations of full-scale trials have been performed. The difference between full-scale and simulated turning circles increased with increasing rudder angle (and consequently drift angle), which may indicate incorrectly modelling of non-linear damping forces. The non-linear damping forces are dependent on the cross-flow drag coefficient, $C_{cf}(x)$. Using $C_{cf}(x)$ predicted by SIMAN, tactical diameter and transfer at 35° rudder angle were significantly underestimated in the simulations. Simulations were also performed using Oltmann's polynomial for $C_{cf}(x)$, which improved the results with exception of transfer and advance at 20° rudder angle. Using Olmann's polynomial underestimated transfer at 20° rudder angle and tactical diameter at 35° rudder angle. Table 8.1 presents the mean differences between measured and simulated results of a turning circle.

Table 8.1: Mean difference [%] between measured and simulated turning circles when the cross-flow drag coefficient is predicted by SIMAN and Oltmann. Positive value indicates that the parameter is overestimated in the simulations.

	Rudder angle	Mean difference between measured and simulated results [%]	
		SIMAN	Oltmann
Tactical diameter	20°	-7.1	-0.6
Transfer	20°	3.1	19.6
Advance	20°	1.0	7.7
Tactical diameter	35°	-30.3	-21.8
Transfer	35°	-12.5	-7.1
Advance	35°	-5.6	-5.9

Full-scale zig-zag manoeuvres were carried out using the DP-system installed on R/V Gunnerus. This solution did not work properly as 10/27, 10/21, 20/44 and 20/39 manoeuvres were obtained instead of 10/10 and 20/20 manoeuvres. Nevertheless, zig-zag trials were simulated at the registered conditions. Stopping tests were simulated in SIMAN as well. SIMAN greatly overestimates the parameters in the zig-zag and stopping tests, see Table 8.2. These differences may be due inaccurate simulation conditions, or modelling issues as R/V Gunnerus is smaller and responds faster than the vessels SIMAN is developed for. However, only a few seconds or degrees difference between the simulated and the measured zig-zag results cause a large percentage difference, and reducing rudder angle in the simulations improves the results.

Table 8.2: Mean difference [%] between simulations and full-scale tests. Positive value indicates that the parameter is overestimated in the simulations.

	Mean difference between measured and simulated results [%]
<i>Zig-zag test:</i>	
Time before 1st counter rudder	21.6
Time from counter rudder to overshoot angle	60.1
Overshoot angle	71.2
<i>Stopping test:</i>	
Track reach	64.0
Time to stop	95.0

It has been shown that SIMAN can be used to investigate R/V Gunnerus' manoeuvring capability, but modifications are necessary. Hence it can be concluded that R/V Gunnerus can be used as a case vessel in order to

investigate how manoeuvring simulation tools predict manoeuvring performance of an unconventional vessel like R/V Gunnerus. CFD-tools need validation in order to be commonly accepted in the commercial market, which R/V Gunnerus can contribute to. There is also a particular need for mathematical models for low speed manoeuvring and R/V Gunnerus can be used as a case vessel for this research.

8.1 Further work

Further investigation and modification of R/V Gunnerus ship motion model is necessary to obtain a complete model. It is recommended to perform PMM tests to predict the hydrodynamic coefficients. The non-linear damping forces require closer study. Full-scale zig-zag manoeuvres should be carried out using a better solution than the present DP-system. Several reruns of the field tests are required in order to predict the precision error of the field tests. Simulations can also be performed in VeSim.

If R/V Gunnerus is going to be used as a case vessel for low-speed manoeuvring problems, it is necessary to carry out field tests and PMM tests for low speed manoeuvres. Bare hull tests is recommended for CFD-purposes.

References

- [1] International Maritime Organization. *Standards for Ship Manoeuvrability*. IMO Resolution MSC.137(76). 2002.
- [2] International Towing Tank Conference. Opened: 27/05/2012. URL: <http://ittc.sname.org/>.
- [3] S. Tjøswold. *Validation of numerical manoeuvring models, Project thesis*. 2011.
- [4] International Maritime Organization. *Explanatory Notes to the Standards for Ship Manoeuvrability*. MSC/Circ. 1053. 2002.
- [5] American Bureau of Shipping. *GUIDE FOR VESSEL MANEUVERABILITY*.
- [6] The Manoeuvring Commitee. “Final Report and Recommendations to the 25th ITTC”. In: *Proceedings of 25th ITTC - Volume 1*. 2008.
- [7] T. E. Berg. *Lecture notes, TMR 4220 Naval Hydrodynamics, Ship Manoeuvring*. Departement of Marine Technology, 2009.
- [8] <http://www.simman2008.dk>. *SIMMAN2008: Workshop for Verification and validation if Ship Manoeuvring Simulation Methods*.
- [9] A. Ross. “Nonlinear Manoeuvring Models for Ships”. PhD thesis. NTNU, 2008.
- [10] T. I. Fossen. *Handbook of Marine Craft Hydrodynamics and Motion Control*. Wiley, 2011.
- [11] T.I. Fossen. *Lecture Notes TTK 4190 Guidance and Control of Vehicle*. Opened: 20/03/2012. URL: <http://www.itk.ntnu.no/fag/gnc/Wiley/Ch 2.pdf>.
- [12] B. Pettersen. *Kompendium Marin teknikk 3 Hydrodynamikk*. Institutt for Marin teknikk, 2007.

- [13] K. Minsaas and S. Steen. *TMR4220 Naval Hydrodynamics FOIL THEORY*. Department of Marine Technology, NTNU, 2008.
- [14] U.S. Centennial of Flight Commission. Opened: 07/02/2012. URL: http://centennialofflight.gov/essay/Theories_of_Flight/Stability_I/I/TH27G8.htm.
- [15] T. E. Berg. *Styring og manøvrering, forelesningsnotater våren 1995*. Institutt for Marin hydrodynamikk, 1995.
- [16] G. Hine D. Clarke P. Gedling. “The Application of Manoeuvring Criteria in Hull Design Using Linear Theory”. In: *The Royal Institution of Naval Architects* (1982).
- [17] D. Clarke. “A two-Dimensional Strip Method for Surface Ship Hull Derivatives: Comparison of theory with Experiments on a Segmented Tanker Model”. In: *Journal of Mechanical Engineering Science* (1972).
- [18] K. Kijima S. Inoue M. Hirano. “Hydrodynamic Derivatives on Ship Manoeuvring”. In: *International Shipbuiling Progress Marine Technology Monthly* (1981).
- [19] T.-I. Lee et al. “On an Empirical Prediction of Hydrodynamic Coefficients for Modern Ship Hulls”. In: *MARSIM'03* (2003).
- [20] K. Kijima and Y. Nakiri. “On the Practical Prediction Method for Ship Manoeuvring Characteristics”. In: *MARSIM 03* (2003).
- [21] A. Ross K. Martinussen E. Ringen. *Simulation of KVLCC1 and KVLCC2 Manoeuvring Motions*.
- [22] Kongsberg. *Seapath 300*. Opened: 23/04/2012. URL: [http://www.km.kongsberg.com/ks/web/nokbg0397.nsf/AllWeb/D2CA490C88C86635C12576400037CA93/\\$file/Datasheet_SEAPATH300_mar12.pdf?OpenElement](http://www.km.kongsberg.com/ks/web/nokbg0397.nsf/AllWeb/D2CA490C88C86635C12576400037CA93/$file/Datasheet_SEAPATH300_mar12.pdf?OpenElement).
- [23] R. Fogt. *Unix Time Conversion*. URL: http://www.onlineconversion.com/unix_time.htm.
- [24] Kongsberg. *Compact dynamic positioning - DP system*. Opened: 23/04/2012. URL: <http://www.km.kongsberg.com/ks/web/nokbg0240.nsf/AllWeb/721E0E70AA59607FC1256DF20044355E?OpenDocument>.
- [25] R. Palacios. *deg2utm*. Opened: 05/03/2012. URL: <http://www.mathworks.com/matlabcentral/fileexchange/10915-deg2utm>.
- [26] The Engineering Toolbox. *UTM to Latitude and Longitude Converter*. URL: http://www.engineeringtoolbox.com/utm-latitude-longitude-d_1370.html.
- [27] E-mail correspondance between Sverre Steen (NTNU), Tom Schultz (Kongsberg Maritime) and Sissel Tjøswold (MSc. student), spring 2012.

- [28] E.Ringen K. Martinussen. “Manoeuvring Prediction During Design Stage”. In: *International Workshop on Ship Manoeuvrability at the Hamburg Ship Model Basin*. HSVA, 2000.
- [29] Olav H. Slaattelid. *Model Tests PK-410, Research Vessel for NTNU. Calm Water Tests*. Tech. rep. MARINTEK, 2005.
- [30] S D. Sharma P. Oltmann. *Simulation of Combined Engine and Rudder Maneuvers using an improved Model of Hull-Propeller-Rudder Interactions*. Technische Uniserität Hamburg-Harburg, 1984.
- [31] The Manoeuvring Commitee. *The Manoeuvring Committee, Final report and recommendations to the 26th ITTC*. draft. 2011.
- [32] S. Steen and J. V. AArnes. *Lecture notes in Experimental Methods in Marine Hydrodynamics*. Department of Marine Technology, NTNU, 2010.
- [33] MARINTEK. *New towing tank multi-purpose carriage*.
- [34] S. Steen. *TMR4247 Marin teknikk 3 - Hydrodynamikk. Motstand og propulsjon, Propell- og foilteori*. Institutt for Marin teknikk, 2007.

Appendix

A.1 Specifications R/V Gunnerus

RV GUNNERUS - LNVZ
Multipurpose research vessel for Norwegian University of Science and Technology (NTNU)

Name	R/V GUNNERUS
Owner	Norwegian University of Science and Technology (NTNU) Faculty of Natural Sciences and Technology
Designed by	Polarkonsult AS, Norway
Built by	Larsnes Mekaniske Verksted, Norway
Delivery year	2006
Port of Registry	Trondheim, Norway
Classification Society	Norwegian Maritime Directorate

Main dimensions

Length over all	(Loa) 31.25 m
Length between pp	(Lpp) 28.90 m
Length in waterline	(Lwl) 29.90 m
Breadth middle	(Bm) 9.60 m
Breadth extreme	(B) 9.90 m
Depth mld. Main deck	(Dm) 4.20 m
Draught, mld	(dm) 2.70 m
Mast height / antenna	14.85 / 19.70 m
Dead weight	107 t

Class, Service Area

Range	Coastal areas out to 20 nautical miles from the coast (Litens Kystfart) Designed and built according to European trade.
Class Notation	DNV + 1A1 + Ice C + E0 + R2 Cargo ship

Deck equipment, scientific equipment and lab facilities

Trawl winches	2 x Mjosund 6 t, (wire D=14 mm, L=1000 m).
Net drum	Mjosund 5 m ³ , D=2000mm, d=320mm
Main deck crane	Palfinger 14 m / 35 tm
CTD crane	HIAB/Mjosund, 5 m / 3.3 tm, Water sampler wire 5 mm/750m CTD wire 6,5 mm/750 m.
Stern mounted A-frame	6 t, hydraulic.
Hydraulic diving platform	500 Kg, 1,5m x 0,8m.
Hydraulic aggregate	Mjosund 110 kW
Capstan	Mjosund 8t/220bar, D=410, d=320, L=300
Anchor winch	Mjosund 2 drums, 20 m/min, 2 x 12,5m ø 22mm K2 chain/ 210m ø22mm. wire
Compressed air	Atlas copco compressor
Workdeck	75 m ²
Wet lab	13.9 m ²
Dry lab	11.8 m ²
Computer lab	11.2 m ²
Container attachment:	5, 10, 15 & 20 feet alongside or 20 feet abeam.
CTD	Saiv
CTD	Sealogger 25, Seabird electronics inc.

Watersampler system Carousel water sampler, 12 x 2,5l bottles. Seabird electronics inc
 Workboat Polarcirkel 560 Work, Yamaha 80hp

Capacities

Crews cabins / berths	6 / 11
Daytime personnel capacity	25 incl. crew
Deadweight	107 t
Deck load	45 t
Fuel oil	44 m ³
Fresh water	11 m ³
Water ballast	62 m ³
Cargo hold	42 m ³
Galley	4,5 m ²
Mess, conference and dayroom	32 m ² With 46" LCD monitor.

Machinery: Diesel electric propulsion

Main electric propulsion	1000 kW (Siemens 2 x 500 kW)
Main generators	3 x Nogva-Scania 450 kW
Bow tunnel thruster	1 x Brunvoll 200 kW
Speed at 100% MCR	12,6 kn
Cruising speed	9,4 kn
Gear	2 x Finnøy
Rudder	2 x Rolls-Royce, Ulstein Hinze Rudder FB-H 1200
Steering gear	2 x Rolls-Royce, Tenfjord SR562-FCPX2

The diesel electric system has been specially designed for low hydroacoustic noise levels.

Diesel generators are mounted on a common double elastic frame and one of the generators are mounted in a noise dampening hood for special low noise mode.

Navigation, communications and electronic equipment

Dynamic Positioning system	Kongsberg SDP-11 / cPos
DP - Reference systems	GPS
	Kongsberg Seatex DPS 232
	HPR, Kongsberg transponders.
	Kongsberg Seatex RADius
Heading, Attitude and Positioning Sensor	Kongsberg Seapath 300
Acoustic positioning system	Kongsberg HiPAP 500
Motion reference unit (MRU)	Kongsberg Seatex
Autopilot	Simrad AP50
Compass, magnet	Nautisk service NS 150-A
Compass, gyro	Simrad GC80 / 85
Bearing repeater	Simrad DR76
Differential positioning sensor	Kongsberg DPS 232
Heading, attitude and positioning sensor	Kongsberg Seatex Seapath 300
GPS	Furuno Navigator GP-90
Radar	Furuno FAR 28x7 /FAR 21x7
Log	Furuno Doppler speed log DS-80
Echo sounder	Furuno FCV-1200L. 38, 50, 200 kHz – 2000m
Echo sounder, multibeam	Kongsberg EM 3002s
Catch monitoring system	Simrad PI54

Chartplotter 1	Telchart (AIS)
Chartplotter 2	Olex (Installed AIS, HT, SB, ITI, MBES)
Chartplotter 3	Olex LT (Office version)
AIS	Furuno FA-150
Navtex	JMC NT900
GMDSS console	
VHF fixed radio	Sailor
VHF handheld radios	Jotron
UHF handheld radios	Icom
Satellite phone	Sailor
Internet in sea	ICE & Telenor mobilt bredbånd
Internet at pier Trondheim	Wireless broadband NTNU.

Safety

MOB boat, inflateable craft	Narwhal 6 persons SOLAS aproved, Propulsion Mariner 20 Hp
Rescue boat davit	Ned Deck Marine
Life rafts	2 x 25 men each
Survival suits	25 Stearns model ISS-590i
Life jackets	Seamaster – 1983, SOLAS Approved
Work vests	25 Regatta
EPIRB	Jotron
SART	Jotron
Aircraft beacon	Jotron
Fire alarm system	Minerva Marine T1008
Fixed system	Engine room, CO2
Fire suit	Draeger
Search light	Tranberg
SAR	SECurus prototype, Apto maritime (Under construction)
Day and night vision	SECurus prototype, Apto maritime (Under construction)
Oil spill monitoring	SECurus prototype, Apto maritime (Under construction)

Details are believed to be correct but not guaranteed

A.2 4-DOF equations of motion

The 4-DOF low frequency model is obtained to describe low-frequency operations, i.e. manoeuvring in calm water. The model is expressed as:

$$\mathbf{M}\dot{\boldsymbol{\nu}} + \mathbf{C}(\boldsymbol{\nu})\boldsymbol{\nu} + \mathbf{D}(\boldsymbol{\nu}) + \mathbf{g}(\boldsymbol{\eta}) = \boldsymbol{\tau}, \quad (\text{A.1})$$

where

- $\boldsymbol{\nu} = [\boldsymbol{\nu}_1 \ \boldsymbol{\nu}_2] = [u, v, p, r]$ is a generalised velocity vector,
- $\boldsymbol{\eta} = [\boldsymbol{\eta}_1 \ \boldsymbol{\eta}_2] = [x, y, \phi, \psi]$ is a position vector, also called Euler angles,
- $\mathbf{M} = \mathbf{M}_{\mathbf{RB}} + \overline{\mathbf{M}}_{\mathbf{A}}^0$ is the systems inertia matrix including added mass,
- $\mathbf{C}(\boldsymbol{\nu}) = \mathbf{C}_{\mathbf{RB}}(\boldsymbol{\nu}) + \mathbf{C}_{\mathbf{A}}(\boldsymbol{\nu})$ is a Coriolis-centripetal matrix including added mass,
- $\mathbf{D}(\boldsymbol{\nu})$ is a damping matrix,
- $\mathbf{g}(\boldsymbol{\eta})$ is a vector of gravitational/buoyancy forces and moments and
- $\boldsymbol{\tau}$ is a vector of control inputs.

A.2.1 Kirchhoff's equations of motion

The 4-DOF model is derived using Kirchhoff's equations of motion. Kirchhoff's equations of motion are a special case of the Euler-Lagrangian equations and are based upon the kinetic energy of a system. They also take Coriolis-centripetal forces, which arise using non-inertial frames, into account.

Kirchhoff's equations of motion are expressed as:

$$\begin{aligned} \frac{d}{dt}\left(\frac{\partial T}{\partial \boldsymbol{\nu}_1}\right) + \mathbf{S}(\boldsymbol{\nu}_2)\frac{\partial T}{\partial \boldsymbol{\nu}_1} &= \boldsymbol{\tau}_1 \\ \frac{d}{dt}\left(\frac{\partial T}{\partial \boldsymbol{\nu}_2}\right) + \mathbf{S}(\boldsymbol{\nu}_2)\frac{\partial T}{\partial \boldsymbol{\nu}_2} + \mathbf{S}(\boldsymbol{\nu}_1)\frac{\partial T}{\partial \boldsymbol{\nu}_1} &= \boldsymbol{\tau}_2, \end{aligned} \quad (\text{A.2})$$

where T is kinetic energy of an object with mass M given by $T = \frac{1}{2}\boldsymbol{\nu}^T \mathbf{M} \boldsymbol{\nu}$ and \mathbf{S} is the skew-symmetric cross-product operator defined as:

$$\mathbf{S}(\boldsymbol{\lambda}) = -\mathbf{S}^T(\boldsymbol{\lambda}) = \begin{bmatrix} 0 & -\lambda_3 & \lambda_2 \\ \lambda_3 & 0 & -\lambda_1 \\ -\lambda_2 & \lambda_1 & 0 \end{bmatrix}, \boldsymbol{\lambda} = \begin{bmatrix} \lambda_1 \\ \lambda_2 \\ \lambda_3 \end{bmatrix}. \quad (\text{A.3})$$

Hence, for the 4-DOF model $\mathbf{S}(\boldsymbol{\nu})$ is expressed as:

$$\begin{aligned}\mathbf{S}(\boldsymbol{\nu}_1) &= \begin{bmatrix} 0 & -w \\ w & 0 \end{bmatrix} \\ \mathbf{S}(\boldsymbol{\nu}_2) &= \begin{bmatrix} 0 & q \\ -q & 0 \end{bmatrix}.\end{aligned}\quad (\text{A.4})$$

A.2.2 Rigid body equation of motion

The mass matrix of a rigid body can be expressed as:

$$\mathbf{M}_{\text{RB}} = \begin{bmatrix} m\mathbf{I}_{2 \times 2} & -m\mathbf{S}(\mathbf{r}_g^b) \\ m\mathbf{S}(\mathbf{r}_g^b) & \mathbf{I}_b \end{bmatrix} \in \mathbb{R}^{4 \times 4}, \quad (\text{A.5})$$

where m is the vessel's mass, $\mathbf{I}_{2 \times 2}$ is the identity matrix, \mathbf{r}_g^b is the location of o_b , i.e. the origin of the body fixed frame relative to the centre of gravity of the vessel, $\mathbf{S}(\mathbf{r}_g^b)$ is a skew-symmetric matrix and \mathbf{I}_b is the inertia matrix.

For a starboard-port symmetric vessel the mass matrix is given as:

$$\mathbf{M}_{\text{RB}} = \begin{bmatrix} m & 0 & 0 & 0 \\ 0 & m & 0 & 0 \\ 0 & 0 & I_x & 0 \\ 0 & 0 & 0 & I_z \end{bmatrix}. \quad (\text{A.6})$$

In the rigid body system is the kinetic energy given as $T_{\text{RB}} = \frac{1}{2}\boldsymbol{\nu}^T \mathbf{M}_{\text{RB}} \boldsymbol{\nu}$. The rigid body Coriolis-matrix is defined using Kirchoff's equations:

$$\begin{array}{ll} \text{mass-terms} & \text{Coriolis-centripetal forces} \\ \overbrace{\frac{d}{dt} \left(\frac{\partial T}{\partial \boldsymbol{\nu}_1} \right)}^{\text{inertia terms}} + \underbrace{\mathbf{S}(\boldsymbol{\nu}_2) \frac{\partial T}{\partial \boldsymbol{\nu}_1}}_{\text{Coriolis-centripetal moments}} & = \boldsymbol{\tau}_1 \\ \overbrace{\frac{d}{dt} \left(\frac{\partial T}{\partial \boldsymbol{\nu}_2} \right)}^{\text{inertia terms}} + \underbrace{\mathbf{S}(\boldsymbol{\nu}_2) \frac{\partial T}{\partial \boldsymbol{\nu}_2} + \mathbf{S}(\boldsymbol{\nu}_1) \frac{\partial T}{\partial \boldsymbol{\nu}_1}}_{\text{Coriolis-centripetal moments}} & = \boldsymbol{\tau}_2 \end{array} \quad (\text{A.7})$$

as:

$$\mathbf{C}_{\text{RB}}(\boldsymbol{\nu})\boldsymbol{\nu} = \begin{bmatrix} -\mathbf{S}(\boldsymbol{\nu}_2) \frac{\partial T}{\partial \boldsymbol{\nu}_1} \\ \mathbf{S}(\boldsymbol{\nu}_2) \frac{\partial T}{\partial \boldsymbol{\nu}_2} + \mathbf{S}(\boldsymbol{\nu}_1) \frac{\partial T}{\partial \boldsymbol{\nu}_1} \end{bmatrix}. \quad (\text{A.8})$$

Utilising $\mathbf{S}(a)b = -\mathbf{S}(b)a$ Equation (A.8) can be written as:

$$\mathbf{C}_{\text{RB}}(\boldsymbol{\nu})\boldsymbol{\nu} = \begin{bmatrix} 0 & -\mathbf{S}(\frac{\partial T}{\partial \boldsymbol{\nu}_2}) \\ -\mathbf{S}(\frac{\partial T}{\partial \boldsymbol{\nu}_1}) & \mathbf{S}(\frac{\partial T}{\partial \boldsymbol{\nu}_2}) \end{bmatrix} \begin{bmatrix} \boldsymbol{\nu}_1 \\ \boldsymbol{\nu}_2 \end{bmatrix}, \quad (\text{A.9})$$

which gives:

$$\mathbf{C}_{RB}(\boldsymbol{\nu}) = \begin{bmatrix} 0 & 0 & 0 & mv \\ 0 & 0 & mv & -mu \\ 0 & -mv & 0 & I_y q \\ -mv & mu & -I_y q & 0 \end{bmatrix}. \quad (\text{A.10})$$

The Coriolis-centripetal matrix, $\mathbf{C}_{RB}(\boldsymbol{\nu})$, is skew-symmetric, and consequently it performs no actual work on the system. This illustrates that the Coriolis-centripetal forces are fictive and arise when a non-inertial reference frame is used.

Kirchhoff's equation of motion for a rigid body system can be expressed as:

$$\mathbf{M}_{RB}\dot{\boldsymbol{\nu}} + \mathbf{C}_{RB}(\boldsymbol{\nu})\boldsymbol{\nu} = \boldsymbol{\tau}_{RB}. \quad (\text{A.11})$$

The first term, $\mathbf{M}_{RB}\dot{\boldsymbol{\nu}}$, may be considered as Newton's second law, while $\mathbf{C}_{RB}(\boldsymbol{\nu})\boldsymbol{\nu}$ can be seen as a correction of the first term when the equation is solved in a non-inertial reference frame.

A.2.3 Equations of motion for ships

A body moving through water will impart kinetic energy to the fluid, and this energy must be included in the equations of motion. This is taken into account as inertial pressure forces, also called added mass. These forces are included in the Kirchhoff's equations using the energy of the added mass. The added mass forces also induce Coriolis-centripetal forces that must be included in the equations of motion.

The inertial pressure forces are proportional to the acceleration of the motion. For a port-starboard symmetric ship is the low-frequency added mass matrix given as:

$$\mathbf{M}_A^0 = - \begin{bmatrix} X_u^0 & 0 & 0 & 0 \\ 0 & Y_v^0 & 0 & 0 \\ 0 & K_v^0 & K_p^0 & K_r^0 \\ 0 & N_v^0 & N_p^0 & N_r^0 \end{bmatrix}, \quad (\text{A.12})$$

where the superscript 0 indicates that the derivatives is defined at low-frequency, which are typically valid for manoeuvring in calm water.

In calm water manoeuvring the total energy of the system is given as:

$$T = \frac{1}{2} \boldsymbol{\nu}^T \mathbf{M} \boldsymbol{\nu}, \quad (\text{A.13})$$

where $\mathbf{M} = \mathbf{M}_{RB} + \mathbf{M}_A^0$. The rigid body mass matrix, \mathbf{M}_{RB} , is defined in the previous section, while \mathbf{M}_A^0 is the low-frequency added mass matrix. The skew-symmetric parts of \mathbf{M}_A^0 do not have any influence on the kinetic energy of the system. Hence, it is only the symmetric parts of \mathbf{M}_A^0 that is of interest:

$$\mathbf{M}_A^0 = \underbrace{\frac{1}{2}(\mathbf{M}_A^0 + (\mathbf{M}_A^0)^T)}_{\text{symmetric}} + \underbrace{\frac{1}{2}(\mathbf{M}_A^0 - (\mathbf{M}_A^0)^T)}_{\text{skew-symmetric}}. \quad (\text{A.14})$$

Consequently can the added mass matrix be defined as:

$$\overline{\mathbf{M}_A^0} = \frac{1}{2}(\mathbf{M}_A^0 + (\mathbf{M}_A^0)^T), \quad (\text{A.15})$$

which gives

$$\mathbf{M} = \mathbf{M}_{RB} + \overline{\mathbf{M}_A^0}. \quad (\text{A.16})$$

By separating the energy of the system into rigid body mass and added mass as:

$$T = T_{RB} + T_A, \quad (\text{A.17})$$

where $T_A = \frac{1}{2}\boldsymbol{\nu}^T \overline{\mathbf{M}_A^0} \boldsymbol{\nu}$, the forces on the rigid body due to added mass are expressed as:

$$\begin{aligned} \boldsymbol{\tau}_{a1} &= -\frac{d}{dt}\left(\frac{\partial T_A}{\partial \boldsymbol{\nu}_1}\right) - \mathbf{S}(\boldsymbol{\nu}_2)\frac{\partial T_A}{\partial \boldsymbol{\nu}_1} \\ \boldsymbol{\tau}_{a2} &= -\frac{d}{dt}\left(\frac{\partial T_A}{\partial \boldsymbol{\nu}_2}\right) - \mathbf{S}(\boldsymbol{\nu}_2)\frac{\partial T_A}{\partial \boldsymbol{\nu}_2} - \mathbf{S}(\boldsymbol{\nu}_1)\frac{\partial T_A}{\partial \boldsymbol{\nu}_1}. \end{aligned} \quad (\text{A.18})$$

Using the same procedure as for the rigid body system, the Coriolis-centripetal forces on the rigid body can be given as:

$$\begin{aligned} X_C &= r \frac{\partial T_A}{\partial v} = -Y_v^0 vr - \frac{1}{2}(N_v^0 + Y_r^0)r^2 - \frac{1}{2}(Y_p^0 + K_v^0)pr \\ Y_C &= -r \frac{\partial T_A}{\partial u} = X_u^0 ur \\ K_C &= 0 \\ N_C &= v \frac{\partial T_A}{\partial u} - u \frac{\partial T_A}{\partial v} = (Y_v^0 - X_u^0)uv + \frac{1}{2}(Y_r^0 + N_v^0)ur + \frac{1}{2}(Y_p^0 + K_v^0)pu. \end{aligned} \quad (\text{A.19})$$

By assuming a symmetric added mass N_v^0/Y_r^0 and Y_p^0/K_v^0 are interchangeable. Further, the Coriolis-centripetal forces can be expressed on matrix form as:

$$\mathbf{C}_A(\boldsymbol{\nu}) = \begin{bmatrix} 0 & 0 & Y_v^0 v + Y_r^0 r + Y_p^0 p \\ 0 & 0 & -X_u^0 u \\ 0 & 0 & 0 \\ -Y_v^0 v - Y_r^0 r - Y_p^0 & X_u^0 u & 0 \end{bmatrix}. \quad (\text{A.20})$$

A.3 Main characteristics of R/V Gunnerus

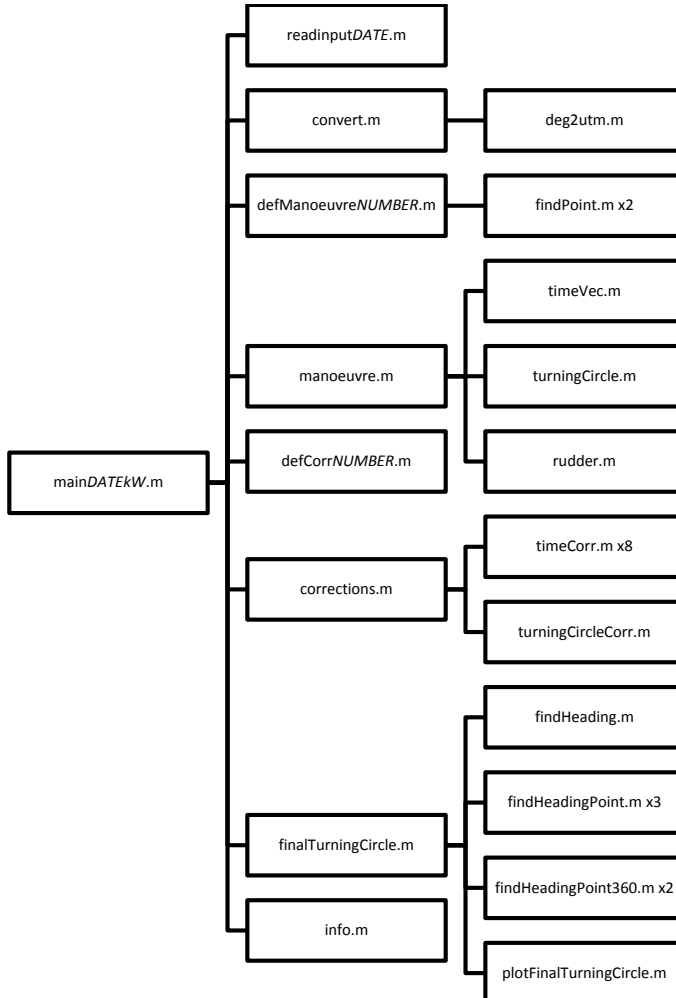
Following characteristics of R/V Gunnerus is used in calculation of hydrodynamic coefficients.

```
%_____
% mainCharacteristics.m
%
% Task: Define main characteristics of R/V Gunnerus to be used in
%        calculation of hydrodynamic coefficients.
%
% _____
% Parameter:      Description:
% T             [m]      Draught
% L             [m]      Ship length (length betw. perp)
% B             [m]      Beam
% Cb            [-]      Block coefficient, from ShipX
% rho           [kg/m^3] Fluid density of sea water
% Delta          [kg]     Displacement, from ShipX
% Nabla          [m^3]    Volume displacement , from ShipX
% BP07           [m]      Half breadt at the height of 0.7R
%                   (R=propeller radius)
% BPS            [m]      Half breadth at the height of propeller shaft
%                   in station 2.0
% Cwa            [-]      Water plane coefficient of aft section (between
%                   station 5 and AP), from ShipX
% Cpa            [-]      Prismatic coefficent of aft section (between
%                   station 5 and AP), from ShipX
%
% Programmed by Sissel Tjoeswold, Spring 2012
%
function [T L B Cb rho Delta Nabla BP07 BPS Cwa Cpa] = ...
mainCharacteristics()
T = 2.75;
L = 28.9;
B = 9.6;
Cb = 0.569;
rho = 1025;
Delta = 447000;
Nabla = 436.672;
BP07 = 3.6;
BPS = 3.5;
Cwa = 0.9844;
Cpa = 0.7099;
end
```

A.4 Analysis of full-scale trials

A.4.1 Turning circles

Flow chart



DATE – specifies which day the trials are from.

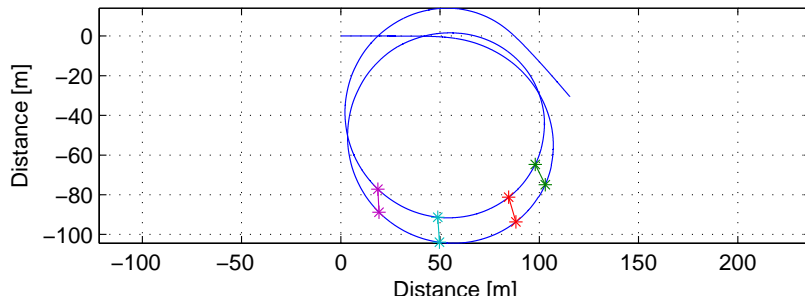
kW – indicates the engine power used at the trial.

NUMBER – specifies which trial that is being investigated.

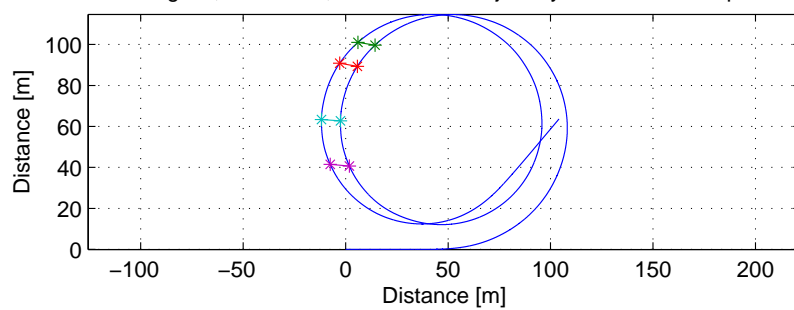
The flow chart is valid for one trial at a time. Consequently, the second and third level are repeated three times in order investigate four trials in one main-script.

Monday 27 February 2012 - 2x425 kW

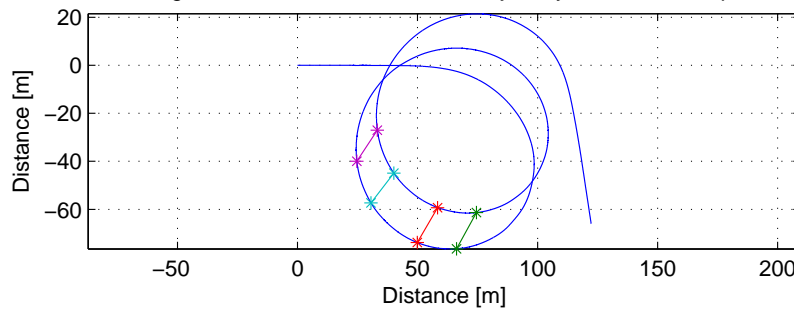
20 deg SB, 2x425 kW, 27/02/2012. Trajectory and corrections points



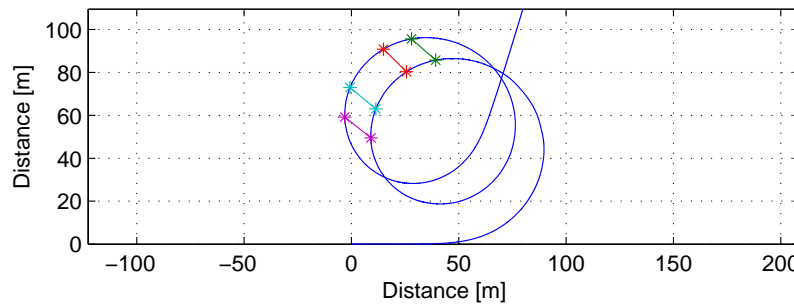
20 deg PT, 2x425 kW, 27/02/2012. Trajectory and corrections points



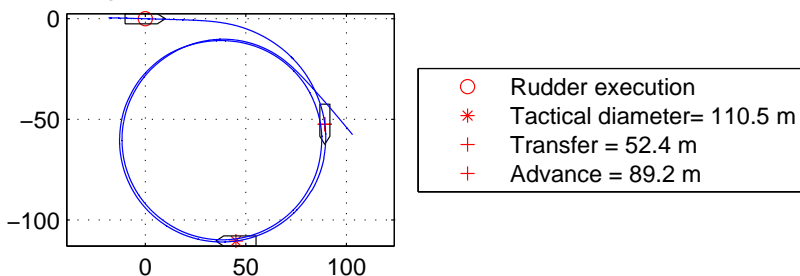
35 deg SB, 2x425 kW, 27/02/2012. Trajectory and correction points



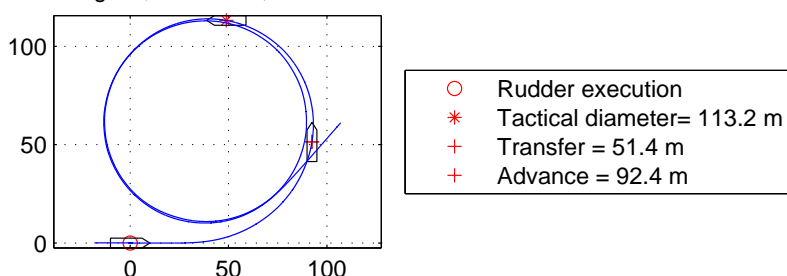
35 deg PT, 2x425 kW, 27/02/2012. Trajectory and correction points



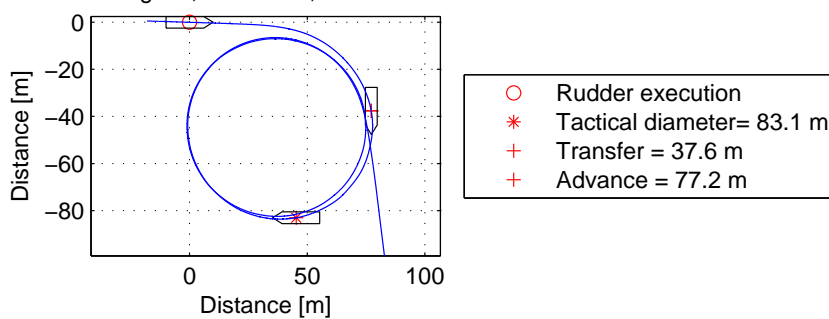
20 deg SB, 2x425 kW, 27/02/2012.



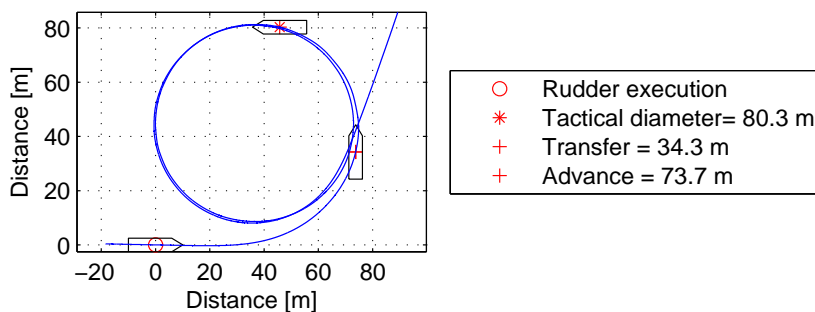
20 deg PT, 2x425 kW, 27/02/2012.

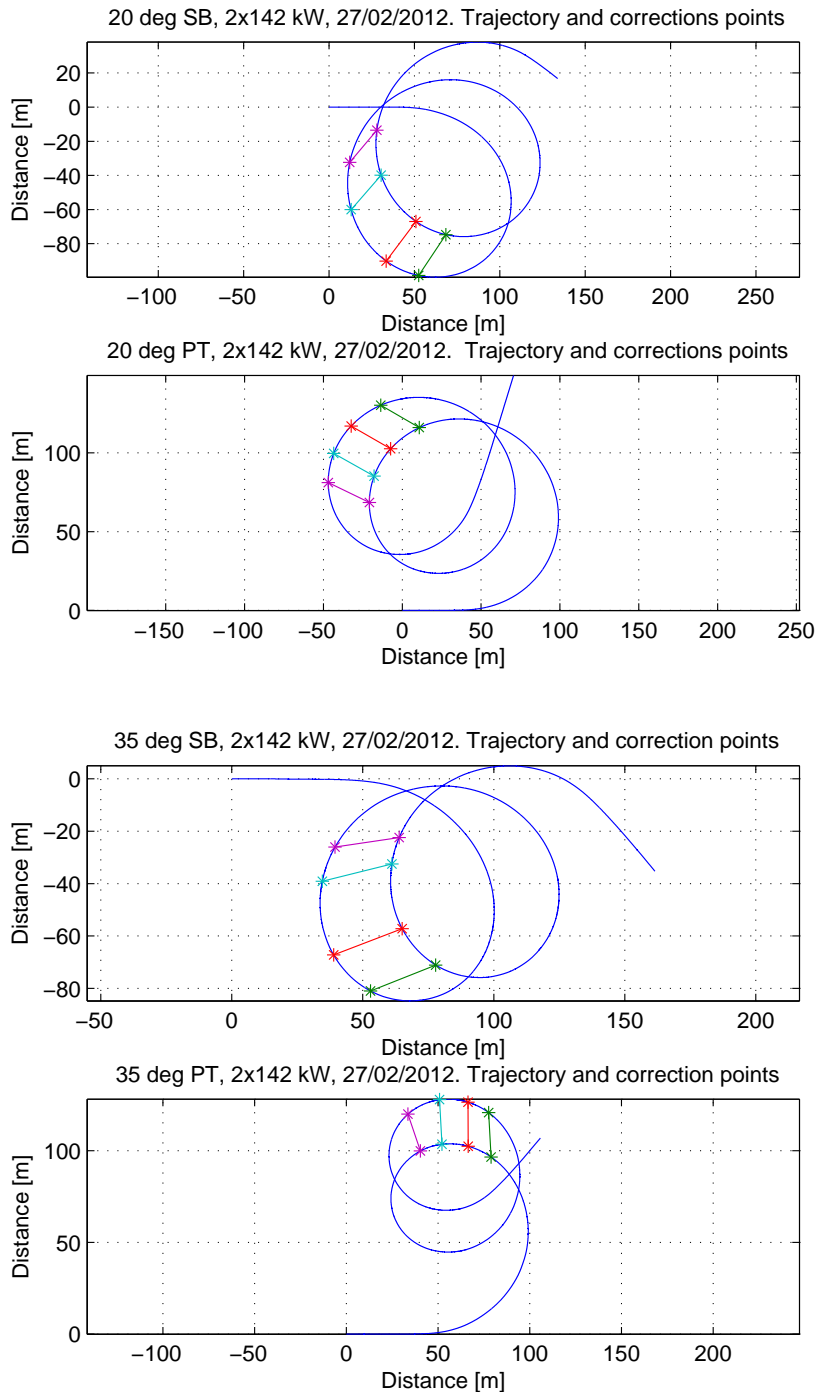


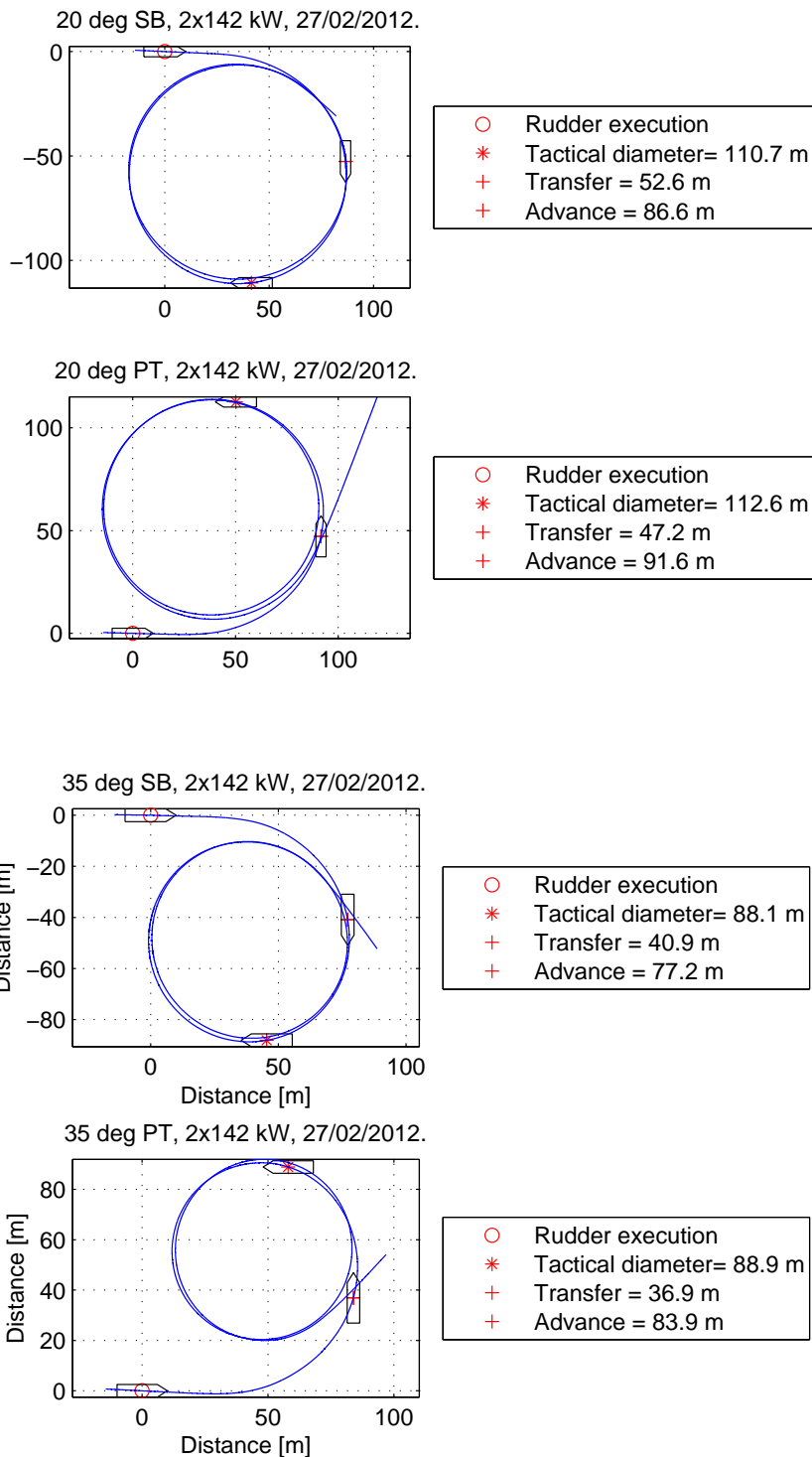
35 deg SB, 2x425 kW, 27/02/2012.

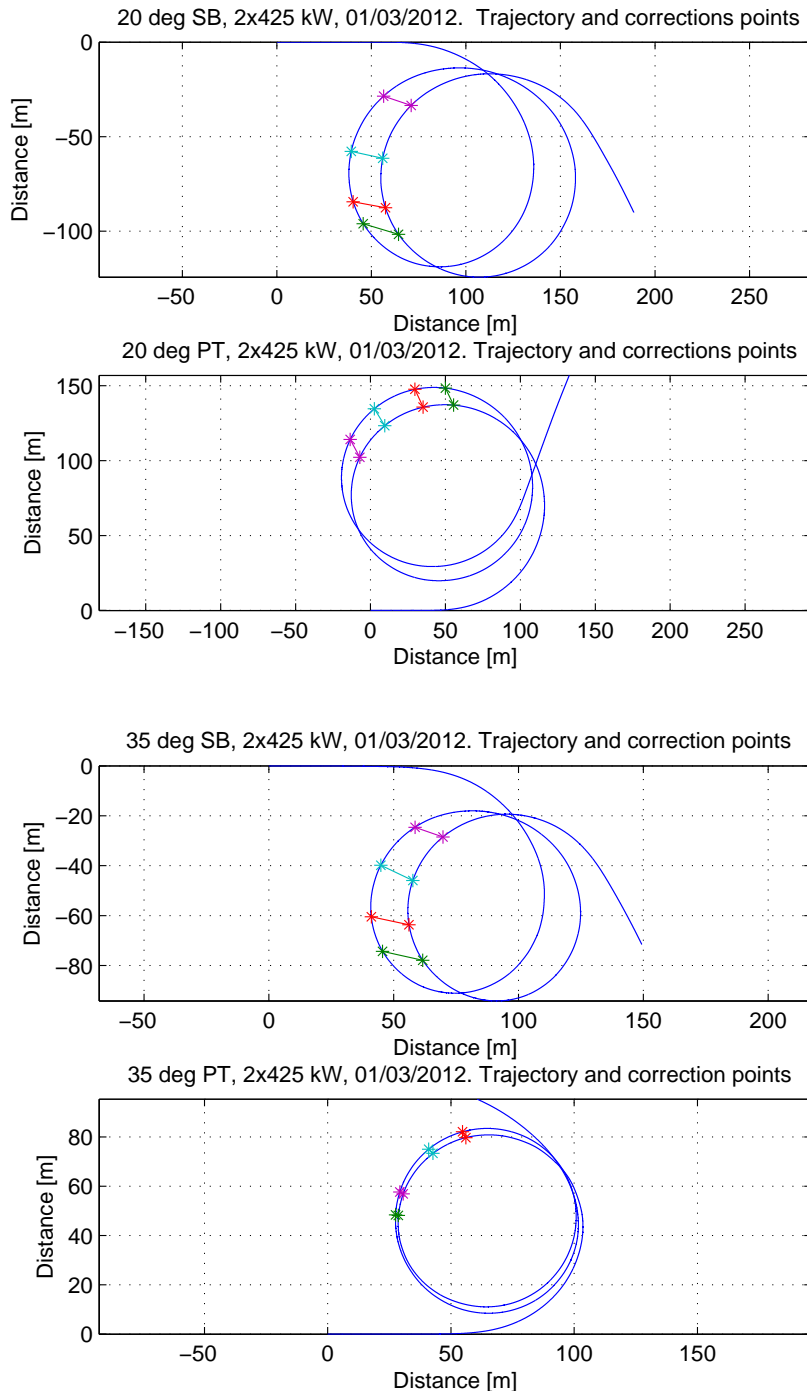


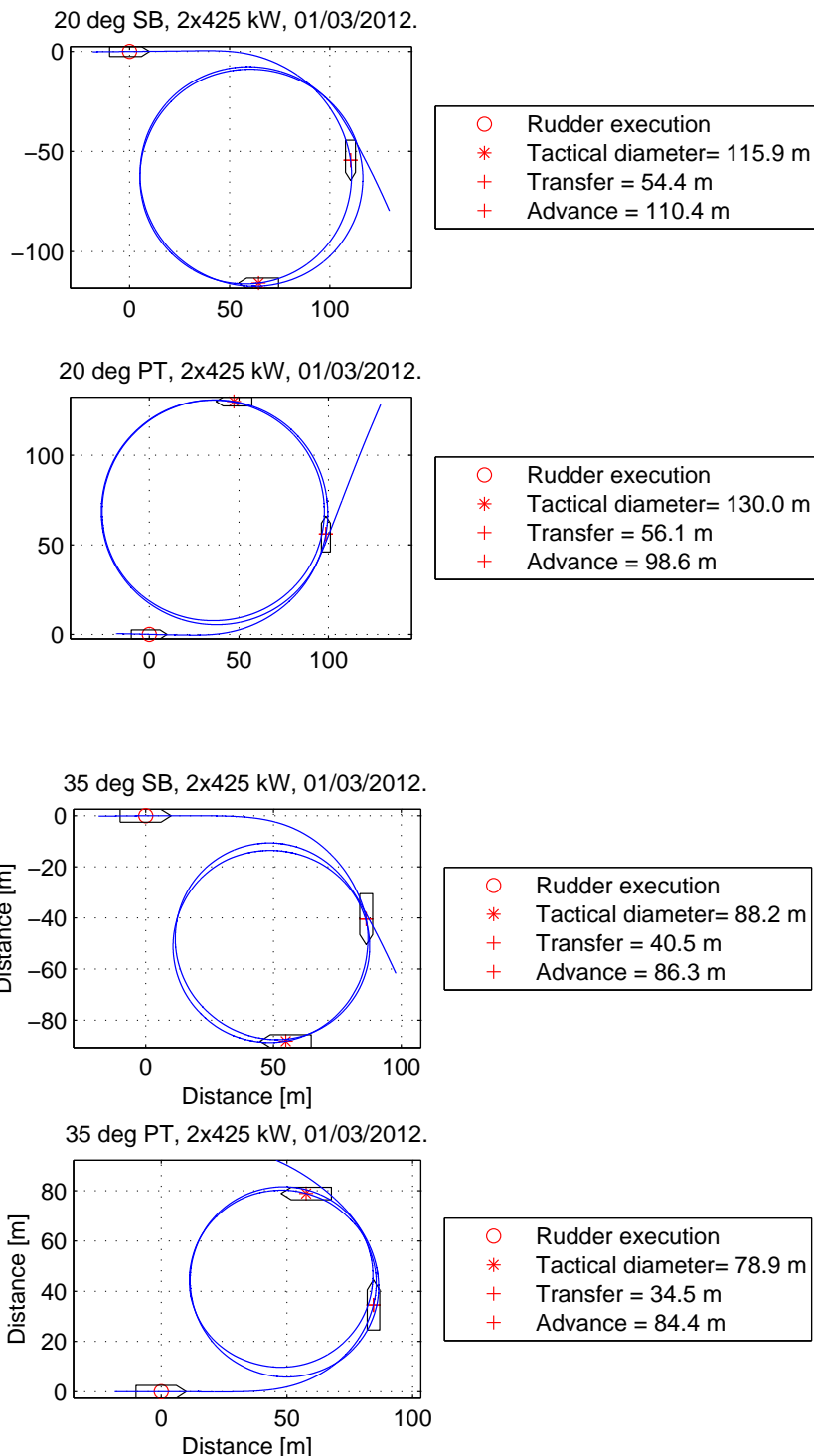
35 deg PT, 2x425 kW, 27/02/2012.



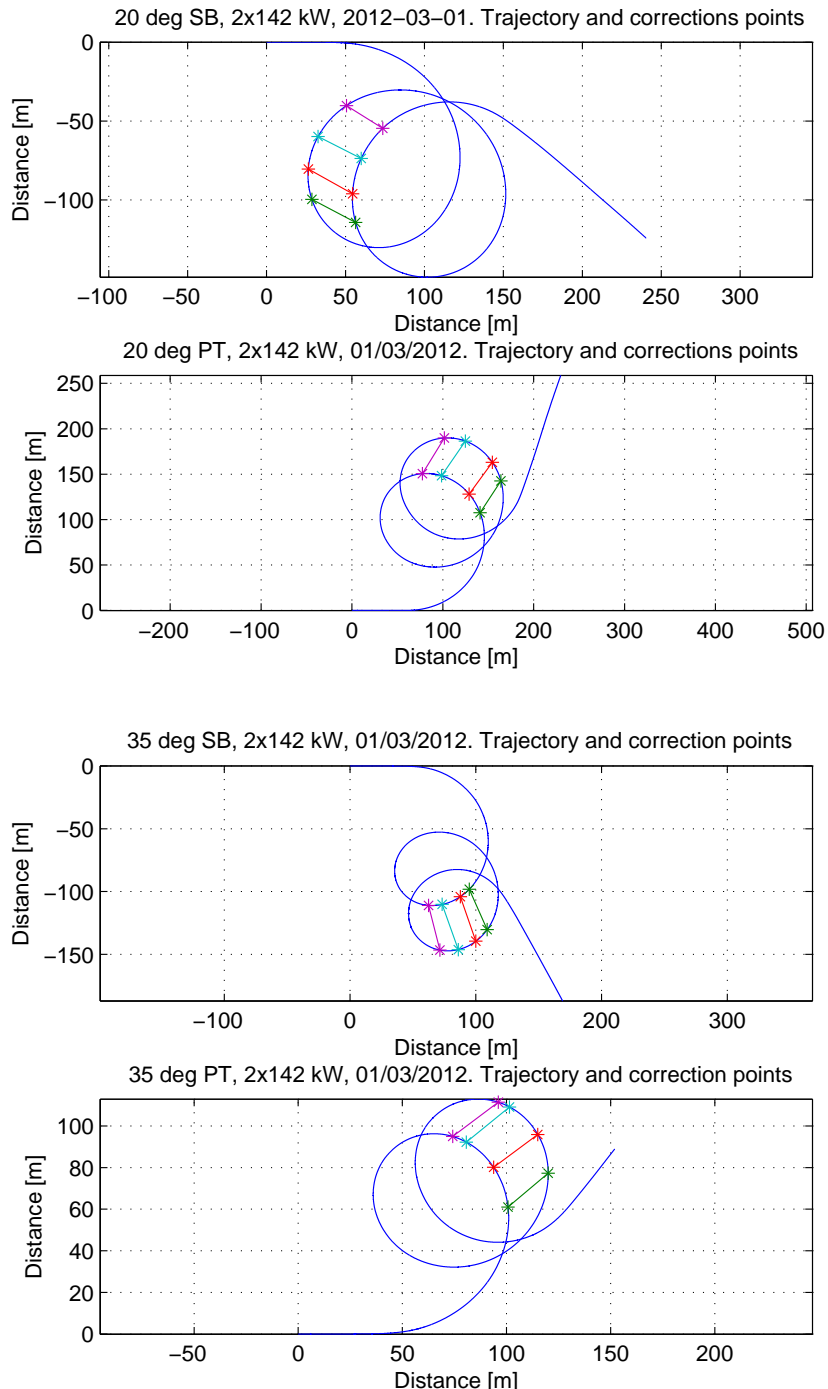
Monday 27 February 2012 - 2x142 kW




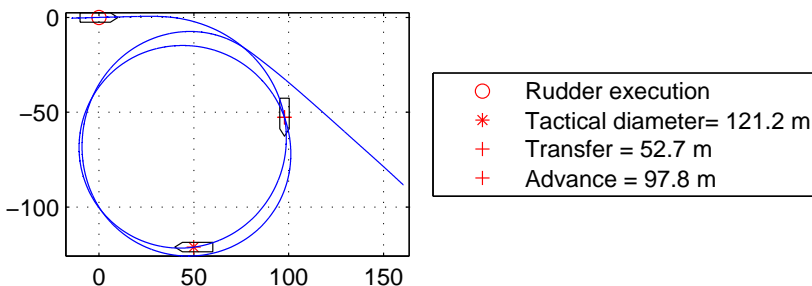
Thursday 1 March 2012 - 2x425 kW



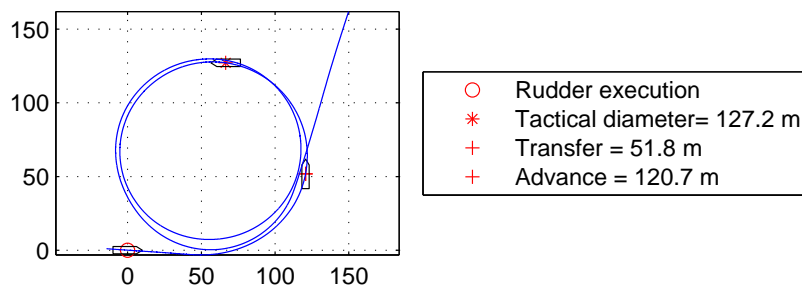
Thursday 1 March 2012 - 2x142 kW



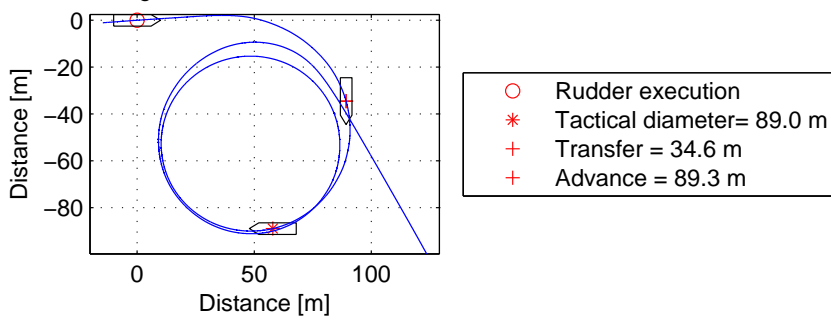
20 deg SB, 2x142 kW, 2012-03-01.



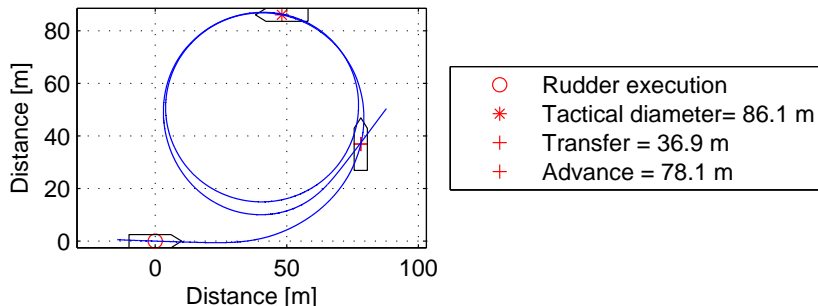
20 deg PT, 2x142 kW, 01/03/2012.



35 deg SB, 2x142 kW, 01/03/2012.

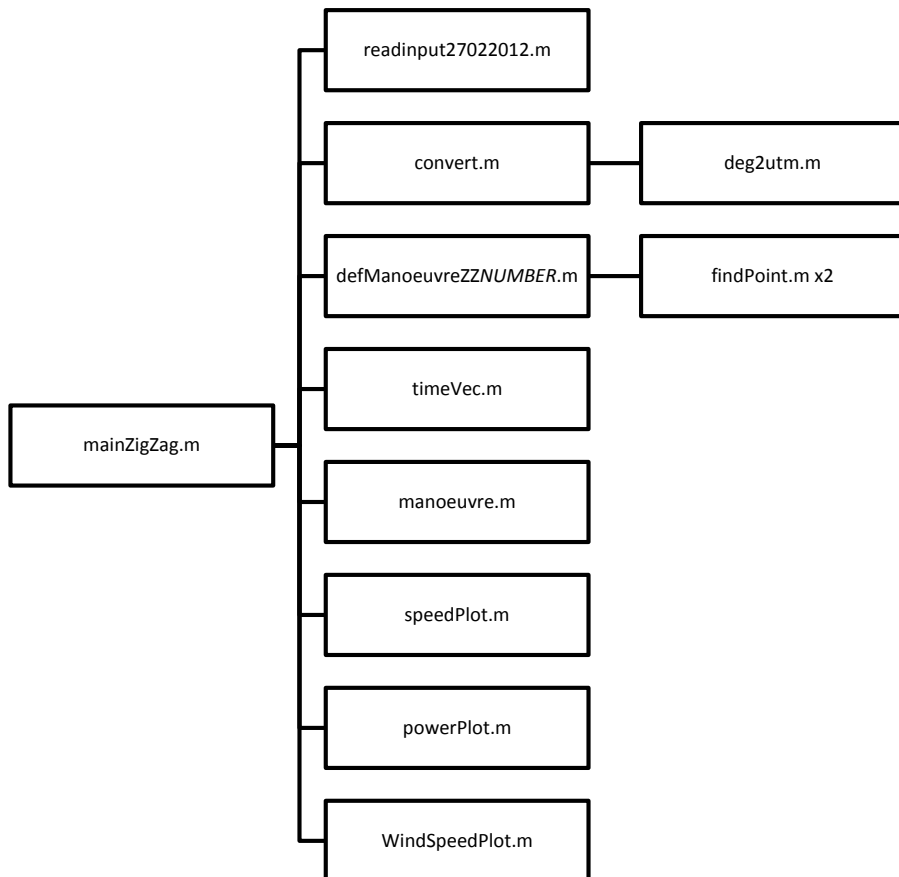


35 deg PT, 2x142 kW, 01/03/2012.



A.4.2 Zig-zag manoeuvres

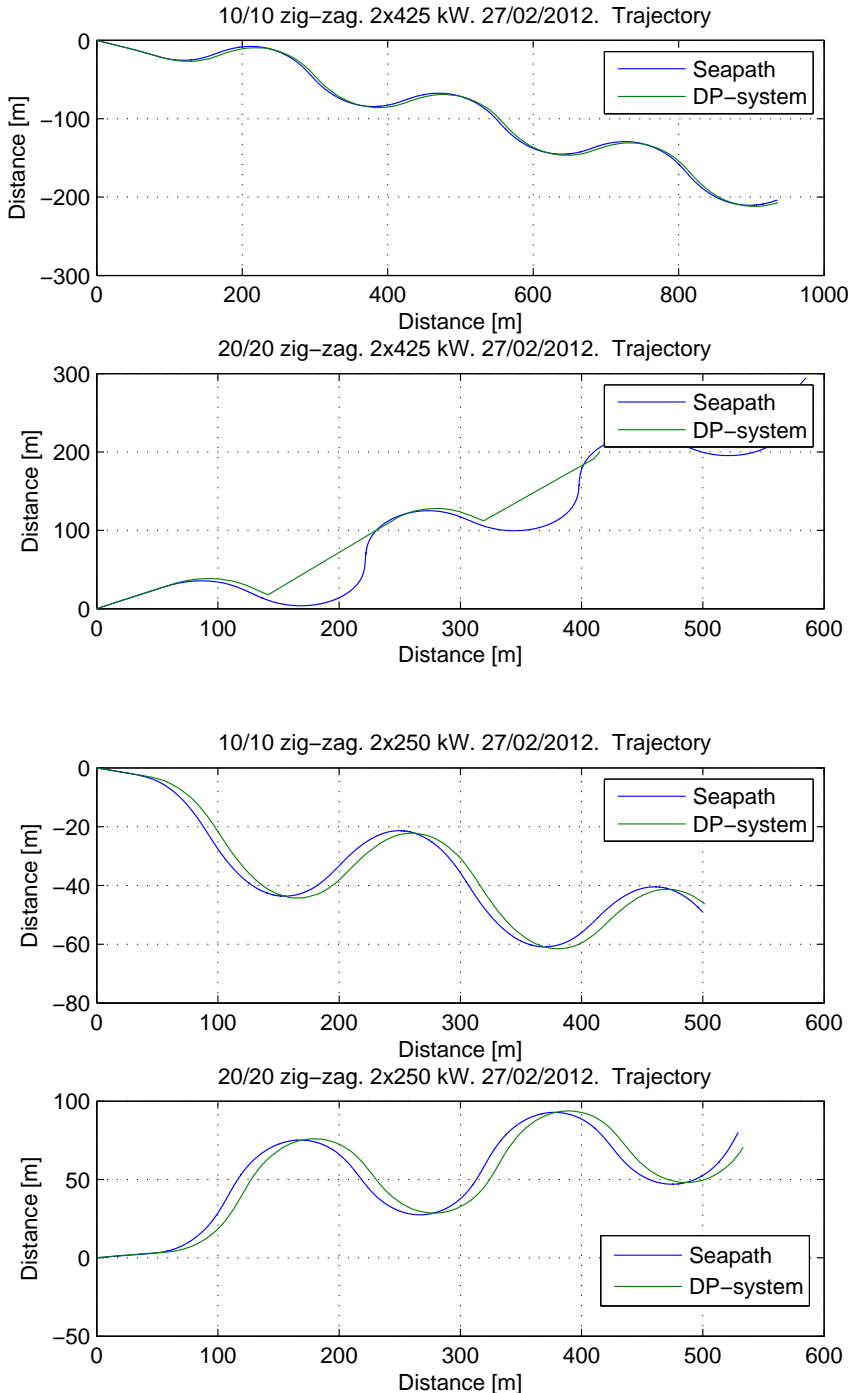
Flow chart

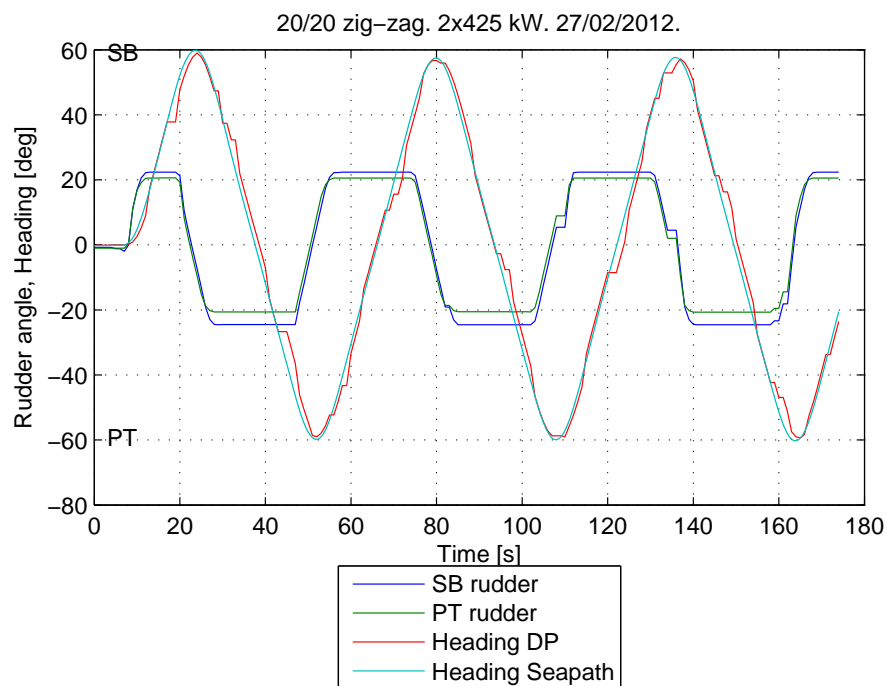
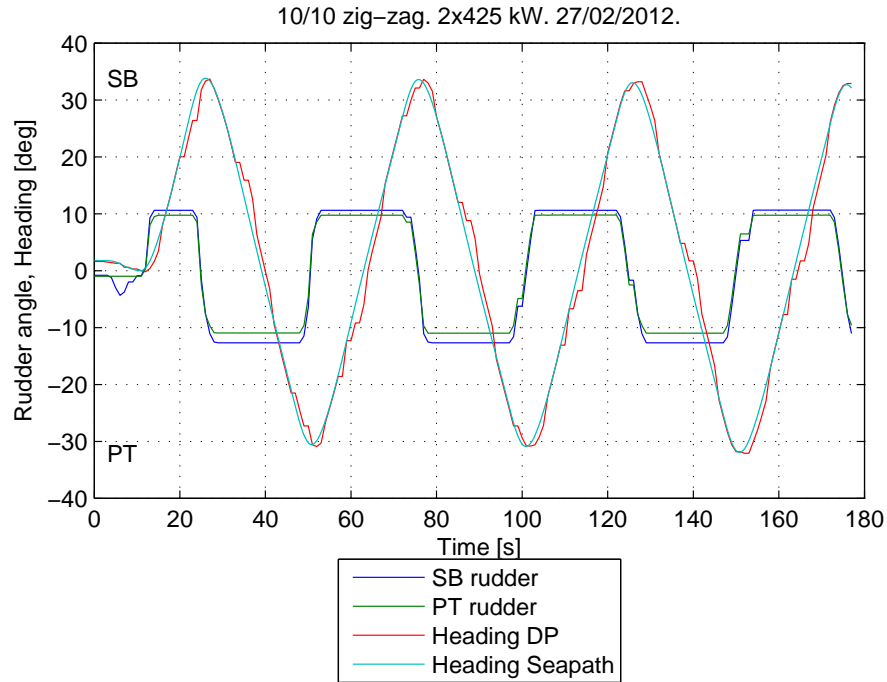


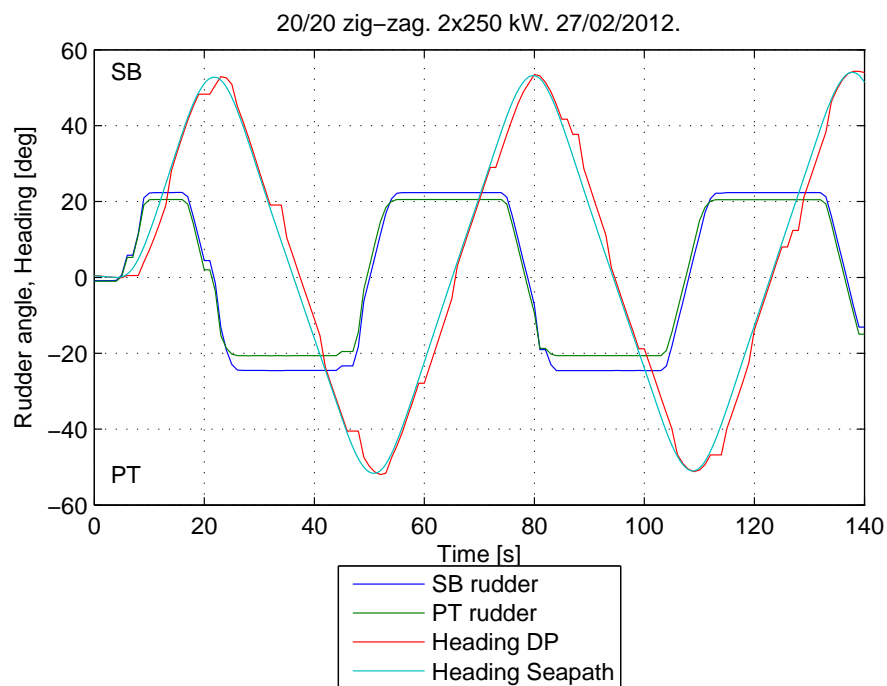
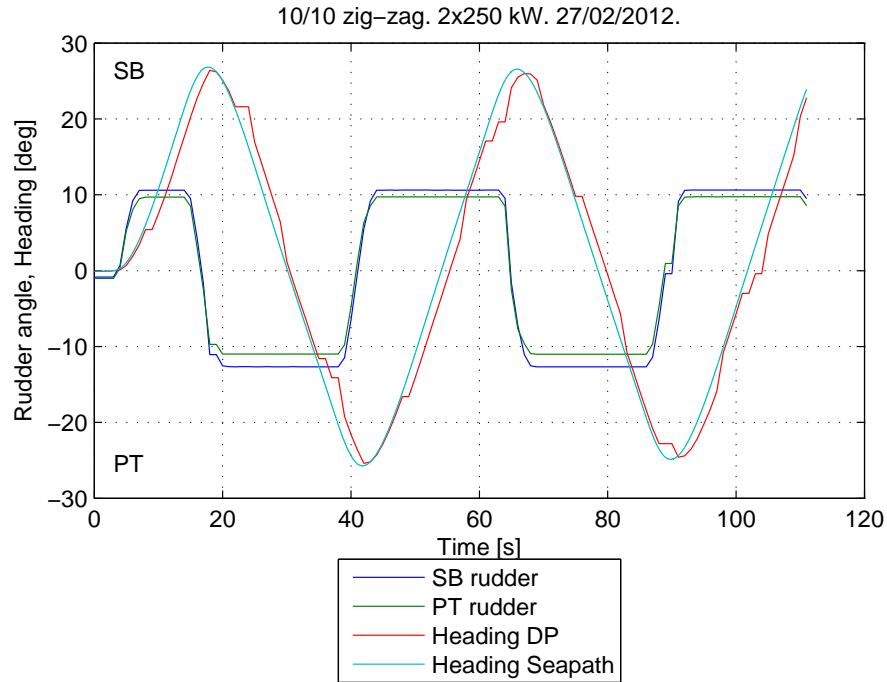
NUMBER – specifies which trial that is being investigated.

The flow chart is valid for one manoeuvre at a time. Consequently, the second and third level are repeated three times in order investigate four manoeuvres in one main-script.

Plots

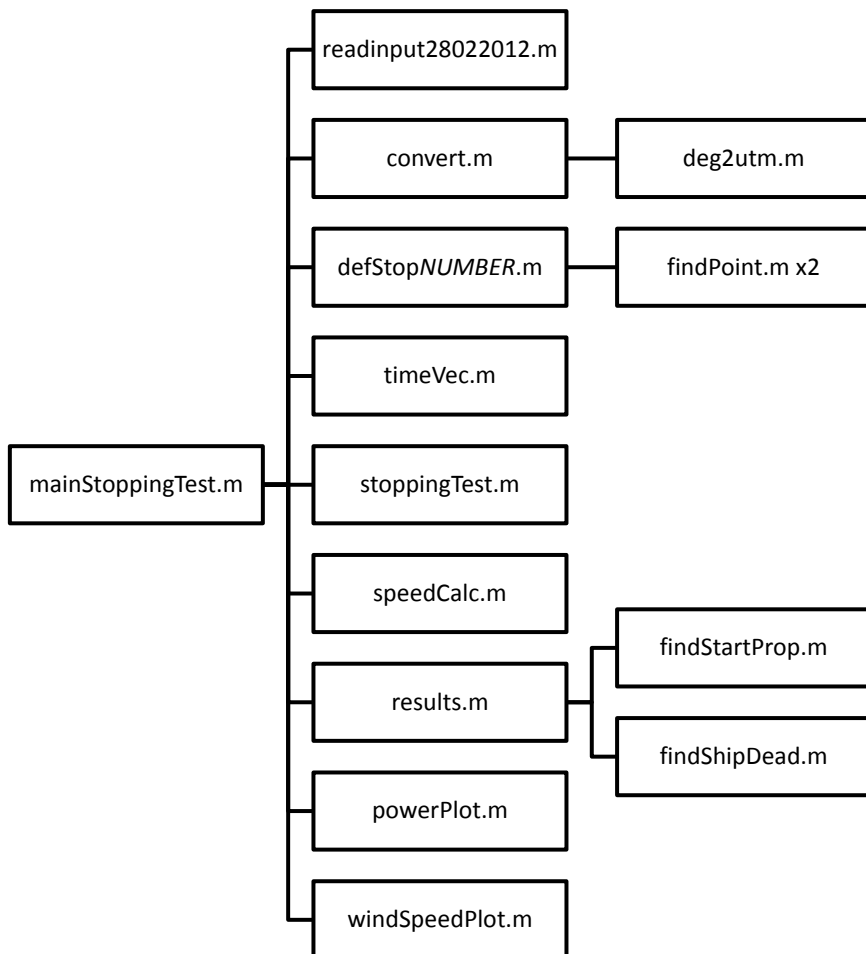






A.4.3 Stopping tests

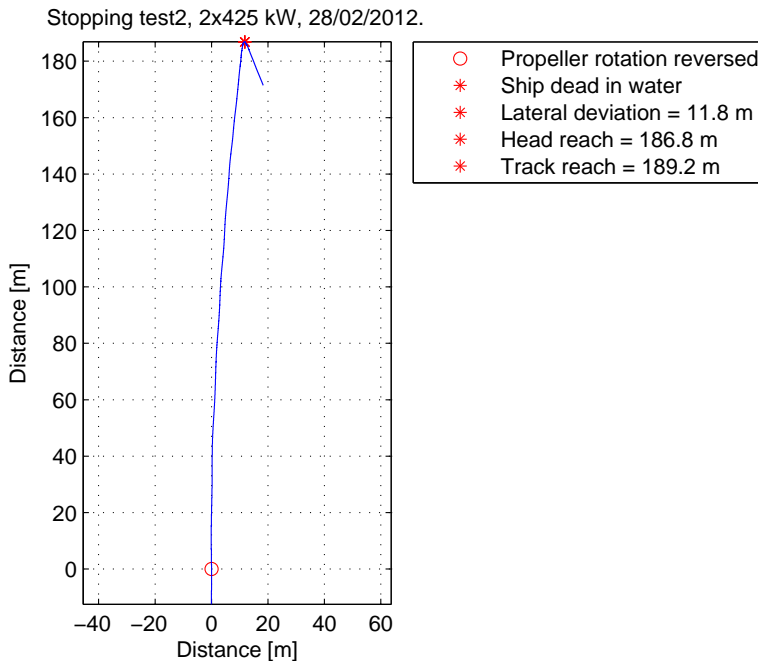
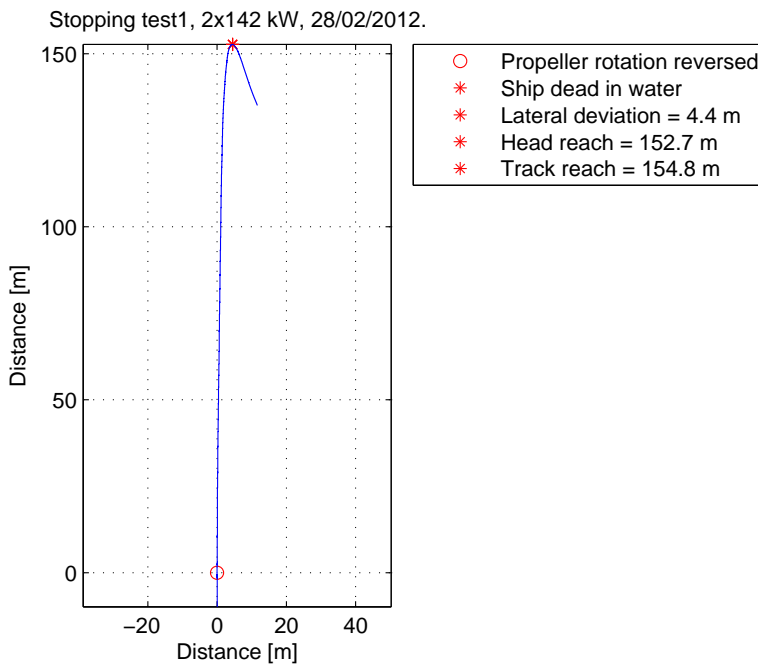
Flow chart



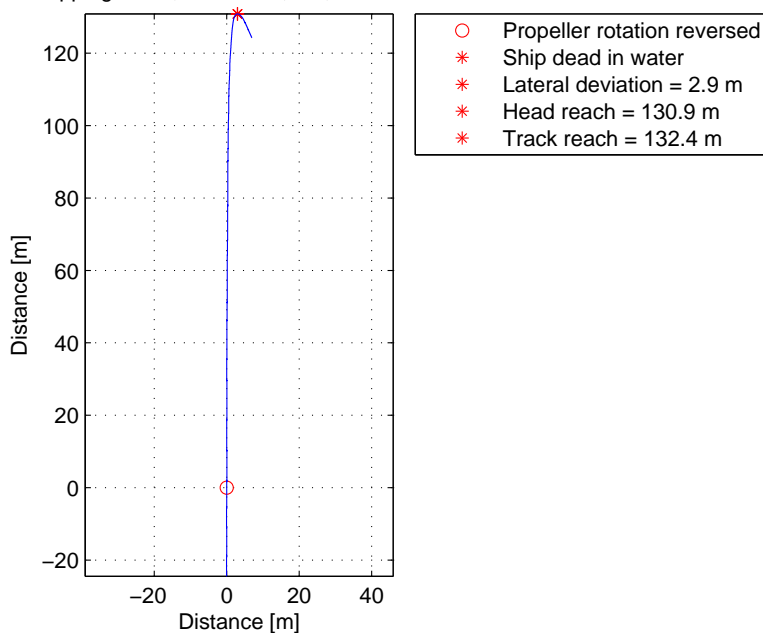
NUMBER – specifies which trial that is being investigated.

The flow chart is valid for one trial at a time. Consequently, the second and third level are repeated two times in order investigate three trials in one main-script.

Results



Stopping test 3, 2x142 kW, DP, 28/02/2012.



A.5 Simulations in ShipX

A.5.1 Effect of wake fraction and thrust deduction on turning circle manoeuvre

The interaction between hull and propeller can be described by wake fraction, w , and thrust deduction, t . The flow around the hull and to the propeller changes due to friction, hull shape and the propeller. The velocity that the propeller experiences will be less than the vessel's speed. The velocity through the propeller can be expressed as [34]:

$$U_A = U(1 - w), \quad (\text{A.21})$$

where U is ship speed and w is wake fraction.

A vessel's resistance and propeller thrust are not equal. The propeller thrust are usually larger than the ship resistance, which may be expressed by the thrust deduction, t .

Wake fraction and thrust deduction must be specified in ShipX Manoeuvring Plug-in. w and t are predicted for R/V Gunnerus in the model tests. The model tests were performed with $T = 2.6$ m and velocities from 8.0 kn to 14.0 kn. As this is the only available information, a sensitivity analysis of how wake and thrust deduction influence the results of a turning circle manoeuvre is carried out. The sensitivity analysis is performed with approach speed at 9.8 kn and 11.9 kn. The values for wake fraction and thrust deduction are chosen based on the model test.

Table A.3: Sensitivity analysis of wake fraction and thrust deduction's influence on turning circle manoeuvres with approach speed at 9.8 kn.

		Advance [m]		Transfer [m]		Tactical diameter [m]	
Rudder angle	[°]	20	35	20	35	20	35
w	[-]	0.260					
t	[-]	0.280	102 79	58 34	118 64		
w	[-]	0.260					
t	[-]	0.234	103 80	59 35	120 65		
w	[-]	0.260					
t	[-]	0.288	101 79	57 34	117 64		
w	[-]	0.271					
t	[-]	0.280	103 80	59 34	120 65		
w	[-]	0.253					
t	[-]	0.280	101 78	57 33	117 64		
w	[-]	0.271					
t	[-]	0.234	104 81	60 35	122 66		
w	[-]	0.253					
t	[-]	0.242	102 79	58 34	118 64		

Table A.4: Sensitivity analysis of wake fraction and thrust deduction's influence on turning circle manoeuvres with approach speed at 9.8 kn.

		Advance [m]		Transfer [m]		Tactical diameter [m]	
Rudder angle	[°]	20	35	20	35	20	35
w	[-]	0.260					
t	[-]	0.280	101 80	54 33	111 62		
w	[-]	0.260					
t	[-]	0.288	100 80	54 33	111 61		
w	[-]	0.271					
t	[-]	0.234	102 81	55 33	114 63		

The results of the sensitivity analysis are given in Table A.3 and Table A.4. The results differs with maximum 4 m. In the model test with $T = 2.6$ m and $U = 9.5$ kn wake fraction and thrust deduction are predicted as respectively 0.260 and 0.280. Using these values give relatively neutral results (i.e. usually not maximum or minimum values). As the results do not differ much and this is the only information available, it chosen to run the simulations with $w = 0.260$ and $t = 0.280$.